technology · applications · instrumentation

tai corporation

(NASA-CR-161619) ANALYSIS OF LOCALIZED FRINGES IN THE HOLOGRAPHIC OPTICAL SCHLIEREN SYSTEM Final Report (TAI Corp., Huntsville, Ala.) 171 p HC A08/MF A01 CSCL 20F

N81-13329

Unclas
G3/35 29510

P.O. Drawer B Farley Station • Huntsville, Alabama 35802 • (205) 881-4999 & 881-1272

Research Study Entitled

"ANALYSIS OF LOCALIZED FRINGES IN THE HOLOGRAPHIC OPTICAL SCHLIEREN SYSTEM"

by

Robert L. Kurtz

FINAL REPORT

Prepared for

George C. Marshall Space Flight Center

MSFC, AL. 35812

Contract Number

NAS8-33509

TABLE OF CONTENTS

(Table of Contents, Cont.)

Section IV (Continued)

SECTION V

(Table of Contents, Cont.)

SECTION VI

SECTION VII

LIST OF FIGURES

Section III

(List of Figures, Continued)

Section IV

(List of Figures, Continued)

Section V

SECTION I

INTRODUCTION

Holography has found wide application in a variety of fields, yet perhaps the most remarkable application of optical holography is the interferometric comparison of diffuse wavefronts. Classical interferometric techniques, such as the Michelson interferometers are restricted to the comparison of wavefronts of simple geometric form, usually plane or spherical from polished surfaces using high quality optics. Holographic interferometry, however, can be used to measure the vector displacement of points on diffuse opaque surfaces or through diffuse transparent mediums of complicated shape. This is a consequence of the high information content of holograms, which makes possible the faithful recording and reconstruction of the optical wavefront scattered from such objects.

The subject of holography per se can be found in many good texts e.g. "Optical Holography" by Collier, Burkhardt and Lin-Academic Press and therefore, will not be discussed here. A knowledge of holography is assumed for this report.

In this report we primarily consider an application of holographic interferometry for which the object is a transparent medium with non-homogeneous refractive index. This constitutes the foundation of measurement techniques used in fluid flow visualization, aerodynamics, heat transfer, plasma diagnostics and stress analysis of transparent models. The technique is based on the analysis of the optical path length change of the object wave as it propagates through a transparent medium. Phase shifts due to variations of the speed of light within the medium give rise to an interference pattern. The resulting interferogram can be analyzed to determine physical properties of the medium

or transparent objects. Such properties include; mass density of fluids, electron densities of plasmas, temperature of fluids, chemical species concentration of fluids, and state of stress in solids. Each of these properties can be related to refractive index, which is measured by interferometry.

The optical wave used to probe transparent objects or mediums can be a simple plane or spherical wave, or it may be a complicated spatial wave scattered by a diffusing screen. When a plane object wave is used, the holographic interferograms are quite similar to those produced by classical instruments such as Michelson or Mach-Zehnder interferometers. There are differences, however, which are of considerable practical importance. When a diffuse object wave is used, holographic methods are unique and provide multidirectional interferometric data. Diffuse light holographic interferometry of phase objects gives rise to fringe localization effects similar to that found with diffuse opaque objects. In this report we discuss methods of recording holographic interferograms of transparent objects and of analyzing the formation and localization of interferometric fringes.

Information about the structure of the refractive index distribution is displayed in two ways or techniques in a holographic interferogram:

1) fringe number, position and spacing,

2) fringe localization/parallax.

Holographic interferometry can be, and is frequently used, to measure vector displacements of points on diffusely reflecting opaque objects. This theory of fringe analysis is reasonably well developed

and localization/parallax plays an important role. While there is an analogy between the fringe localization theory of opaque bodies and that for transparent (phase) objects, the analysis of holographic interferograms of transparent media, on the other hand, has thus far virtually been based exclusively on fringe number, position and spacing. The role of localization has been largely ignored.

Fringe analysis in the case of transparent mediums are quite complicated because fringe shifts are associated by path integrals through the object rather than with a single phase shift due to reflections at a single object point. As a consequence of this, the determination or computational reconstruction of a refractive index field based on fringe number, position and spacing, requires that the object field be viewed from a large number of viewing directions, ideally over a 180^{o} range of angles. This required range can be reduced if the object field has known symmetries. It is important, therefore, to develop a theory of fringe localization in diffusely illuminated transparent media, to see if it augments conventional fringe analysis in useful ways. At the very least, fringe localization must provide information which is useful for approximate reconstruction of refractive index fields when the range of viewing angles is restricted to less than 180^{o} (the usual case in practice). Ultimately, a new reconstruction theory could result. Either result would be extremely useful.

The phenomenon of fringe localization is always useful in the sense that it discloses symmetries of the field, assists the viewer in locating the field in space, and helps one to form a qualitative impression of the structure of the field.

A distinction should be drawn between two separate and related localization problems.

1. The forward problem: Given a refractive index distribution, determine the fringe localization surface for a specified viewing direction.

2. The inverse problem: Using the measured fringe localization surface for a specified viewing direction, determine the refractive index distribution (or use the measurements to augment reconstruction based on fringe number, position and spacing). Of course, the inverse problem is the most formidable. We treat both problems in this report.

Section II of this report discusses a review of the literature, and Section III provides a determination of the feasibility and application of localized fringes to the Holographic Optical Schlieren System (HOSS). Section IV of this report provides the theoretical models for fringe formation - both problems, while Section V treats the application and implementation of localized fringe formation model to density/refractive index changes in a transparent medium. Conclusions and recommended areas for further study constitute Sections VI and VII respectively.

SECTION II

REVIEW OF LITERATURE

Since its introduction in 1965 the field of holographic interferometry has become somewhat confused by the very large number of papers published on the problem of interpreting the fringe patterns observed. Most of the papers have dealt with the fringe patterns created by diffusely reflecting opaque bodies [1-111]. Only a relative few papers have dealt directly with the reconstruction of refractive index fields from multi-directional interferometric data of diffusely illuminated transparent media. Because of the similarity of the two problems, much of the theoretical model development for holographic interferometry of opaque bodies provides a good analogy for the theoretical model development for refractive transparent media.

Contributions of the Seventies

The past ten years have produced a steady stream of papers on holographic interferometry, many of them dealing with the problems of interpretation. Emphasis has remained centered on the zero-order fringe (ZF) technique [39] using a multiple-hologram approach. The three-hologram technique was described in detail by Shibayama and Uchiyama [112], Hecht et. al. [113], and Eweres et. al. [114]. A vector approach was used by Macáková [115] to obtain the direction and magnitude of the displacement from a single hologram. Bijl and Jones [116, 117] used a tensor approach to obtain three-dimensional strains from three separate holograms. The problem of establishing a common datum point between the separate holograms in the multiple-hologram was overcome by Abramson [118], who used a length of elastic rubber strip fixed at one end to the object

and at the other end to the (stationary) holographic bench. Using the same technique, after measuring fringe positions to an accuracy of $\lambda/100$, the rubber strip idea was also used by Hung et. al. [120] who suggested that an alternative to using three separate holograms was to use a single hologram plate and to record three double-exposure holograms on it using three different illumination directions. This technique avoids the need for fringe projection inherent in the original three-hologram method, since all the fringe patterns can be photographed from the same viewing direction. The need for some simplification of the analysis if holographic interferometry is to become a widely used engineering tool was stressed by Hansche and Murphy [12,122], who showed that if the geometry of the object and the expected direction of the displacement are known a priori, then the analysis from first principles can be very straightforward. Specific applications of the ZF technique have been described by several authors [123-126]. Comparisons of the ZF technique with the fringe counting (FC) and fringe localization (FL) techniques were made in papers by Sollid [127] and Hansche and Murphy [121]. The combination of the ZF technique (to measure line-of-sight displacements) with speckle interferometry (to measure in-plane displacements) has been suggested by Velzel [128] and by Adamas and Maddux [129].

The fringe counting (FC) technique, introduced originally by Aleksandrov and Bonch-Bruevich [29], has also been developed in recent years . Kohler [130] proposed the use of cut-out masks in the hologram plane to dictate the way in which the viewing direction is changed.

Landry and Wise [131] proposed a semi-automatic method of data analysis for the FC technique, and a similar scanning method, but using the real image from the hologram, was suggested by Bellani and Sona [132]. A paper by King [133] combined the advantages of the multiple-hologram methods (the accurate measurement of all the components of motion) with the simplicity of the FC technique. He used two holograms mounted perpendicularly to each other. The FC technique has been compared with the ZF (zero-order fringe) and FL (fringe localization) techniques by several authors, including Sollid [127] and Hansche and Murphy [121].

The fringe localization (FL) technique, pioneered by Haines and Hildebrand [10], has also had its adherents. Dubas and Schumann [134] used the criterion of maximum fringe visibility to define the plane of localization of the fringes. The FL method was also used by Ashton et.al. [135], and was discussed in two papers by Stetson [136, 137]. Hansche and Murphy [121] compared the technique with the fringe counting (FC) method.

The Haidinger fringe/hologram fringe (HF) technique, first proposed by Tsujiuchi et.al. [71, 99] and Gates [74, 98], has been taken up and developed by other workers, notably by Boone and DeBacker [138, 139].

The problem of fringe localization has continued to attract attention, with contributions from several authors [134, 136, 137, 140-143].

The application of moiré techniques to holographic interferometry has generated some considerable interest. Twin apertures in the hologram plane were used by Velzel [128] to produce moiré fringes which are contours of equal in-plane displacement, while Der et. al. [144] used a four-exposure technique to obtain moiré fringes which gives the difference between two

displacements of the object. Moiré fringes were also used by Hariharan and Hegedus [145] in a method designed to eliminate the effects of spurious movements of the object and to record only symmetrical deflections. Moiré fringe theory has also been used to explain and interpret holographic interferograms - the images can be regarded as moiré fringes between the two complex gratings making up the two holograms. This line of approach has been developed by such authors as Abramson [146-148] and Gori and Mallamace [19].

Abramson has developed his holo-diagram technique in a series of papers [118,148,149] and has also introduced an 'analogue computer' based on the holo-diagram and stretched strings to facilitate the interpretation of holographic interferograms [118,148]. The use of the holo-diagram has been extended to time-averaged holography and the study of vibrations by Bjelkhagen [150]. An interesting set of photographs of holographic interferograms was also published by this team [151].

A detailed account of vibration analysis by time-averaged holography is outside the scope of this paper, but it should perhaps be recorded that a considerable amount of work has been put into this branch of holography. The reader is referred to the literature for further details of this topic and particularly to the contributions of Wilson [152-154] on vibration mode patterns. Stetson [155-158] on non-sinusoidal vibrations and higher-order fringes, Bjelkhagen [150] on the use of Abramson's holo-diagram, and Vikram on vibrating objects undergoing constant acceleration [159] and on a technique for extending the range of time-averaged holography [160].

Several techniques using two or more separate holograms, instead of either one double-exposure hologram or a single-exposure hologram and the original object, have been proposed. Havener and Radley [18] called their method, which was used with phase objects, 'dual-hologram interferometry'. A similar approach, also using phase objects, was described by Gori and Mallamace [19]. A multiplex technique, in which several images of the object in different states are recorded either on separate hologram plates or on different parts of the same plate, was described in a paper by Hariharan and Hegedus [20]. Finally, a novel approach by Abramson [21, 161] uses two holographic plates sandwiched together; the holograms can be manipulated either separately, or together as a single 'sandwich hologram' as an aid to fringe interpretation.

Other contributions to the field of holographic interferometry during the past few years have included the further development by Stetson [136, 162, 163] of his generalized mathematical theory of fringe formation, the use of projected fringes to reduce the sensitivity of holographic interferometry [164], the use of temporally modulated illumination [165], the use of a double pulsed laser for work with impact-loaded objects [166], considerations of errors and accuracy attainable in holographic interferometry [119, 167],the use of a small frequency shift to achieve fringe interpretation down to better than $\lambda/100$ [168], a Fourier transform method of analysis [169], and the application of holographic interferometry to a wide variety of problems, such as the stretching of rubber [135], stresses in rigid pavements subjected to simulated traffic loads,

the monitoring of plant growth and other applications [172-176].

In general, the many techniques proposed for the interpretation of holographic interferograms can be classified according to four main groups of techniques as defined by Briers. These are:

1) The fringe localization techniques (FL)

Historically this technique was the first reported technique for interpreting holographic interferograms. The technique utilizes the fact that for certain types of motion or optical pathlength change, the fringes are localized at some distance from the image. In calculations this distance is used as a parameter. The method is powerful in determining the in-plane component of motion or optical pathlength change (the component in the plane perpendicular to the line of sight). The other components of displacements can be found, in principle, by repetitive measurements of fringe spacing and localization from different observation directions. Nevertheless, the effectiveness of the procedure is limited by the normally small size of typical interferograms. Usually for asymmetric conditions the range of angles to be covered by the hologram recordings are $\pm 90^{o}$. So the components of motion, with the exception of the in-plane one, are very difficult to measure with some accuracy. Another disadvantage of the FL technique is the difficulty to locate the plane of fringes to some accuracy.

This method is one of the primary subjects of this report and will be treated in detail below.

2) The fringe counting technique FC

This technique, [29,74] also makes use of the fact that the fringes

are, in general, located at some distance from the surface of the reconstructed image. The optical system used for viewing the fringes is focused on the image and is stopped down until the fringes are clearly visible. The surface point under consideration is viewed continuously from different directions and then the displacement component is determined by counting the number of fringes passing across the image point. The method gives the component of translation of the point in a direction perpendicular to the bisector of the two extreme lines of sight and in the plane containing these lines of sight. Other components of motion can be measured to a limited accuracy as in the case of the FL method. In spite of its rather convenient application in determining a complex object motion, the FC method does not suit measurement of the three-dimensional motion to the accuracy required by the industry. Due to its relative simplicity the FC technique remains a very useful holographic method even in its original form and the more so with improvements and developments especially for the rapid, semi-quantitive interpretation of interferograms.

This technique is also known as the parallax method and is a function of the size and geometry of the viewing aperture used.

3) The hologram or Haidinger fringe technique (HF)

The FL and FC techniques both use the fact that the fringes are localized in a plane remote from the image to measure the in-plane components of translation of the object. They interpret any fringes localized at a distance from the image as being due to a displacement with an in-plane component. However, it has been reported by several authors that

pure line-of-sight translation (i.e., displacement along the z-axis) also gives rise to fringe patterns with similar localization properties. Gates [74] described such fringes as 'curved bands', while other authors were more specific and reported them as concentric circles centered on the line of sight [62,64,71]. These fringes can be used to measure the line of sight translation that produced them.

The explanation of these fringes is that they are Haidinger fringes (fringes of equal inclination) and are due entirely to the variation in path difference across the object caused by the change in angle of view. They are identical to the fringes seen in the Michelson interferometer in diverging light. Although their origin is easy to explain, and they can be used to measure rigid-body translations along the line of sight, one might think that they would be a possible source of error when using the FL or FC techniques to measure in-plane displacements. However, this is unlikely to be the case since the holographic system is much less sensitive to rigid-body translations along the line of sight than it is to in-plane displacements. (This becomes less valid at large angles of view, but for an angle of view as large as 45^{0} there is still an order of magnitude difference in sensitivity.) Secondly, the curvature of the fringes will indicate that some line-of-sight displacement has occurred. If the fringes are concentric circles centered on the line of sight, the displacement is entirely along the line of sight. If the center of the fringe system is off-axis (possible out of the field of view), the displacement has components both along and perpendicular to the line of sight. For the present,

however, we would point out that if the curvature of the fringes is not too great, the FL or FC techniques will still give the in-plane component of the displacement.

4) The zero-order fringe (ZF) technique

The zero-order fringe method was first described by Ennos [39], although it is really the direct application of classical interferometry techniques to holographic interferometry. It is based on the first-principles argument that the change in optical path from the source to the observer (the fringe order, m, can only be determined absolutely if a known zero-order fringe is in the field of view. In many cases it will be known that a particular point on the object has remained stationary between the two holographic exposures, and the fringe order can be determined by counting fringes from such a point. A technique which has been used by several authors [118-120,126] consists of fixing one end of a strip of rubber to a point on the object, and fixing the other end firmly to the holographic bench; fringe counting can then be commenced from the latter point, which is known to have undergone zero displacement. Ennos [39] and Sollid [72] suggested that a zero-order fringe could be identified from the fact that there would be no parallax between it and the image; this approach must be adopted with caution. However, we have already seen that rotations about an axis in the plane of the object produce a system of parallel fringes, all of which display no parallax with the image.

Once the fringe order at all points on the image is known, the problem then becomes one of pure geometry - relating the change in optical path for each point to the actual displacement of that point. There are two schools of thought regarding this problem. One approach is to consider

the general case of arbitrary illumination and viewing conditions and to derive a set of equations from which the three components of the displacement can be calculated. Other authors have taken the view that the resulting expressions are so complex for the general case that it is better to treat each case on its own merit and to devise an experimental arrangement which will simplify the calculation of the displacement from first principles.

Considering the generalized approach first, it should be pointed out that, in general, three separate holograms will be required if all three components of the displacement are to be measured. Each hologram gives the component of the diplacement parallel to the bisector of the illumination and viewing directions [39]. Most authors have used vector analysis methods to derive equations connecting the displacement components of each point on the object with the path differences calculated from the three holograms. In his original paper on the technique, Ennos [39] predicted that this would be a 'formidable task' in the general case, and this has certainly proved to be so. The problem has been attacked by several authors, among whom we might mention Sollid [72], Stetson [60], Shibayama and Uchiyama [112], Hecht et.al. [113] and Bijl and Jones [116,117] but the resulting equations are usually very complex, and either difficult or tedious to apply in practice. The equations become more manageable, at the expense of some loss of generality, if the viewing directions, (i.e. the positions of the three holograms) are specified in certain ways. For example, Sampson [76], in a paper which perhaps deserves to be more widely known than it is, described a technique in which the object under

test is rotated about specific axes for the second and third holograms, the illumination and viewing conditions remaining fixed.

Relation Between Localization of Interference Fringes in Classical and Holographic Interferometry [177,178]

W. H. Steel [177]provides a descriptive account of both classical and hologram interferometry which shows many common features. In each, the position of fringe localization is found by a similar ray construction and the fringe visibility is derived from the amplitude distribution in a diffraction pattern near focus. Steel maintains that the van Cittert-Zernike theorem leads to the useful result that the theory of fringe visibility in an interferometer with an extended source is the same as the theory of diffraction of coherent radiation. Since the technique of hologram interferometry is an example of the diffraction and interference of coherent waves, it might be expected to have a theory equivalent to that of classical interferometry. The descriptive treatment given by Steel points out an equivalence and shows that the results obtained by other more mathematical theories can be derived, or at least made plausible, by a simple physical argument.

M. Meler [178] demonstrates graphically and experimentally that the localization of interference fringes in classical interferometry is a special case of the localization in holographic interferometry.

Fringe Localization and Holographic Interferometry of Transparent Objects in Refractive Index Phase Fields [179-204]

Optical interferometry can be used to determine or reconstruct the refractive index field of a transparent medium by measuring changes in optical pathlength of light rays due to their passage through the medium. Because refractive index is a function of other physical properties of the medium such as temperature, density, or state of stress, interferometric measurements are useful in a number of scientific and technological applications. Classical interferometers display the phase variations of a single plane wave that has passed through the test object. This provides sufficient information to reconstruct only those fields that are axisymmetric or those that have no variation in the direction of the optical axis. Holographic interferometry provides a practical technique for simultaneously recording phase variations in many wavefronts that traverse the test object in a variety of directions. Data obtained by such multidirectional interferometry consists of the optical pathlength changes of a collection of rays due to their passage through a refractive index field.

The pathlength ϕ_i of a ray that can be determined by interferometry is defined by

$$\int_{s_i} f(x,y,z)\,ds_i = \phi_i, \qquad (1)$$

where $f(x,y,z) = n(x,y,z) \cdot n_0$ is the refractive index relative to some reference field n_0 and where the path integral is evaluated along the ray path s_i. Equation (1) can be considered to be a functional equation from which local values of the real scalar function $f(x,y,z)$ can be determined when ϕ_i is given for a large collection of rays.

In general the light rays passing through n (x,y,z) are refracted and follow a curved path. In many interferometric applications, however, ray curvature is minor and the integral in Eq. (1) can be evaluated along straight lines. In this refractionless limit Eq. (1) is linear [205].

Note that in the refractionless limit a two-dimensional field f(x,y) can be considered without loss of generality, since any arbitrary plane within a three-dimensional field can be studied. This is verified by the analysis of Berry and Gibbs [206]. It is convenient, then, to rewrite Eq. (1) in the form

$$\int_S f(x,y)ds = \phi(\rho,\theta), \qquad (2)$$

where ds is a differential element of the geometric ray path and $\phi(\rho,\theta)$ is the pathlength of the ray specified by the polar coordinates (ρ,θ). All possible rays are included in the range $-90^o<\theta\leq 90^o$. The range of θ over which data is actually collected is referred to here as the angle of view. In practice it is often less than 180^o. For example, in holographic interferometry utilizing diffuse illumination, the angle of view is determined by the aperture of the hologram, the angular aperture of the illuminated diffuser, and the extent of the test object.

Only a few previous papers have dealt directly with the reconstruction of refractive index fields from multidirectional interferometric data. Rowley [207] was apparently the first to consider the solution of Eq. (2) in this context. Assuming the value of $\phi(\rho,\theta)$ to be known for all possible straight rays through the object in a given plane, he derived an expression for the two-dimensional Fourier transform of f(x,y). Alwang et.al.[208] reported that A. Pal had obtained the solution for f(x,y) as a function of $\phi(\rho,\theta)$.

To avoid a troublesome singularity in an integrand, he introduced a resolution parameter the optimum value of which is dependent upon the structure of the field being studied. This method was used to measure the density distribution in a slot flame. This same solution has also been derived by Junniger and van Haeringer [209], who proposed using a Taylor series expansion of $f(x,y)$ to determine the principal value of the integral. Tanner [210] showed that the principal value of the integral should be finite in practical applications. Alwang et al [208] also discussed a discrete element technique in which the phase object is considered to be divided into N finite grid elements, each of which has a uniform refractive index. Equation (2) is then replaced by a system of N simultaneous linear equations in N unknowns (the refractive indices of the grid elements). This technique was found to be extremely sensitive to such factors as grid size. Although little detail regarding this technique was presented, it was apparently not too satisfactory.

Matulka and Collins [211] considered a different approach to the problem. Their analysis technique is based on earlier work by Maldonado and Olsen [212] on plasma emissions. In this approach $f(x,y)$ is expanded in the mean sense in terms of a complete set of orthogonal functions within a circular region outside of which $f(x,y)$ is assumed to vanish. An important criterion for selecting the set of expansion functions is that they be invariant in form to a rotation of coordinate axes in order to avoid algebraic complexity when the path integral in Eq. (2) is evaluated for various ray directions. Such a set was developed by Maldonado [213]. The coefficients of this expansion can be determined by substituting

it into the integral equation and orthogonalizing the resulting equations. Matulka and Collins [211] showed this inversion technique to be capable of generating quite accurate results, although convergence was not always rapid (a 1700-term expansion was required in the case of an axisymmetric distribution with a severe discontinuity). This method of analysis requires that in the absence of symmetry, data must be obtained over a 180^{o} range-of-viewing angle in order to carry out the necessary orthogonalization. This technique tends to be efficient when the distribution is nearly axisymmetric, particularly when the distribution is Gaussian or nearly so. The paper by Matulka and Collins [211] is especially noteworthy because their scheme was reduced to practice; experimental measurements were made of the density distribution in both axisymmetric and slightly non-axisymmetric (11^{o} of tilt), free-air jets.

References

1. D. Gabor, Nature 161 (1948) 777-78.
2. Idem, Proc. Phys. Soc. A 197 (1949) 454-87.
3. Idem, Proc. Phys. Soc. B 64 (1951) 449-69.
4. E. N. Leith and J. Upatnieks, J. Opt. Soc. Am. 52 (1962) 1123-30.
5. Idem, ibid. 53 (1963) 1377-81.
6. R. L. Powell and K. A. Stetson, Opt. Soc. Am. Spring Meeting (1965), Paper FA16.
7. Idem, J. Opt. Soc. Am. 55 (1965) 1593-8.
8. M. H. Horman, Appl. Opt. 4 (1965), 333-6.
9. B. P. Hildebrand and K. A. Haines, ibid. 5 (1966) 172-3.
10. K. A. Haines and B. P. Hildebrand, ibid. 5 (1966) 595-602.
11. Idem, IEEE Trans. Inst. Meas. 15 (1966) 149-61.
12. J. M. Burch, Prodn. Engr. 44 (1965) 431-42.
13. J. M. Burch, A. E. Ennos and R. J. Wilton, Nature (1966) 1015-16.
14. R. J. Collier, E. T. Doherty and K. S. Pennington, Appl. Phys. Letters 7 (1965) 223-5.
15. R. E. Brooks, L. O. Heflinger and R. F. Wuerker, Ibid. 7 (1965) 248-9.
16. L. O. Heflinger, R. F. Weurker and R. E. Brooks, J. Appl. Phys. 37 (1966) 642-9.
17. J. W. C. Gates, Nature 220 (1968) 473-4.
18. G. Havener and R. J. Radley, Opto-electronics 4 (1972) 349-57.
19. F. Gori and F. Mallamace, Opt. Commun. 8 (1973) 351-4.
20. P. Hariharan and Z.S. Hegedus, ibid. 9 (1973) 152-5.
21. N. Abramson, Appl. Opt. 13 (1974) 2019-25.

References, con't

22. R. J. Collier, C. B. Burkhardt and L. H. Lin, Optical Holography, Academic Press, 1971).

23. K. A. Stetson and R.L. Powell, Opt. Soc. Am. Ann. Mtg. (1965) Paper WF13.

24. Idem, J. Opt. Soc. Am. 55 (1965) 1694-5.

25. Idem, ibid. 56 1966) 1161-6.

26. J. M. Burch and A. E. Ennos, Opt. Soc. Am. Spg. Mtg. (1966), paper WF14.

27. E. Archbold, J.M. Burch and A. E. Ennos, J. Sci. Instrum. 44 (1967) 489-94.

28. H. Nassenstein, Phys. Letters 21 (1966) 290-1.

29. E. B. Aleksandrov and A. M. Bonch-Bruevich, Zh. Tekh. Fiz. 37 (1967) 360-9. (Translation in Sov. Phys.Tech. Phys. 12 (1967) 258-65.)

30. K. A. Haines and B. P. Hildebrand, Phys. Letters 19 (1965) 10-11.

31. B. P. Hildebrand and K. A. Haines, ibid. 21 (1966) 422-3.

32. Idem, J. Opt. Soc. Am. 57 (1967) 155-62.

33. A. E. Ennos, Contemp. Phys. 8 (1967) 153-70.

34. J. D. Redman, J. Sci. Instrum. 44 (1967) 1032-3.

35. M. Lurie, Opt. Soc. Am. Spring Mtg. (1967), Paper ThF14.

36. D. B. Neumann, J. Opt. Soc. Am. 58 (1968) 447-54.

37. T. Tsuruta, N. Shiotake, J. Tsujiuchi amd K. Matsuda, Jap. J. Appl. Phys. 6 (1967) 661-2.

38. N. E. Barnett, Opt. Soc. Am. Ann. Mtg. (1967) paper WA17.

39. A. E. Ennos, J. Phys. E. (J. Sci. Instrum.) 1 (1968) 731-4.

40. M. Lurie, J. Opt. Soc. Am. 58 (1968) 614-19.

41. M. Lurie and M. Zambuto, Appl. Opt. 7 (1968) 2323-5.

42. E. Archbold and A. E. Ennos, Nature 217 (1968) 942-3.

References, con't.

43. J. S. Zelenka and J. R. Varner, Appl. Opt. 7 (1968) 2107-10.

44. W. G. Gottenberg, Exp. Mech. 8 (1968) 405-10.

45. L. H. Tanner, J. Phys. E. (J. Sci. Instrum.) 1 (1968) 517-22.

46. P. J. Magill and A. D. Wilson, J. Appl. Phys. 39, (1968) 4717-25.

47. E. R. Robertson and J. M. Harvey (eds.), Engineering Uses of Holography, Procs. of Symposium, Strathclyde, 1968 (Cambridge Univ. Press, 1970.)

48. W. R. Bradford, ibid., pp. 57-70.

49. J. N. Butters, ibid., pp. 57-70

50. M. R. Wall, ibid., pp. 355-80.

51. B. P. Hildebrand, ibid., pp. 401-33.

52. J. Der Hovanesian and J. Varner, ibid., pp. 173-84.

53. N. Abramson, ibid., pp. 45-55.

54. Idem, Appl. Opt. 8, 1235-40.

55. Idem, Optik 30 (1969) 56-71.

56. J. D. Briers, Appl. Opt. 10 (1971) 519-24.

57. M. Lurie, in (47), pp. 397-9.

58. K. A. Stetson, ibid., pp. 307-31.

59. M. Zambuto and M. Lurie, Appl. Opt. 9 (1970) 2066-72.

60. K. A. Stetson, Optik 29 (1969) 386-400.

61. N. E. Molin and K. A. Stetson, ibid. 31 (1970) 157-77; 281-91.

62. J. C. Vienot, C. Froehly, J. Monneret and J. Pasteur, in [47], pp. 133-50.

63. J. C. Vienot, Nouv. Rev. d'Opt. Appl 1 (1970) 91-106.

64. C. Froehly, J. Monneret, J. Pasteur and J. C. Vienot, Opt. Acta 16 (1969) 343-62.

65. E. Archbold, A. E. Ennos and P. A. Taylor in Optical Instruments and Techiques, Proc. Eighth Cong, ICO, Reading (1969) ed. J. Home Dickson (Oriel Press, 1970) pp. 265-75.

References, con't.

66. E. Archbold, J.M. Burch and A. E. Ennos, Opt. Acta 17 (1970) 883-98.

67. J. M. Burch, Proc. Spie Seminar on Developments in Holography, (1971) pp. 149-56.

68. J. A. Leendertz, J. Phys. E. (J. Sci. Instrum.) 3 (1970) 214-18.

69. J. N. Butters and J. A. Leendertz, Opt. Laser Technol 3 (1971) 26-30.

70. P. M. Boone and R. Verbiest, Opt. Acta 16 (1969) 555-67.

71. J. Tsujiuchi, N. Takeya and K. Matsuda, ibid., 16 (1969) 709-22.

72. J. E. Sollid, Appl. Opt. 8 (1969) 1587-95.

73. C. M. Vest, ibid. 12 (1973) 612-13.

74. J. W. C. Gates, Opt. Technol 1 (1969) 247-50.

75. G. M. Brown, R. M. Grant and G. W. Stroke, J. Acoust. Soc. Am. 45 (1969) 1166-79.

76. R. C. Sampson, Exp. Mech. 10 (1970) 313-20.

77. A. D. Wilson, Appl. Opt. 9 (1970) 2093-7.

78. T. Tsuruta, N. Shiotake and Y. Itoh, Jap. J. Appl. Phys. 7 (1968) 1092-100.

79. T. Tsuruta, N. Shiotake and Y. Itoh, Opt. Acta 16 (1969) 723-33.

80. S. Walles, Arkiv. for Fysik 40 (1970) 299-403.

81. Idem, Opt. Acta 17 (1970) 899-913.

82. W. T. Wellford, Opt. Commun. 1 (1969) 123-5.

83. Idem, ibid. 1 (1970) 311-14.

84. J. Pastor, G. E. Evans and J. S. Harris, Opt. Acta 17 (1970) 81-96.

85. J. S. Zelenka and J. R. Varner, Appl. Opt. 8 (1969) 1431-4.

86. N. E. Molin and K. A. Stetson, J. Phys E.(J. Sci. Instrum.) 2 (1969) 609-12.

87. N. Abramson, Appl. Opt. 9 (1970) 97-101.

88. E. Champagne and L. Kersch, Opt. Soc. Am. An. Mtg. (1969) paper ThF14.

References, con't.

89. J. R. Varner, Appl. Opt. 9 (1970) -2098-100.

90. P. M. Boone, Opt. Technol. 2 (1970) 94-8.

91. J. C. Vienot, J. Bulabois and J. Pasteur, (eds.), Application de Holographie, Proc. Symposium, Besancom (1970), Universite' de Besancon.

92. C. Aplin, B. Maronne and C. Minard, ibid., Paper 4-6.

93. D. Bul and R. Jones, ibid., Paper 5-3.

94. A. R. Luxmoore and C. House, ibid. Paper 5-2.

95. M. R. Wall, ibid., Paper 4-9.

96. J. E. Sollid, ibid., Paper 4-8.

97. J. Monneret, ibid., Paper 4-3.

98. J. W. C. Gates, ibid., Paper 4-4.

99. J. Tsujiuchi and K. Matsuda, ibid., Paper 4-5.

100. W. T. Welford, ibid., Paper 4-2.

101. P. M. Boone, ibid., Paper 5-1.

102. N. Abramson, ibid., Paper 4-7.

103. R. G. N. Hall, ibid., Paper 9-5.

104. C. R. Hazell and S. D. Liem, ibid., Paper 6-4.

105. C. T. Moffat and B. M. Watrasiewicz, ibid., Paper 6-2.

106. F. M. Mottier, ibid., Paper 6-5.

107. A. J. Waddell, W. Kennedy and P. Waddell, ibid., Paper 6-6.

108. E. DeBazelaire and B. Prade, ibid., Paper 5-6.

109. J. Nicolas, ibid., Paper 5-4.

110. I. K. Leadbetter, ibid., Paper 17-1.

111. E. R. Robertson and S. B. Elliott, ibid., Paper 10-6.

112. K. Shibayama and H. Uchiyama, Appl. Opt. 10 (1971) 2150-4.

References, con't.

113. N. L. Hecht, J. E. Minardi, D. Lewis and R. L. Fusek, ibid. 12 (1973) 2665-76.

114. W. M. Ewers, E. Fritzsch, K. Grunewald and H. Wachutka, Optik 40 (1974) 57-68.

115. M. Macakova, Opt. Appl. 4 (1) (1974) 45-9.

116. D. Bijl and R. Jones, Opt. Acta 21 (1974) 105-18.

117. R. Jones, ibid. 21 (1974) 257-66.

118. N. Abramson, Appl. Opt. II (1972) 1143-7.

119. C. A. Sciammarella and J. A. Gilbert, ibid. 12 (1973) 1951-6.

120. Y. Y. Hung, C. P. Hu, D. R. Henley and C.E. Taylor, Opt. Commun. 8 (1973) 48-51.

121. B. D. Hansche and C. G. Murphy, ISA Trans. 11 (1) (1972) 1-14.

122. Idem. Appl. Opt. 13 (1974) 630-5.

123. A. D. Wilson, ibid. 10 (1971) 908-12.

124. O. J. Burchett and J. L. Irwin, Mech. Eng. 93 (3) (1971) 27-33.

125. H. Michael, Appl. Opt. 12 (1973) 1111-3.

126. T. Matsumoto, K. Iwata and R. Nagata, ibid, 13 (1974) 1080-4.

127. J. E. Sollid, Opt. Commun. 2 (1970) 282-8.

128. C. H. F. Velzel, ibid. 7 (1973) 302-4.

129. F. D. Adams and G. E. Maddux, Appl. Opt. 13 (1974) 219-20.

130. H. Kohler, Optik 39 (1974) 229-35.

131. M. J. Landry and C. M. Wise, Appl. Opt. 12 (1973) 2320-7.

132. V. F. Bellani and A. Sona, ibid. 13 (1974) 1337-41.

133. P. W. King, ibid. 13 (1974) 231-3.

134. M. Dubas and W. Schumann, Opt. Acta 21 (1974) 547-62.

135. R. A. Ashton, D. Slovin and H. J. Gerritsen, Appl. Opt. 10 (1971) 440-1.

References, con't.

136. N. E. Molin and K. A. Stetson, Optik 33 (1971), 399-422.

137. K. A. Stetson, J. Opt. Soc. Am 64 (1974) 1-10.

138. P. M. Boone, Opt. Laser Technol. 4 (1972) 162-6.

139. P. M. Boone and L. C. Debacker, Optik 37 (1973) 61-81.

140. P. M. Boone and L. C. DeBacker, Optik 37 (1973) 61-81.

141. W. H. Steel, Opt. Acta 17 (1970) 873-81.

142. M. A. Machado Gama, Opt. Commun. 8 (1976) 362-5.

143. I. Prikryl, Opt. Acta 21 (1974) 675-81.

144. V. K. Der, .D. C. Holloway and W. L. Fourney, Appl. Opt. 12 (1973) 2552-4.

145. P. Hariharan and Z. S. Hegedus, Opt. Commun. 11 (1974) 127-31.

146. N. Abramson, Nature-Phys Sci. 231 (1971) 65-7.

147. Idem, Appl. Opt. 10 (1971) 2155-61.

148. Idem, Optik 37 (1973) 337-46.

149. Idem, Appl. Opt 9 (1970) 2311-20.

150. H. Bjelkhagen, Opt. Laser Technol. 5 (1973) 172-5.

151. N. Abramson and H. Bjelkhagen, Appl. Opt. 12 (1973) 2792-6.

152. A. D. Wilson, J. Opt. Soc. Am. 60 (1970) 1068-71.

153. A. D. Wilson and D. H. Strope, ibid. 60 (1970) 1162-5.

154. A. D. Wilson, ibid. 61 (1971) 924-9.

155. K. A. Stetson, ibid. 61 (1971) 1359-62.

156. Idem, ibid. 62 (1972) 197-8.

157. Idem, ibid. 62 (1972) 698-700.

158. Idem, Appl. Opt. 11 (1972) 1725-31

159. C. S. Vikram, Opt. Commun. 8 (1973) 355-7.

160. Idem Appl. Opt. 12 (1973) 2808.

References, con't.

161. N. Abramson, ibid. 14 (1975) 981-4.

162. K. A. Stetson, J. Opt. Soc. Am. 60 (1970) 1378-88.

163. Idem, Appl. Opt. 14 (1975) 272-3.

164. S. H. Rowe, J. Opt. Soc. Am. 61 (1972) 1599-603.

165. C. C. Aleksoff, Appl. Opt. 10 (1971) 1329-41.

166. J. W. C. Gates, R. G. N. Hall and I. N. Ross, Opt. Laser Technol. 4 (1972) 72-5.

167. T. Matsumoto, K. Iwata and R. Nagata, Appl. Opt. 12 (1973) 961-7.

168. R. Dandliker, B. Ineichen and F. M. Mottier, Opt. Commun. 9 (1973) 412-16.

169. G. Tribillon and J. F. Miles, Opt. Commun. 11 (1974) 123-6.

170. W. T. Caussignac, in Recent Advances in Optical Physics, Proc. Tenth Cong. ICO, Prague (1975).

171. J. D. Briers, ibid.

172. K. A. Stetson, in Holographic Nondestructive Testing, ed. R.K. Erf (Academic Press, 1974) pp.181-220.

173. I. Prikryl, in Recent Advances in Optical Physics, Proc, Tenth Cong. ICO, Prague (1975).

174. G. B. Brandt, Appl. Opt. 8 (1969) 1421-9.

175. P.M. Boone, Opt. Acta 22 (1975) 579-89.

176. J. D. Briers, in Recent Advances in Optical Physics, Procs. Tenth Cong. ICO, Prague (1975)

177. M. Miler in Optics Comm. 28, 2, 1979.

178. W. H. Steel in Optic Acta 17, 12, 1970.

179. D. W. Sweeney & C. M. Vest - Appl. Opt. 12, 11, 1973.

180. L. H. Tanner, J. Sci. Inst., 44, 1967.

181. Z. Fuzessy Inst. of Phy., 1979.

182. K. A. Haines & B. P. Hildebrand, IEEE, 15, 4, 1966.

References, con't.

183. W. L. Howes and D. R. Buchele, JOSA, 56, 11, 1966.

184. Tadad Tsuruta et.al., Optics Acta, 16,6, 1968.

185. K. A. Stetson, Optics 29, 4, 1969.

186. K. A. Stetson, JOSA, 60, 10, 1970.

187. P.J. Trotter, J. Phy. Chem. 74, 6, 1970.

188. W. T. Welford - Optics Comm. 1, 7, 1970.

189. R. D. Matulka, J. Appl. Phys, 42, 3, 1971.

190. H. G. Junginger, Opts. Comm., 5, 1, 1972.

191. K. A. Stetson, JOSA, 64, 1, 1974.

192. I. Prikryl - Optica Acta, 21, 8, 1974.

193. K. Iwata - Optica Acta, 25, 1, 1977.

194. C. M. Vest and D. W. Sweeney, Appl. Optics 9, 10, 1970.

195. C. M. Vest, JOSA, 64, 9, 1974.

196. C. M. Vest, Appl. Optics, 14, 7, 1975.

197. D. Nobis and C. M. Vest, Appl. Optics, 17, 14, 1978.

198. E. E. Anderson et.al., Appl. Optics, 14, 1, 1975.

199. K. W. Beach et.al., JOSA, 63, 5, 1973.

200. H. Svenson, Opt. Acta 1, 1, 1954.

201. D. W. Sweeney and C. M. Vest, Inst. J. Heat Mass Trans. 17, 1974.

202. H. M. Dobbins, JOSA, 63, 3, 1973.

203. W. Aung, et.al., Rev. Sci. Inst. 42, 12, 1971.

204. C. M. Vest, Holog Int., (Academic Press, 1979)

205. W. Hauf and U. Grigull, in Advances in Heat Transfer, J. P. Hartnett and T. F. Irvine, eds. (Academic Press, NY, 1970), Vol. 6.

References, con't.

206. M. V. Berry and D. F. Gibbs, Proc. Roy. Soc. London A314, 143 (1970).

207. P. D. Rowley, J. Opt. Soc. Am. 59, 1496 (1969).

208. W. Alwang, et.al., Item 1, Final Report, Pratt and Whitney, PWA-3942 [NAVAIR (Air-602) Contract], 1970.

209. H. G. Junginger and W. van Haeringen, Opt. Commun. 5, 1 (1972).

210. L. H. Tanner, J. Sci. Instrum. 3,987 (1970).

211. R. D. Matulka and D. J. Collins, J. Appl. Phys. 42, 1109 (1971).

212. C. D. Maldonado and H. N. Olsen, J. Opt. Soc. Am. 56, 1305 (1966).

213. C. D. Maldonado, J. Math Phys. 6, 1935 (1965).

SECTION III

DISCUSSION OF SIMULATED HOLOGRAPHIC OPTICAL SCHLIEREN SYSTEM (HOSS)

In this section we seek to determine the feasibility and to demonstrate the application of localized fringes in holographic interferometry using transparent objects in general and in fluid visualization via the HOSS in particular. To this end holographic data has been obtained experimentally from two different holographic arrangements and several different test objects which were immersed in a transparent fluid of known constant index of refraction or known variation of index of refraction. The two holographic arrangements are; a typical off-axis sideband configuration, and a scaled-down version of the original HOSS, which we here call the "simulated HOSS". Schematics of both of these systems are provided and discussed below. We intend first to determine the feasibility of fringe localization via holographic interferometry using two different holographic arrangements and secondly to demonstrate the application of these localized fringes to the quantitative analysis of fluid flow visualization via the simulated HOSS.

Feasibility Demonstration of Holographic Fringe Localization

Figure 1 provides a schematic of the first holographic arrangement used to determine and demonstrate the feasibility of fringe localization. The system employed an argon laser which operated at 514.5 nm wavelength and after expansion and spatial filtering the object and reference beams were both rendered parallel prior to being incident on the test cell and hologram respectively. The object beam was incident on a diffuser glass, prior to entering the cell, so as to satisfy the extended source requirement necessary for the localization of fringes. Upon passage through the

cell, the object beam interfered with the reference beam to form the hologram record. The Polaroid film holder is useful for recording the holographic real image upon reconstruction.

Figure 2 provides a schematic of the test cell which was constructed of acrylic with 6.5 mm wall thickness. The cell dimensions were 104 mm depth x 280 mm width x 152 mm height. The diffuser glass was 130 x 130 mm and was centered on the 76.2 mm diameter object beam. (See top of figure 2.) Two hollow acrylic cylinders were placed at either end of the test cell and centered in the object beam. Each cylinder was 25 mm in diameter. Regular tap water was now poured in to fill the test cell. A double exposure (frozen fringe) hologram was recorded through the test cell as shown in bottom of figure 2. The first exposure was taken of the test cell with the water at ambient temperature. Prior to the second exposure small pieces of ice were introduced into each of the hollow acrylic tubes. This provided a temperature or density gradient in the volume of each hollow cylinder. Upon taking the second exposure and properly processing the hologram, the real images were reconstructed in several planes and recorded using the Polaroid film back. In this reconstruction the Polaroid film could be placed along any plane in the reconstructed three-dimensional real image. The relatively large aperture of the system allowed for critical focusing (fringe localization) in the real image.

Figure 3 displays the seven planes in the real image at which photographs were recorded. The photographs of the real image taken at these seven locations are shown in figure 4 and are numbered corresponding to

the planes of their location as shown in figure 3. Photograph number 1 is at the back of the test cell adjacent to the diffuser, number 7 is at the other end of the test cell closest to the hologram. These seven photographs readily display that the various fringes are indeed localized discretely throughout the cell.

A second double exposure was taken using the same identical procedure except a third hollow, acrylic cylinder was added slightly off-center from the first two as shown in figure 5. Upon reconstruction of the real image as before, we display in figure 6, photographs of eleven different planes recorded throughout the volume of the real image. The numbers of the photographs of figure 6 correspond respectively to the numbered planes indicated in figure 5, as before. Again the fringe localization is apparent with position.

In both of the previous cases the reconstruction aperture was large. This was necessary if the fringe localization was to be critically positioned.

Using the same off-axis hologram arrangement and the same test vessel filled with water as before,we employed a different test object with a different means of creating density variations within the cell.

In this case twelve precision resistors of twelve ohms each were soldered together to simulate a crystal boundary during growth. The input and output for the voltage source was taken across the volume diagonally as shown in figure 7. The cube so formed was 12.7 mm per side.

First a real-time (live fringe) hologram was employed in order to observe the response of the resistor cube to current. It was found that

approximately 5 volts provided enough power to the circuit to cause observable heat flow in the water in which the cube was submerged. The resistance of the water across the volume diagonally was about 500 ohms, thus making a short circuit of the resistors by the water improbable.

Next, a double exposure (frozen fringe) hologram was now taken of the test cell and cube, first with ambient conditions and second with power on the cube. As before, the real image of the double exposed hologram was reconstructed with a large aperture beam and photographs were recorded in five planes of the real image of the test cell volume as shown in figure 8. Figure 9 displays photographs of the real image corresponding to the planes located as shown in figure 8. Again the localization of fringes is very apparent.

Therefore, as stated in the literature and demonstrated above, the localization of fringes in a diffusely illuminated transparent medium via holography is a very real and predictable phenomenon, and simple feasibility is verified.

We now describe the second holographic arrangement employed experimentally, the simulated HOSS arrangement.

Figure 10 presents the schematic of the present HOSS configuration. Figure 11 presents a schematic of our scaled-down version of the HOSS. All HOSS parameters were satisfied except we employed half-size optics mirrors and worked with a three (3) inch optics instead of a six (6) inch as in the HOSS. Data taken with the scaled-down HOSS compare sufficiently well with that from HOSS. A modification of this scaled-down version of HOSS was then made to conveniently allow localized fringe holograms to be

made using diffuser glass illumination of the test cell. This modified HOSS or simulated HOSS is shown schematically in figure 12.

We have stated at the outset that two different holographic arrangements were employed. There is, however, no real difference in that both are forms of off-axis sideband arrangements. However, the physical geometric parameters are different and this is of importance in that we can quantify them and that the remaining data will be from a geometry essentially identical to the HOSS system of NASA.

Therefore, using the holographic arrangment having the geometry of the simulated HOSS of figure 12 we investigate various objects in a transparent medium using diffuse illumination. The cell employed was identical to that described earlier. The object in the experiment was two heating elements.

Two soldering pencil heads were integrated into the base of the test cell. Each possessed a female threaded core which normally served to receive the soldering pencil tip. In the various cases discussed below, this served as a mounting for the various objects used.

The two heating elements so mounted in this experiment were: a simple soldering tip and a 25mm diameter cup-shaped disc. Figure 13 displays the location of both the large and small heating elements in the test cell. Three separate double exposure holograms were recorded with the object, each allowing a different magnitude of heating to occur between the first and final exposure. The first exposure was in all

cases taken at ambient conditions. The second exposure was at: 30 sec after first with heat on, 60 sec after first with heat on, 90 sec after first with heat on. The photographs of the real image of each of these are shown in figures 14, 15 and 16 respectively with the locating plane of each photograph identified as shown in figure 13.

In further support of the demonstration of localized fringe feasibility we will briefly present the results of another experiment. With the holographic arrangement as before, the object this time was a small aluminum cube, approximately 15 mm per side, attached to the heating element closest to the diffuser and immersed in water in the test cell. After completion of the required double exposure the real image was reconstructed and photographs were taken in four planes of the real image. The location of the planes is shown in figure 17, the four respective holograms are displayed in figure 18. It will be noted for this case the plane of best focus (localization) occurs at position 2, the center of the cube.

From the foregoing it is obvious that it is quite feasible to produce localized fringes using diffuse illuminated holographic interferometry. It is not so obvious how easily or how accurately one can quantitatively specify where this localization physically occurs. This will be the subject of the section on theory to be discussed below.

Demonstration of Localized Fringe Application

We have previously alluded that the fringe localization is a function of the geometric parameters of the holographic arrangement employed. We have determined, and the literature states, that the localization of

fringes is a critical function of the aperture size and geometry used for the reconstruction of the holographic real image. We have further seen from the literature survey that the fringe localization technique (FL) and the fringe counting technique (FC) i.e., parallax technique, are closely related. We wish now to present the results of an experiment which verify this and which demonstrate the utility of both of these methods and which further exhibit the discreteness of localization of the fringes as well as illustrate the dependence of the localization on still another parameter - the geometric perspective or viewing angle.

As additional parameter dependence is unfolded in this manner, it becomes clear that the theoretical description of the phenomena of localized fringes is indeed a complex one.

For this experiment two heating elements of the same size were employed in the localized fringe mode as before, except now we have positioned an accurate temperature probe within the test cell to provide quantitative magnitude of the temperature field. (Quantitative information will be extracted from this hologram in Section V.

A double exposure was recorded with the first exposure at ambient conditions and no heat flow. Both heating elements were energized for thirty(30) seconds and a second exposure recorded. The temperature probe was located near the edge of the heat plume closest to the hologram.

Upon proper development the real image was projected out and Polaroid photographs were recorded.

Figure 19 displays a schematic of the hologram real image projection

technique for fringe localization and parallax demonstration. The hologram was positioned so that the line passing through the center of both heating elements intersected the hologram one inch from the right-hand side (see line A and insert A, figure 19).

With appropriate adjustment of the Polaroid film plane in the real image, photographs 1 and 2 of figure 20, were recorded with this "A" perspective. The fringe localization is most evident. Photo number 1 shows the fringes localized in the vicinity of the heating element furthest from the hologram. Note the out-of-focus temperature probe. Photo number 2 shows the fringes localized in the vicinity of the heating element nearest the hologram. Note the temperature probe in-focus.

If the reconstruction beam is shifted to the other side of the hologram, we then have the perspective "B" of figure 19. With appropriate adjustment of the Polaroid film plane in the real image, photographs 3 and 4, figure 20, were recorded with this "B" perspective. Again, the fringe localization is most evident. Further, the parallax now is most striking. Photograph number 3, analogous to number 1, shows the fringes localized in the vicinity of the heating element furthest from the hologram (temperature probe out-of-focus). Photograph number 4, like number 2, shows the fringes localized in the vicinity of the heating element nearest the hologram (temperature probe in-focus).

Comparison of photographs 1 with 3 and 2 with 4 dramatically demonstrates the fringe localization and parallax and how the presence of one plume can obstruct the contrast of another set of fringes.

The phenomenon of localized fringes as generated by the diffuse illumination of a transparent medium also allows for the viewing of fringes from different directions within the limitations of the hologram's aperture. In the situation where there are two or more disturbances in the test cell, it appears advantageous to be able to choose a viewing direction where the light passes only through a single disturbance and is not affected by the other disturbances in the cell. On obtaining a photograph (or image) where the fringes are due only to a single radially symmetric disturbance, the index of refraction and thus the temperature within the disturbance can be calculated in two ways. The first is a quick and easy way of obtaining the average temperature readings across lines through the disturbance, the second generates a fairly detailed map of index of refraction in a cross section of the radially symmetric disturbance. Both of these will be discussed and pursued in Section V.

SECTION IV

MATHEMATICAL THEORY ON THE FORMATION AND ANALYSIS OF LOCALIZED FRINGES IN A TRANSPARENT MEDIUM

General Background, Model Formulation and Fringe Interpretation

The process of holography provides an interferometric tool which is linear in time, in the sense that two or more object wavefronts can be recorded sequentially in time and later both wavefronts can be reconstructed simultaneously with interferometric comparison. For example, consider a typical off-axis sideband arrangement similar to that used earlier in Section I with slight modification. Figure 1 displays our intended configuration. The phase object could be a transparent solid or a transparent solid in a transparent fluid, etc. In any case, consider the refractive index distribution within the phase object to be given by $n_1(x,y,z)$, during an initial holographic exposure and $n_2(x,y,z)$ during the final holographic exposure of a double exposure hologram. On proper development and reconstruction of this hologram, two waves are reproduced simultaneously

$$U_{o1} = a_1(x,y) \exp\left[i \frac{2\pi}{\lambda} \Phi_1(x,y)\right]$$

$$\xi$$

$$U_{o2} = a_2(x,y) \exp\left[i \frac{2\pi}{\lambda} \Phi_2(x,y)\right]$$

where $\phi = \int n ds$,

The irradiance becomes

$$I(x,y) = 2\left\{1 + \cos\frac{2\pi}{\lambda}\left[\Phi_2(x,y) - \Phi_1(x,y)\right]\right\} \tag{1}$$

where we have assumed that $a_1(x,y) = a_2(x,y)$ = uniform unit amplitudes.

If, as in most practical cases, the refractive index during one exposure is uniform and constant, n_0, then the fringe pattern is

$$I(x,y) = 2\left[1 + \cos\left(\frac{2\pi}{\lambda}\Delta\Phi(x,y)\right)\right] \tag{2}$$

where

$$\Delta\Phi(x,y) = \int [n_1(x,y,z) - n_0]\, ds$$

is the optical path difference, and the equation representing a bright fringe is

$$\Delta\Phi(x,y) = \int [n(x,y,z) - n_0]\, ds = N\lambda \tag{3}$$

For the simple case where the refractive index $n_1(x,y,z)$ varies only in the y direction, i.e., $n(x,y,z) = n(y)$, then the integration in equation (3) is easily performed and the optical pathlength difference is

$$\Delta\Phi(x,y) = [n(y) - n_0]\, l$$

where l is the total length of the phase object.

The fringe spacing, of the holographic interferometric fringes, is determined by the product of n.

If the refractive index n(y) varies linearly as

$$n(y) = n_0 + n'y$$

the fringe pattern produced is a series of equally spaced parallel fringes, and

$$\Delta\Phi(x,y) = [n_0 + n'(y) - n_0]\,\ell = N\lambda$$

with

$$y = N\lambda/n'\ell \quad ; \quad N = 1, 2, 3, \cdots.$$

If, however, the refractive index, n(x,y,z) is a distribution similar to that which occurs in the measurement of thermal boundary layers, then

$$n(y) = n_0 - n_1 \exp(-ay)$$

and the fringes are parallel straight lines with <u>variable</u> spacings, and

$$\Delta\Phi(x,y) = [n_0 - n_1 e^{-ay} - n_0]\,\ell = N\lambda \tag{4}$$

with

$$y = \frac{1}{a} \ln\left(\frac{N\lambda}{n'\ell}\right); \qquad N = 1, 2, 3, \cdots.$$

The spacing is large in regions of small gradient and small in regions of large gradient.

There is another class of index of refraction distribution of great practical importance in aerodynamics, heat and mass transfer and plasma diagnostics. It is the radially symmetric distribution and is found in radially symmetric phase objects.

We provide the first exposure to it here and treat it in depth later during fringe analysis along with experimental evidence of its behavior with regard to localized fringes.

Figure 2 provides a schematic of a radially symmetric phase object n(r) and allows the definition of notation necessary for discussion. A plane wave traveling in the z direction is used to interrogate the object. This is indicated by the typical ray shown in the figure.

The optical path difference, $\Delta\phi(x)$, for a two-exposure hologram is determined via equation 3, with $dz = (r^2 - x^2)^{-\frac{1}{2}} r\, dr$ to be

$$\Delta\Phi(x) = 2\int_x^R \frac{[n(r)-n_o]\, r\, dr}{(r^2-x^2)^{1/2}} \tag{5}$$

The integral in equation 5 is the Abel transform of $[n(r)-n_o]$ and is found to be quite instrumental in the evaluation of fringes of radially symmetric phase objects. The interferogram displays contours of the Abel transform of a radially symmetric object. We address this subject in some detail in later sections.

As stated at the outset, holographic interferometry is differential in time, that is the two waves constituting the first and second exposure object wavefronts are separated temporally rather than spatially. For example, in a Mach-Zehnder interferometer, only one wave passes through the phase object. This wave then interferes with a plane comparison wave which is separated in geometric space and has traveled a different path through the interferometer.

In a holographic interferometer, however, both the object and comparison waves travel across and through precisely the same object space, but at different times. Holographic interferometers are then single path interferometers. This important feature is what permits the use of test sections with windows of rather poor optical quality.

In classical interferometry, if a test section window is not optically flat and homogeneous, it will introduce a pathlength error or noise term $\Delta\phi_n(x,y)$ into an optical wave passing through it. Let $\Delta\phi(x,y)$ represent the pathlength difference due to the phase objects inside the test section and remember that it is the contours of this $\Delta\phi(x,y)$ which we desire the interferometer to display as a fringe pattern.

In a Mach-Zehnder interferometer, the fringe pattern for this test section and phase object would be:

$$I(x,y) = 2\left\{1 + \cos\frac{2\pi}{\lambda}\left[\Delta\Phi(x,y) + \Delta\Phi_n(x,y)\right]\right\} \tag{6}$$

Thus the presence of the noise term $\Delta\phi_n(x,y)$ due to the poor quality windows produces pathlength variations leading to errors in the fringe pattern which can be eliminated only by the use of optically flat homogeneous windows so that $\Delta\phi_n(x,y)$ is a constant.

In holographic interferometry, only changes in pathlength between exposures are displayed. Therefore, since the same test section, windows and phase objects used above are present during both holographic exposures, the effects of $\Delta\phi_n(x,y)$ are cancelled and the expression for the holographic fringes is given by equation (2) as:

$$I(x,y) = 2\left\{1 + \cos\frac{2\pi}{\lambda}\Delta\Phi(x,y)\right\} \tag{7}$$

It should be noted, however, that errors due to refraction by curved test section windows occuring between exposures are not cancelled and must be accounted for in quantitative measurements.

An interferogram described by equation (2) above is called an infinite fringe interferogram. This means that an infinitely wide fringe results when $\Delta\phi(x,y) = 0$. Further, this type of interferogram displays contours of constant value of $\Delta\phi(x,y)$. There is a sign ambiguity in such interferograms, however, because $+\Delta\phi(x,y)$ and $-\Delta\phi(x,y)$ yield the same fringe pattern. This is a result of the cosine being an even function. Because of this, interpretation of the fringes from such an interferogram is ambiguous. That is, we cannot determine if the optical pathlength increases or decreases from one fringe to the next. This sign ambiguity can be removed by the use of a priori knowledge of the specific experiment and by introducing reference fringes into the interferogram. These fringes are most commonly parallel, straight, "wedge fringes" with equal spacing corresponding to a constant phase gradient of known sign. The resulting interferograms are called finite fringe interferograms and are commonly used in classical interferometry.

Fringe Localization in Transparent Media: Development of Basic Equation[+]

Holographic interferometry can be used to visualize and measure refractive index fields in transparent media. If the medium is a liquid, knowledge of the refractive index distribution enables one to calculate the spatial distribution of density throughout the field. If the object (transparent medium) under study is illuminated with diffused light, such as that scattered by a ground glass screen placed between the source and the object, the fringes of holographic interferometry have a distinct three dimensional nature. They exhibit spatial localization, i.e., they are localized. To the observer they appear to be suspended in space in the object location or perhaps in front of or behind it. As the observer changes viewing direction, the fringes appear to change form, shift about and change position of localization.

Information about the structure of the refractive index distribution is displayed in two ways in a holographic interferogram:

(1) Fringe number, position and spacing

(2) Fringe localization

As mentioned earlier, holographic interferometry can also be used to measure vector displacement of points on diffusely reflecting opaque objects. In the case of opaque objects, fringe localization plays an important role, either directly or indirectly, in the analysis of holographic interferograms and further, the theory of analysis for these objects is well developed. The analyses of holographic interferograms of transparent media, on the other hand, has thus far been based almost ex-

[+]Appreciation is gratefully acknowledged to Dr. Charles Vest of the University of Michigan for his consultation on the theory development for this section.

clusively on fringe number, position and spacing and the role of localization has been largely ignored. Fringe analysis in the case of transparent media is quite complicated because fringe shifts are associated with path integrals through the object rather than with a single phase shift due to reflection at a single point as in the case of opaque objects. As a consequence of this complication, the determination or computational reconstruction of a refractive index field has conventionally been based on fringe number, position and spacing which requires that the object field be viewed from a large number of viewing directions, ideally over a 180^{o} range of angles. This required range can be reduced if the object field has known symmetries. It is important, therefore, to develop a theory of fringe localization in diffusely illuminated transparent media to provide augmentation of conventional fringe analysis in useful ways. At the very least, this additional information of fringe localization must provide information which is useful for approximate reconstruction of refractive index fields when the range of viewing angles is practically restricted to less than 180^{o} (the usual case in practice). At best a new reconstruction theory might ultimately result. Either result would aid the present conventional method of analysis.

There exist two distinctly separate but related localization problems which are defined in terms of what we know and what we desire to determine from a given holographic interferometry experiment. We draw the following distinction:

(1) The Forward problem: Given a refractive index distribution, Δn, determine the surface in which the fringes appear to localize when viewed from a specified direction, i.e.,

$$\underset{\text{known}}{\Delta n} \Longrightarrow \underset{\text{calculate}}{f\ (\text{Loc})}$$

(2) The Inverse problem: Using physical measurements of fringe localization, f (Loc), determine the refractive index distribution, Δn, or use the measurements to augment reconstruction based on fringe number, position and spacing, i.e.,

$$\underset{\text{calculated}}{\Delta n} \Longleftarrow \underset{\text{meas.}}{f\ (\text{Loc})}$$

Our first task here is to set forth a theory for the forward problem, which will form a basis for subsequent exploration of the role of fringe localization in the inverse problem. Finally, in this section we provide an application of the theory to the analysis of localized fringes.

Model for Fringe Formation in the Forward Problem

Ideally the description of formation of interferometric fringes in diffused light should be developed in the context of diffraction theory; however, this approach is more complicated and mathematically cumbersome than is necessary to meet the objectives of the current task. Therefore, a simplified model, which has been satisfactorily used to develop a complete and practical theory of fringe formation and interpretation for opaque objects, will be used. This model is modified to address an ideal case of the diffuse illumination of transparent media. In this section we present and explain this model.

Figure 3, drawing on the treatment for opaque bodies (Section I, ref. [1-111]), presents the optical elements which are considered in a discussion of the fringes of holographic interferometry for a transparent medium. At the left is a diffuser, illuminated from behind by a column of laser light. Light transmitted and scattered by the diffuser then passes through the object space. During an initial holographic exposure the refractive index in this object space is known to be n_0, which often is uniform throughout the region. During a second exposure (or observation in the case of real time interferometry) the distribution of refractive index throughout this object space is $n\ (x,y,z)$.

Our objective is to study this difference of refractive index:

$$f\ (x,y,z) = n\ (x,y,z) - n_0 = \Delta n$$

These wavefronts in turn pass to the hologram where each is recorded, processed and later holographically reconstructed. On reconstruction the optical field transmitted through and diffracted by the hologram (shown to the right of the hologram in figure 3) is accessible to the observer who may form an image on a screen, photograph the interferogram with a camera, or visually observe it with an unaided eye. Any viewing system used by the observer to investigate this image has a particular, finite entrance aperture. Such an aperture is indicated schematically in figure 3.

For convenience, consider the diffuser to be a plate of ground glass whose front surface has some random microscopic variation so that the phase of light scattered by it varies randomly in phase from point to point. Let P and M be two typical points on the diffuser surface. The effect of the change in the refractive index field f (x,y,z) is to slightly distort the optical wavefront which passes through it at the time of the second exposure, relative to that which passed through it at the time of the first exposure. If, as in many practical cases, this distortion is very small, we can, to a satisfactory degree of approximation, describe the effect of f (x,y,z) as a phase shift of light rays whose path direction through the field remains unchanged. We refer to this as the refractionless limit and say that f (x,y,z) is a phase object. The errors and effect of such an approximation will be treated later in this paper.

To fix ideas in relation to figure 3, we can also think of f (x,y,z) as causing a very slightly distorted and displaced image of the diffuser.

This idea is shown schematically in figure 3. P' and M' are the new apparent location of the points P and M respectively.

Because the interferogram is formed in diffuse, coherent light, it will include laser speckle - a small-scale random interference pattern. This is indicated schematically by the finely spaced irradiance variation falling under the cosinusoidal envelope of the holographic interferometry fringes in the observation plane of figure 3. The scale of the speckle is controlled by the size of the aperture. If the aperture is large, the speckle size will be small; if the aperture is small, the speckle size will be large. Specifically if, b_s, is the typical speckle size, it is given in terms of figure 3 by

$$b_s \equiv 1.22 \frac{\lambda z_o}{D} \tag{8}$$

where λ is the wavelength of light employed and D is the aperture diameter.

In the reconstructed image of the hologram, and as a result of the first exposure, light is scattered by the diffuser at and in the neighborhood of P and gives rise to a complex amplitude of light, $U_o(x,y,z)$ in the observation plane a distance, z, from the diffuser. The corresponding irradiance $I(x,y,z)$ observed through the aperture would be recognized as a speckle pattern. In holographic interferometry, as a result of the second exposure, a second optical wave is present and can be thought of as scattered by the diffuser at and in the neighborhood of point P' on the effectively distorted and displaced diffuser. The corresponding complex amplitude, $U_o'(x,y,z)$ differs in fine detail from $U_o(x,y,z)$. If we could compare the corresponding speckle patterns $I_o(x,y,z)$ and

$I_o'(x,y,z)$ they would be uncorrelated at an arbitrary plane z = constant, that is their fine structure would be completely different. However, there exists one special value of z, where for a given observation direction, $U_o(x,y,z)$ and $U_o'(x,y,z)$ will be nearly identical, except for a small relative displacement and a variation in phase whose spatial scale is large compared with the value of b_s. The irradiance pattern of this particular value of z consists of a speckle structure modulated by a broad, cosinusoidal variation which is the pattern of fringes of holographic interferometry. The fringes are localized at this special value of z for this particular viewing direction. In the next segment of this section, equations are derived for determining this localization distance, z.

The localization equations will be based on the assumption that for purposes of fringe pattern computation, we need only consider the change in optical pathlength, $\Delta\phi$, discussed earlier, of light scattered by apparent corresponding points such as P and P', and that the light from P and P' will travel to a point in the observation plane along nearly straight, coincident rays. The equivalent model for fringe formation with opaque objects successfully predicts all important phenomena. The present model will be indirectly verified by experimentally checking predictions of the theory. These results will be presented later in this document.

As this model is pursued, we conclude that fringe localization occurs where $U_o(x,y,z)$ and $U_o'(x,y,z)$ are most nearly matched. Near

such locations, $I_0(x,y,z)$ and $I_0'(x,y,z)$ are most nearly matched and overlap. This position will be calculated by using simple geometric optics and by requiring the optical pathlength change $\Delta\phi$ between light scattered by the apparent points P and P' to be equal to that of light scattered by pairs of matched apparent points M and M'.

Derivation of Fringe Localization Equations in the Forward Problem

Consider a refractive index distribution backlighted by a laser illuminated diffuser as in figure 3. It is convenient to redraw the configuration as shown in figure 4. Using the model of fringe formation introduced above and assuming the refractionless limit to apply, it is useful to imagine a field f(x,y,z) to be located in front of the diffuser where

$$f(x,y,z) = n(x,y,z) - n_0 \tag{9}$$

is the change of refractive index under study. It is unnecessary to explicitly consider the hologram per se in this analysis. The function of the hologram is merely to make the two wavefronts, passing through n_0 and n(x,y,z), from the first and second exposures respectively, simultaneously accessible. In some cases it will be convenient to use vector notation to locate a point in the object field, which in this notation will be

$$f(\vec{r}) = f(\hat{i}x + \hat{j}y + \hat{k}z) \tag{10}$$

The coordinate system may be arbitrarily positioned in space, but for our purposes it is helpful to imagine it attached to the diffuser.

An observer looking toward point $P(x_p, y_p, 0)$ receives a small cone of ray pairs with a mean propagation vector of $\vec{K}_2$. Each of the ray pairs necessary for comparison originate at the same point on the diffuser. The pairs result from the first and second exposure and are designated in figure 4 by solid and dotted lines. Note that there are two pairs shown

in the cone. Each pair consists of one solid and one dotted line respectively. Each pair in this case represents a point in the neighborhood of $P\ (x_p,y_p,0)$ on the diffuser. The two pairs so represented could be thought of in terms of our P and M discussed earlier. To carry it further consider the uppermost pair in figure 4, let this solid line represent the wavefront resulting from P of the first exposure, let the dotted line of this pair (uppermost) represent the wavefront resulting from P (call it P') of the second exposure. Repeat this analogy for the lowermost pair (one dotted one solid) and call it M and M' . Observe though, that here we say, P and P' are the same point and their respective wavefronts are altered as a result of one exposure through a field n_o, and a second exposure through a field n(x,y,z). They are related through a change in refracture index distribution of

$$f(\vec{r}) = n(x,y,z) - n_o$$

Now for such a ray pair the optical pathlength difference is

$$\Delta\Phi = \int f(\vec{r})\, ds = N\lambda \tag{11}$$

where ds is the differential distance along the ray in question. This ray is in the direction specified by $\hat{K}_2$ the unit vector coincident with $\vec{K}_2$. Recall that

$$\vec{r} = \hat{i}x + \hat{j}y + \hat{k}z \tag{12}$$

and note that

$$\vec{r}_p = \hat{i}x_p + \hat{j}y_p \tag{13}$$

so that we can write

$$\Delta\Phi = \int f(\vec{r}_p + \hat{K}_z s)\, ds = N\lambda \tag{14}$$

With this the optical pathlength change can be determined by the usual fringe counting procedure as shown at the first of this section.

In order to understand localization, we must recognize that the imaging system is focussed on some plane, normal to $\vec{K}_z$, which contains the point Q (X,Y,z) shown in figure 4. The location of Q and the aperture of the imaging lens determine the extent of the cone of ray pairs. If Q is located at an arbitrary position in space the optical pathlength difference, $\Delta\phi$, will be different for each ray pair in the cone. In this case the observer will not see the desired interference fringes, he will only see a speckle pattern. However there will be a specific location of Q (X,Y,z) at which $\Delta\phi$ is nearly identical for each ray pair in the cone. This is the precise position of fringe localization, at this location the observer will see very distinct holographic interferometry fringes.

Analytically, we determine localization by seeking the points Q along all rays propagating parallel to $\vec{K}_z$ for which the change of $\Delta\phi$ with small changes in viewing direction is zero. It is convenient to describe changes in viewing direction by changing the location of the point P $(x_p, y_p, 0)$. (It should be emphasized that it is the change in direction which is important, introducing x_p and y_p is merely an algebraic convenience.)

From vector algebra the limiting value of $\Delta\phi$ along Δs employs the directional derivative of $\Delta\phi$ and with the above we can write the condition

for localization as

$$\boxed{d(\Delta\Phi) = \frac{\partial(\Delta\Phi)}{\partial x_p} dx_p + \frac{\partial(\Delta\Phi)}{\partial y_p} dy_p = 0} \tag{15}$$

We wish to evaluate the two partials on the right-hand side of equation (15).

Recall from equation (11) that

$$\Delta\Phi = \int f(\vec{r})\, ds$$

taking the partial derivative with respect to x_p first, we have

$$\frac{\partial(\Delta\Phi)}{\partial x_p} = \frac{\partial}{\partial x_p}\left(\int f(\vec{r})\, ds\right) \tag{16}$$

If we maintain that $f(\vec{r})$ decays smoothly to zero and is zero outside of some finite region we can integrate over the limits $\pm\infty$. In this case we can take the derivative operation inside the integral and

$$\boxed{\frac{\partial(\Delta\Phi)}{\partial x_p} = \int_{-\infty}^{+\infty} \frac{\partial}{\partial x_p} f(\vec{r})\, ds} \tag{17}$$

The integrand of equation (17) can be written as

$$\frac{\partial f(\vec{r})}{\partial x_p} = \frac{\partial f}{\partial x}\frac{\partial x}{\partial x_p} + \frac{\partial f}{\partial y}\frac{\partial y}{\partial x_p} + \frac{\partial f}{\partial z}\frac{\partial z}{\partial x_p} \tag{18}$$

The first factor in each product on the right in equation (18) depends only on the index distribution, f, and on the coordinates of the point P, at which the derivatives of f are evaluated. The second factor in each product is independent of f and depends only on the direction in which

the derivative is being computed. This observation suggests that $\partial f / \partial x_P$ can be thought of as the dot product of two vectors, one depending only on f and the coordinates of P, the other depending only on the direction of ∂x_P and in fact we can write

$$\frac{\partial f(\vec{r})}{\partial x_P} = \left(\frac{\partial f}{\partial x}\hat{i} + \frac{\partial f}{\partial y}\hat{i} + \frac{\partial f}{\partial z}\hat{k}\right) \cdot \left(\frac{\partial x}{\partial x_P}\hat{i} + \frac{\partial y}{\partial x_P}\hat{i} + \frac{\partial z}{\partial x_P}\hat{k}\right)$$

Since $\vec{r} = x\hat{i} + y\hat{j} + z\hat{k}$ we have

$$\frac{\partial f(\vec{r})}{\partial x_P} = \left(\frac{\partial f}{\partial x}\hat{i} + \frac{\partial f}{\partial y}\hat{i} + \frac{\partial f}{\partial z}\hat{k}\right) \cdot \frac{\partial \vec{r}}{\partial x_P}$$

Now the quantity in parenthesis is just the gradient of f and we have

$$\frac{\partial f(\vec{r})}{\partial x_P} = \nabla f \cdot \frac{\partial \vec{r}}{\partial x_P} \tag{19}$$

Substitution of equation (19) into equation (16) produces

$$\boxed{\frac{\partial(\Delta\Phi)}{\partial x_P} = \int_{-\infty}^{+\infty} \nabla f \cdot \frac{\partial \vec{r}}{\partial x_P}\, ds} \tag{20}$$

By analogy, the second partial on the right-hand side of equation (15), becomes

$$\boxed{\frac{\partial(\Delta\Phi)}{\partial y_P} = \int_{-\infty}^{+\infty} \nabla f \cdot \frac{\partial \vec{r}}{\partial y_P}\, ds} \tag{21}$$

We now wish to evaluate the partials in the integrand of equations (20) and (21). We start with that of equation (20), $\partial \vec{r} / \partial x_P$.

Recall that from equations (12-30),

$$\vec{r} = \vec{r}_p + \hat{K}_z S \tag{22}$$

where $$\vec{r}_p = x_p \hat{i} + y_p \hat{j} \tag{23}$$

&

$$\vec{K}_z = K_{zx}\hat{i} + K_{zy}\hat{j} + K_{zz}\hat{k} \tag{24}$$

then

$$\frac{\partial \vec{r}}{\partial x_p} = \frac{\partial}{\partial x_p}\left[\vec{r}_p + \vec{K}_z S\right] \tag{25}$$

using equations (23) and (24) in (25)

$$\boxed{\frac{\partial \vec{r}}{\partial x_p} = \hat{i} + \left(\frac{\partial K_{zx}}{\partial x_p}\hat{i} + \frac{\partial K_{zy}}{\partial x_p}\hat{j} + \frac{\partial K_{zz}}{\partial x_p}\hat{k}\right)S} \tag{26}$$

By analogy the partial of equation (21), becomes

$$\boxed{\frac{\partial \vec{r}}{\partial y_p} = \hat{j} + \left(\frac{\partial K_{zx}}{\partial y_p}\hat{i} + \frac{\partial K_{zy}}{\partial y_p}\hat{j} + \frac{\partial K_{zz}}{\partial y_p}\hat{k}\right)S} \tag{27}$$

Substitution of equation (26) into (20) and (27) into (21) produces,

$$\boxed{\frac{\partial(\Delta\Phi)}{\partial x_p} = \int_{-\infty}^{\infty} \nabla f \cdot \left[\hat{i} + \left(\frac{\partial K_{zx}}{\partial x_p}\hat{i} + \frac{\partial K_{zy}}{\partial x_p}\hat{j} + \frac{\partial K_{zz}}{\partial x_p}\hat{k}\right)S\right] ds} \tag{28}$$

&

$$\boxed{\frac{\partial(\Delta\Phi)}{\partial y_p} = \int_{-\infty}^{\infty} \nabla f \cdot \left[\hat{j} + \left(\frac{\partial K_{zx}}{\partial y_p}\hat{i} + \frac{\partial K_{zy}}{\partial y_p}\hat{j} + \frac{\partial K_{zz}}{\partial y_p}\hat{k}\right)S\right] ds} \tag{29}$$

We pause now to define a specific shorthand notation for the expression of the partial derivatives, e.g.

$$\frac{\partial K_{zx}}{\partial x_p} \equiv K_{zx}^{x_p} \quad ; \quad \frac{\partial K_{zx}}{\partial y_p} \equiv K_{zx}^{y_p}$$

$$\frac{\partial K_{zy}}{\partial x_p} \equiv K_{zy}^{x_p} \quad ; \quad \frac{\partial K_{zy}}{\partial y_p} \equiv K_{zy}^{y_p} \tag{30}$$

$$\frac{\partial K_{z\bar{z}}}{\partial x_p} \equiv K_{z\bar{z}}^{x_p} \quad ; \quad \frac{\partial K_{z\bar{z}}}{\partial y_p} \equiv K_{z\bar{z}}^{y_p}$$

These will be used throughout the remainder of this derivation.

Let's rewrite equations (28) and (29) in terms of this shorthand notation

$$\boxed{\frac{\partial(\Delta\Phi)}{\partial x_p} = \int_{-\infty}^{+\infty} \nabla f \cdot \left[\hat{i} + \left(K_{zx}^{x_p}\,\hat{i} + K_{zy}^{x_p}\,\hat{j} + K_{z\bar{z}}^{x_p}\,\hat{k}\right)s\right] ds} \tag{31}$$

$$\boxed{\frac{\partial(\Delta\Phi)}{\partial y_p} = \int_{-\infty}^{+\infty} \nabla f \cdot \left[\hat{j} + \left(K_{zx}^{y_p}\,\hat{i} + K_{zy}^{y_p}\,\hat{j} + K_{z\bar{z}}^{y_p}\,\hat{k}\right)s\right] ds} \tag{32}$$

We now address the integrand of equation (31) and perform the indicated operation.

$$\nabla f \cdot \left[\hat{i} + \left(K_{zx}^{x_p}\hat{i} + K_{zy}^{x_p}\hat{j} + K_{zz}^{x_p}\hat{k}\right) s\right]$$

$$= \left(\frac{\partial f}{\partial x}\hat{i} + \frac{\partial f}{\partial y}\hat{j} + \frac{\partial f}{\partial z}\hat{k}\right) \cdot \left[\hat{i} + \left(K_{zx}^{x_p}\hat{i} + K_{zy}^{x_p}\hat{j} + K_{zz}^{x_p}\hat{k}\right) s\right]$$

$$= \frac{\partial f}{\partial x} + \frac{\partial f}{\partial x} K_{zx}^{x_p} s + \frac{\partial f}{\partial y} K_{zy}^{x_p} s + \frac{\partial f}{\partial z} K_{zz}^{x_p} s \qquad (33)$$

Using another addition to the shorthand notation

$\partial f / \partial x \equiv f^x$ etc., equation (33) becomes

$$\nabla f \cdot \left[\hat{i} + \left(K_{zx}^{x_p}\hat{i} + K_{zy}^{x_p}\hat{j} + K_{zz}^{x_p}\hat{k}\right) s\right]$$

$$= f^x + f^x s K_{zx}^{x_p} + f^y s K_{zy}^{x_p} + f^z s K_{zz}^{x_p} \qquad (34)$$

By analogy the integrand of equation (32) becomes:

$$\nabla f \cdot \left[\hat{j} + \left(K_{zx}^{y_p}\hat{i} + K_{zy}^{y_p}\hat{j} + K_{zz}^{y_p}\hat{k}\right) s\right]$$

$$= f^x s K_{zx}^{y_p} + f^y + f^y s K_{zy}^{y_p} + f^z s K_{zz}^{y_p} \qquad (35)$$

Substitution of equation (34) into equation (28) and substitution of equation (35) into equation (29) finally produces the evaluation of the partials of interest from equation (15). Therefore equation (28) becomes

$$\frac{\partial(\Delta\Phi)}{\partial x_p} = \int_{-\infty}^{+\infty} \left[\left(1 + K_{zx}^{x_p} s\right) f^x + K_{zy}^{x_p} f^y s + K_{zz}^{x_p} s\right] ds \qquad (36)$$

and equation (29) becomes

$$\boxed{\frac{\partial(\Delta\Phi)}{\partial y_P} = \int_{-\infty}^{+\infty}\left[K_{zx}^{y_P} f^x S + \left(1 + K_{zy}^{y_P} S\right) f^y + K_{z\bar{z}}^{y_P} f^{\bar{z}} S\right] ds} \tag{37}$$

With equations (36) and (37) the localization condition, equation (15) becomes

$$d(\Delta\Phi) = \int_{-\infty}^{+\infty}\left[\left(1 + K_{zx}^{x_P} S\right) f^x + K_{zy}^{x_P} f^y S + K_{z\bar{z}}^{x_P} S\right] ds \; dx_P$$

$$+ \int_{-\infty}^{+\infty}\left[K_{zx}^{y_P} f^x S + \left(1 + K_{zy}^{y_P} S\right) f^y + K_{z\bar{z}}^{y_P} f^{\bar{z}} S\right] ds \, dy_P = 0 \tag{38}$$

If the viewing aperture is of roughly the same dimension in all directions, i.e., a symmetric aperture like a circular or square aperture, then dx_P and dy_P can be varied independently in equation (38) above, which is the equivalent of the original equation (15), the localization condition. Therefore the two integral terms above in equation (38) must vanish independently, i.e., can be set independently equal to zero.

Therefore we have that:

$$\int_{-\infty}^{+\infty}\left[\left(1 + K_{zx}^{x_P} S\right) f^x + K_{zy}^{x_P} f^y S + K_{z\bar{z}}^{x_P} S\right] ds = 0 \tag{39}$$

ξ

$$\int_{-\infty}^{+\infty}\left[K_{zx}^{y_P} f^x S + \left(1 + K_{zy}^{y_P} S\right) f^y + K_{z\bar{z}}^{y_P} f^{\bar{z}} S\right] ds = 0 \tag{40}$$

In order to render the above equations for the localization condition into useful form, it now remains to determine expressions for the various

components of $\vec{K}_z$ and their respective derivatives.

To this end we direct attention to figure 5 which reproduces a part of figure 4 with certain modifications.

As shown in figure 5 the vector $\vec{K}_z$ points from P $(x_p, y_p, 0)$ to the observation point Q (X, Y, z) which is held fixed while the derivatives are taken. The distance $\overline{PQ}$ is denoted by ρ. The various components of vector $\vec{K}_z$ are as follows.

$$\overline{PQ} = \rho = \left[(X - x_p)^2 + (Y - y_p)^2 + z^2\right]^{1/2} \tag{41}$$

and

$$\left.\begin{aligned} K_{zx} &= \frac{X - x_p}{\rho} \\ K_{zy} &= \frac{Y - y_p}{\rho} \\ K_{zz} &= \frac{z}{\rho} \end{aligned}\right\} \tag{42}$$

taking the partials of these components, noting that X,Y,z are parameters (held fixed) and not functions of x_p and y_p, we find:

$$K_{zx}^{x_p} = \left(\rho \frac{\partial}{\partial x_p}(X - x_p) - (X - x_p)\frac{\partial \rho}{\partial x_p}\right)\rho^{-2}$$

$$= \left[-\rho - (X - x_p)\left(\frac{1}{2}\left[(X - x_p)^2 + (Y - y_p)^2 + z^2\right]^{-1/2} 2(X - x_p)(-1)\right)\right]\rho^{-2}$$

$$= \rho^{-2}\left[-\rho + \frac{(X - x_p)^2}{\rho}\right]$$

$$\therefore \quad \boxed{K_{zx}^{x_p} = -\frac{1}{\rho}\left(1 - K_{zx}^2\right)} \tag{43}$$

Since $\vec{K}_z$ is a unit vector, we can write

$$K_{zx}^2 + K_{zy}^2 + K_{zz}^2 = 1 \tag{44}$$

Also from the third line of equation (42), we have

$$\rho = \frac{z}{K_{zz}} \tag{45}$$

Using equations (44) and (45), equation (43) becomes:

$$K_{zx}^{x_p} = \frac{-K_{zz}}{z}\left(1-(1-K_{zy}^2-K_{zz}^2)\right)$$

$$= \frac{-K_{zz}}{z}\left(1-1+K_{zy}^2+K_{zz}^2\right)$$

or

$$\boxed{K_{zx}^{x_p} = \frac{-K_{zz}}{z}\left(K_{zy}^2+K_{zz}^2\right)} \tag{46}$$

All the other derivatives of $\vec{K}_z$ components can be evaluated in this way to give:

$$K_{zx}^{x_p} = \frac{-K_{zz}}{z}\left(K_{zy}^2+K_{zz}^2\right) \quad ; \quad K_{zx}^{y_p} = \frac{K_{zz}}{z} K_{zx} K_{zy}$$

$$K_{zy}^{x_p} = \frac{K_{zz}}{z} K_{zx} K_{zy} \quad ; \quad K_{zy}^{y_p} = \frac{-K_{zz}}{z}\left(K_{zx}^2+K_{zz}^2\right) \tag{47}$$

$$K_{zz}^{x_p} = \frac{K_{zz}}{z} K_{zx} K_{zy} \quad ; \quad K_{zz}^{y_p} = \frac{K_{zz}}{z} K_{zy} K_{zz}$$

Substitution of the appropriate expressions from equation (47) back into equations (39) and (40) provides the criteria for fringe localization.

$$\int_{-\infty}^{+\infty}\left\{\left[1-\frac{K_{zz}}{z_1}\left(K_{zy}^{\,2}+K_{zz}^{\,2}\right)s\right]f^{x}+\frac{K_{zz}}{z}K_{zx}K_{zy}f^{y}s+\frac{K_{zz}}{z}K_{zx}K_{zz}f^{z}s\right\}ds=0 \tag{48}$$

$$\int_{-\infty}^{+\infty}\left\{\frac{K_{zz}}{z}K_{zx}K_{zy}f^{x}s+\left[1-\frac{K_{zz}}{z}\left(K_{zx}^{\,2}+K_{zz}^{\,2}\right)s\right]f^{y}+\frac{K_{zz}}{z_1}K_{zy}K_{zz}f^{z}s\right\}ds=0 \tag{49}$$

Here the subscript, 1, has been introduced to emphasize that z_1 is the z coordinate of the point of localization along the ray in question. Such localization tends to form near steep gradients of refractive index.

These equations (48) and (49) relate the surface of fringe localization to the distribution of refractive index change and the geometry of the holographic system.

In the above equations the distance s, is the distance from P to Q along the ray whose specific length we seek. If this distance s is measured from the diffuser, in figures 4 and 5, that is the plane z=o then

$$s=\frac{z}{K_{zz}} \tag{50}$$

Incidentally recalling equation (45) we see that

$$\rho = \frac{z}{K_{zz}} = s$$

and one value of s is the directed distance $\overline{PQ}$.

Expanding equations (48) with substitution of equation (50) we have:

$$\int_{-\infty}^{+\infty} f^x ds - \int_{-\infty}^{+\infty} \frac{K_{zz}}{z}\left(K_{zy}^2 + K_{zz}^2\right)\frac{z}{K_{zz}} f^x ds + \int_{-\infty}^{\infty} \frac{K_{zz}}{z_1} K_{zx} K_{zy} f^y \frac{z}{K_{zz}} ds$$

$$+ \int_{-\infty}^{+\infty} \frac{K_{zz}}{z} K_{zx} K_{zz} f^z \frac{z}{K_{zz}} ds = 0$$

$$\int_{-\infty}^{+\infty} f^x ds - \int_{-\infty}^{+\infty} \frac{\left(K_{zy}^2 + K_{zz}^2\right) z f^x ds}{z_1} + \int_{-\infty}^{+\infty} \frac{K_{zx} K_{zy} f^y z}{z_1} ds$$

$$+ \int_{-\infty}^{+\infty} \frac{K_{zx} K_{zz} f^z z}{z_1} ds = 0$$

Transposing

$$\int_{-\infty}^{+\infty} f^x ds = \int_{-\infty}^{+\infty} \frac{\left(K_{zy}^2 + K_{zz}^2\right)}{z_1} z f^x ds + \int_{-\infty}^{+\infty} \frac{K_{zx} K_{zy} f^y z}{z_1} ds + \int_{-\infty}^{+\infty} \frac{K_{zx} K_{zz} f^z z}{z_1} ds$$

Crossmultiplying $z_1 \int_{-\infty}^{\infty} f^x ds$ and performing the same operations on equation (49) we have:

$$z_1 = \frac{\int_{-\infty}^{+\infty} \left[\left(K_{zy}^2 + K_{zz}^2\right) f^x - K_{zx} K_{zy} f^y - K_{zx} K_{zz} f^z\right] z \, ds}{\int_{-\infty}^{\infty} f^x ds} \qquad (51)$$

$$z_1 = \frac{\int_{-\infty}^{+\infty} \left[- K_{zx} K_{zy} f^x + \left(K_{zx}^2 + K_{zy}^2\right) f^y - K_{zy} K_{zz} f^z\right] z \, ds}{\int_{-\infty}^{+\infty} f^y ds} \qquad (52)$$

This is the general localization criteria which is referenced to the coordinate frame in the plane of the diffuser. Once a specific field of refractive index, f(x,y,z), has been substituted into equations (51) and (52), each equation represents a surface in the object space. The intersection of these surfaces is the curve of localization. The curve of localization is the locus of all points of fringe localization when the entire object field is viewed in a single observation direction, $-\vec{K}_z$. (If the object field is relatively wide this may require the use of a telecentric telescope, consisting of two lenses separated by a distance equal to the sum of their focal lengths, and having a small aperture at the center of the focal plane between them.)

(It should also be noted that if one wishes to write the equation of a surface or curve of localization in the (X,Y,z) coordinate system of figure 4, the following transformation must be made.)

$$X = x - \left(\frac{K_{zx}}{K_{zz}}\right) z$$

$$Y = y - \left(\frac{K_{zy}}{K_{zz}}\right) z$$

Insight into the significance of the localization condition can be gained by considering the case in which the interferogram is viewed along the z axis. In this case $\vec{K}_z = \vec{K}$ and equations (51) and (52) become

$$z_l = \frac{\int_{-\infty}^{+\infty} f^x z \, dz}{\int_{-\infty}^{+\infty} f^x \, dz} \tag{53}$$

and

$$z_1 = \frac{\int_{-\infty}^{+\infty} f^y z \, dz}{\int_{-\infty}^{+\infty} f^y \, dz} \tag{54}$$

Thus in this perspective, directed along the z axis, the fringes localized where the first moments of f^x and f^y vanish, that is where the rate of change of the gradients in the x and y direction is zero.

The question now arises: Can this interpretation be extended to arbitrary viewing directions? Of course it can because the orientation of the original (x,y,z) coordinate axes is arbitrary. However once the coordinate axes are fixed, the equations can still be written in a compact form in terms of ∇f for an arbitrary viewing direction $\vec{K}_z$. To do so, we introduce two unit vectors $\hat{K}_h$ and $\hat{K}_v$ which are the projections of $\hat{i}$ and $\hat{j}$ respectively onto the observation plane which is normal to $\vec{K}_z$. The vector $\hat{K}_h$, is normal to $\vec{K}_z$, is a unit vector, and is coplanar with $\vec{K}_z$ and $\hat{i}$:

$$\hat{K}_h \cdot \hat{K}_z = 0 \tag{55}$$

$$|\hat{K}_h| = 1 \tag{56}$$

$$\hat{K}_h \cdot \vec{K}_z \cdot \hat{i} = 0 \tag{57}$$

Similarly, $\hat{K}_v$ is normal to $\vec{K}_z$, is a unit vector, and is coplanar with $\vec{K}_z$ and $\hat{j}$:

$$\hat{K}_v \cdot \hat{K}_z = 0 \tag{58}$$

$$|\hat{K}_v| = 1 \tag{59}$$

$$\hat{K}_v \cdot \vec{K}_z \cdot \hat{i} = 0 \tag{60}$$

The solution of these equations is

$$\hat{K}_h = \frac{\hat{i}\left(K_{zy}^2 + K_{zz}^2\right) - \hat{j} K_{zx} K_{zy} - \hat{k} K_{zx} K_{zz}}{\left(K_{zy}^2 + K_{zz}^2\right)^{1/2}} \tag{61}$$

$$\hat{K}_v = \frac{-\hat{i} K_{zx} K_{zy} + \hat{j}\left(K_{zx}^2 + K_{zy}^2\right) - \hat{k} K_{zy} K_{zz}}{\left(K_{zx}^2 + K_{zz}^2\right)^{1/2}} \tag{62}$$

Comparison of the components of $\hat{K}_h$ with the coefficients in the numerator of equation (51) indicates that the first localization condition can be written as

$$Z_l = \frac{\left(K_{zy}^2 + K_{zz}^2\right) \int_{-\infty}^{+\infty} \hat{K}_h \cdot \nabla f \, z \, dz}{\int_{-\infty}^{+\infty} f^x \, dz} \tag{63}$$

However

$$z = K_{zz} S \tag{64}$$

$$dz = K_{zz} \, ds \tag{65}$$

so

$$Z_l = \frac{K_{zz}^2 \left(K_{zy}^2 + K_{zz}^2\right)^{1/2} \int_{-\infty}^{+\infty} \hat{K}_h \cdot \nabla f \, s \, ds}{K_{zz} \int_{-\infty}^{+\infty} f^x \, ds} \tag{66}$$

Finally, we note that

$$K_{hx} = \left(K_{zy}^2 + K_{zz}^2\right)^{1/2}$$

so

$$z_l = \frac{K_{zz} K_{hx} \int_{-\infty}^{+\infty} \hat{K}_h \cdot \nabla f \, s \, ds}{\int_{-\infty}^{+\infty} f^x \, ds} \tag{67}$$

and

$$z_l = \frac{K_{zz} K_{vy} \int_{-\infty}^{+\infty} \hat{K}_v \cdot \nabla f \, s \, ds}{\int_{-\infty}^{+\infty} f^y \, ds} \tag{68}$$

In summary, equations (51) and (52) are the solutions of the forward problem of fringe localization. For a given f(x,y,z) they describe the curve of fringe localization. These two equations can also be written in the more compact, but not necessarily more convenient form of equations (67) and (68).

Investigations into the Reconstruction of Refractive Index Distribution - The Inverse Problem - Fringe Analysis

We have presented a detailed discussion of the forward problem. This process carried us figuratively from inside the phase object out to the hologram and the effects of the phase object determined the pattern of the fringes in the subsequent interferogram.

The problem to be addressed here is the inverse of the forward problem and this process attempts to take us back in time, as it were. That is we must take what the interferogram has to offer and walk, figuratively, back through the holographic process and seek to determine what refractive index distribution of a phase object could have existed to cause or create our given interferogram.

We will see that in the general asymmetric case this is indeed a formidable problem. We will, however, present, sometimes only in outline form, what represents the current state of existing knowledge on the subject. Much of this section is drawn from various sources and as such will be appropriately referenced. The basis for most of this section closely follows that of C. M. Vest of University of Michigan, which was done, for this project, under a consultant arrangement by Vest with the TAI Corporation.

Inversion Techniques[1]

The pathlength change $\Delta\phi$ for an interferogram can be evaluated, as shown earlier by use of

$$\Delta\Phi(x,y) = \int [n(x,y,z) - n_o]\, dz = N\lambda \tag{68a}$$

This equation must then be inverted to determine $[n(x,y,z) - n_o]$. The degree of complexity involved in the required inversion depends on the

geometry of the holographic arrangement used, as shown earlier, but depends primarily on the structure of the phase object. In practice we are generally confronted with three cases.

(1) Two-dimensional phase objects, with no variation in the z direction (direction of propagation).

(2) Radially symmetric phase objects.

(3) Asymmetric phase objects.

Each of these will be discussed in turn.

Two-Dimensional Phase Objects

Inversion of the above equation for this type of phase object structure is relatively simple. Consider that the phase object of interest has a length, L, in the direction of propagation of the illumination wave and let this be along the z axis of a rectangular Cartesian coordinate system. The change in refractive index to be determined by inversion is then only a function of x and y. In this case the above equation becomes

$$N(x,y)\lambda = \int_0^L [n(x,y,z) - n_0]\, dz$$

$$= [n(x,y,z) - n_0]\, L$$

therefore

$$\Delta n = [n(x,y,z) - n_0] = \frac{N(x,y)\lambda}{L} \tag{68b}$$

This relation, though simple to determine, is often quite useful because flow around airfoils, temperature distributions near long heated cylinders and many other structures encountered in practice are two-dimensional or approximately two-dimensional.

Radially Symmetric Phase Objects

This particular structure is quite commonly encountered in investigations of flow around cones, jets, thermal plumes, flames, plasma arcs, and many other practical situations. We have mentioned it in a previous section and we will use it again, in connection with analysis of original experimental data, in the next section.

Objects of this structure may be either spherical, cylindrical or cubic etc., dependent on how we orient them with respect to the propagation axis. In either case its refractive index is a function of radius only. For convenience let

$$f(r) = n(r) - n_o$$

Figure 2, of the background subsection of this section depicts an optical ray traveling in the z direction through a radially symmetric phase object. Since

$$dz = d(r^2 - x^2)^{1/2} = (r^2 - x^2)^{-1/2} r\, dr$$

equation (68a) becomes

$$N(x)\lambda = 2\int_x^R \frac{f(r)\, r\, dr}{(r^2 - x^2)^{1/2}} \tag{69}$$

In order to conveniently treat equation (69) we must assume that the phase object decays smoothly to zero at large radius, and has no included discontinuities. However many phase objects encountered in practice behave this way and the constraint is acceptable. It is convenient to rewrite equation (69) as

$$N(x)\,\lambda = 2\int_{x}^{\infty} \frac{f(r)\,r\,dr}{(r^2-x^2)^{1/2}} \tag{70}$$

The right-hand side of equation (70) is the Abel transform of f(r) The inversion formula for this is well-known, it can be derived by classical methods[2] or more conveniently by transform methods[3]. It is given by

$$f(r) = -\frac{\lambda}{\pi}\int_{r}^{\infty} \frac{\left(\frac{dN}{dx}\right)dx}{(x^2-r^2)^{1/2}} \tag{71}$$

From this we observe that an interferogram of a radially symmetric phase object displays contours of constant value of the Abel transform of $n(r) - n_o$.

In the analysis of interferometric data the fringe order number, N(x) is known only at a finite number of discrete locations and must be inverted numerically. Various inversion schemes can be used and must be based on either equations (70) or (71). Our first approach is to consider that the phase object is divided into a specific number, I, of discrete annular zones or elements of constant width, Δr, as shown in figure 6. The objective is to determine I discrete values of f(r) from data consisting of I discrete values of N(x). To solidify what is actually happening observe figure 6 and consider that the interferogram furnishes the discrete values of the fringe order number for the position along the positive x axis of figure 6. Our impending analysis will determine the discrete values of f(r) from data for N(x) along this direction and for the I values of the annular elements. Since the structure is radially symmetric we can in

effect rotate those values of f(r) so determined through 2π about the y axis to fully generate the required concentric annular zones of values of f(r).

Inversion methods based on approximating equation (70) lead to a system of algebraic equations which must be solved. We consider that each annular element has a uniform refractive index. The index of each annular element is also discrete from that of its neighbor elements, yet it is considered to be so closely matched that a smooth transition occurs with no real discontinuity being present. Let f_i denote the value of $n - n_o$ for the element $r_i \leq r \leq r_{i+1}$, where $r_i = i \cdot \Delta r$. (This provides for the final summation of the radial position.)

With this approximation equation (70) becomes

$$N_i \lambda = 2 \sum_{K=i}^{I-1} f_K \int_{r_K}^{r_{K+1}} \frac{r\,dr}{(r^2 - r_i^2)^{1/2}} \tag{72}$$

The integral in equation (72) has the value

$$\left(r_{K+1}^2 - r_i^2\right)^{1/2} - \left(r_K^2 - r_i^2\right)^{1/2} = \Delta r \left\{\left[(K+1)^2 - i^2\right]^{1/2} - (K^2 - i^2)^{1/2}\right\}$$

thus

$$N_i \lambda = 2 \sum_{K=i}^{I-1} f_K \, \Delta r \left\{\left[(K+1)^2 - i^2\right]^{1/2} - (K^2 - i^2)^{1/2}\right\}$$

so

$$\sum_{K=i}^{I-1} A_{Ki} f_K = \left(\frac{\lambda}{2\Delta r}\right) N_i \tag{73}$$

Where the coefficients A_{ki} are

$$A_{Ki} = \left\{ \left[(K+1)^2 - i^2 \right]^{1/2} - \left(K^2 - i^2 \right)^{1/2} \right\} \tag{74}$$

Equation (73) represents a set of simultaneous algebraic equations which must be solved for the unknown values of f_k. The solution is reduced in complication since the coefficients A_{ki} form a matrix of lower triangular form, so that

$$\frac{\lambda}{2\Delta r} N_{(I-1)} = A_{(I-1),(I-1)} f_{(I-1)}$$

$$\frac{\lambda}{2\Delta r} N_{(I-2)} = A_{(I-2),(I-2)} f_{(I-2)} + A_{(I-1),(I-2)} f_{(I-1)}$$

$$\frac{\lambda}{2\Delta r} N_{(I-3)} = A_{(I-3),(I-3)} f_{(I-3)} + A_{(I-2),(I-3)} f_{(I-2)}$$

$$+ A_{(I-1),(I-3)} f_{(I-1)}$$

The outermost element, see figure 6, is located so that $f_I = 0$. Each value of f should be calculated in sequence starting at the outer radius and working towards the center. The coefficients given by equation (74) have been computed and tabulated by Hauf and Grigull[4] up to I=25.

Alternative inversion schemes can be developed by using more complex representations of $f(r)$: each different representation yields a different set of coefficients A_{ki} for use in equation (73) [ref. 5-17].

To summarize, many methods are available, all based on the numerical approximation of equations (70) and (71), for the analysis of the interferograms of radially symmetric phase objects. The best method for any specific application is, of course, dependent on the phase object structure, orientation, data accuracy and data point density. A study by Kulagin[17] suggests that the method of Nestor and Olsen[10] is the best general purpose method and can be expected to give reasonable accuracy and have low sensitivity to errors in the data. The safest procedure is to try several methods with known functions f(r) similar to the one expected to be measured, and to compare the methods with regard to accuracy and sensitivity to random errors in the data.

Asymmetric Phase Objects

Determination of an asymmetric refractive index distribution requires analysis of a large number of interferograms, each recorded from a different viewing direction. Holographic interferometry is ideally suited for recording such data, which is termed multi-directional interferometric data. However the determination of the necessary refractive index distribution from such data is at best a most complicated effort. Even though this subject has been investigated only recently there are many approaches to various inversion schemes. One fact stands out as common to most of the inversion techniques and that is the role of still another transform, the Radon transform. An interferogram of an asymmetric phase object displays contours of constant value of the Radon transform of $n(r,\phi) - n_o$. So we see that the Radon transform plays the same role for asymmetric

inversion that the Abel transform plays for the radially symmetric inversion.

Various inversion methods are treated in the literature in references 18 through 34.

In this section we intend only to provide an outline of the analysis of the inverse problem of fringe localization for the asymmetric phase object. We classify it in two forms: First it is given in the spatial domain. In this case the objective is to derive a set of algebraic equations which directly relates the unknown refractive index to measured values of fringe localization. Second, the problem is considered by using the Fourier transform, because this approach is so useful for the analysis of reconstruction from fringe order data. In each approach, we first review the corresponding analysis of reconstruction from fringe order data.

Spatial Domain

Reconstruction from Pathlength Measurements

Consider that the refractive index of an asymmetric phase object is given by $n(x,y,z) - n_0$. We address the problem of determining this distribution in a particular plane z = constant. In this plane the refractive index can be denoted in Cartesian coordinates by

$$f(x,y) = n(x,y) - n_0 \tag{75}$$

and in cylindrical coordinates as

$$f(r,\phi) = n(r,\phi) - n_0 \tag{76}$$

both represent the same physical distribution in two different coordinate systems. Figure 7 provides the notation for data recorded in a particular

viewing direction. Using this notation the expression for optical path-length difference is

$$N(P,\theta)\cdot\lambda = \int_{-\infty}^{+\infty}\int f(r,\phi)\,\delta[P - r\sin(\phi-\theta)]\,dx\,dy \qquad (77)$$

Θ specifies the given observation direction and $N(P,\phi)$ is the fringe order data read from the interferogram in the manner discussed throughout this section. δ is the Dirac delta function so the integral on the right-hand side equation (77) represents the line integral of $f(r,\phi)$ along a straight ray passing through the phase object. The limits as before assume that the phase object decays smoothly to zero at the edges of the field. The right-hand side of equation (77) is the two dimensional Radon transform of $f(r,\phi)$ [18]. The inverse of equation (77) is

$$f(r,\phi) = \frac{\lambda}{2\pi^2}\int_{-\frac{\pi}{2}}^{\frac{\pi}{2}}\int_{-\infty}^{\infty}\frac{\partial N/\partial P\,dP}{r\sin(\phi-\theta)-P} \qquad (78)$$

This inversion was given by Berry and Gibbs[19] and is a special case of the inverse Radon transform discussed in references 18 through 23.

Interferometric data consisting of a set of measured values of fringe order number $N(P,\Theta)$ must be inverted numerically. Inversion schemes can be based on numerical approximations of either equation (77) or (78). Methods based on approximating equation (78) lead to a system of algebraic equations which must be solved. To this end consider the region occupied by the phase object to be divided into discrete rectangular elements of dimension Δx by Δy, where from figure 8,

$$\Delta X = \frac{L_x}{M+1} \quad ; \quad \Delta y = \frac{L_y}{N+1}$$

Consider that each rectangular element has a uniform index of refraction. Let f_k denote the value of refractive index change of the element centered on the point $x = m\Delta x$, and $y = n\Delta y$, where m and n are integers. The subscript k is related to m,n by

$$K = n(M+1) + m + 1 \tag{79}$$

Let the fringe order number N_i, be associated with the i^{th} ray traversing the phase object. This ray is specified by the coordinates P,θ. If A_{ki} denotes the length of the segment of the i^{th} ray which lies in the k^{th} element, the total optical pathlength difference for the i^{th} ray is given by

$$\sum_{K=1}^{K} A_{Ki} f_K = \lambda N_i \tag{80}$$

Where K=(M+1)(N+1) is the total number of elements. Equation (80) is a finite sum approximation to equation (77). The coefficients can be determined geometrically[24] as: A_{ki}=

$$\Delta x \sec\theta \qquad \text{for } |b| \leq \frac{\Delta y - \Delta x|\tan\theta|}{2}$$
$$\text{and } |\tan\theta| \leq \frac{\Delta y}{\Delta x}$$

$$\Delta y \sec\theta \qquad \text{for } |b| \leq \frac{\Delta x|\tan\theta| - \Delta y}{2}$$
$$\text{and } |\tan\theta| > \frac{\Delta y}{\Delta x}$$

$$\frac{\sec\theta}{|\tan\theta|}\left(\frac{\Delta x\,|\tan\theta|+\Delta y}{2}-|b|\right) \qquad \text{for } \frac{|\Delta y-\Delta x\,|\tan\theta||}{2}<|b| \leqslant \frac{\Delta y+\Delta x\,|\tan\theta|}{2},$$

$$\Delta y \qquad \text{for } |c|<\frac{\Delta x}{2} \text{ and } |\tan\theta|=\infty$$

$$0 \qquad \text{for } |b|>\frac{\Delta x\,|\tan\theta|+\Delta y}{2}$$

$$0 \qquad \text{for } |c|>\frac{\Delta x}{2} \text{ and } |\tan\theta|=\infty$$

Where

$$b = P\sec\theta + m\Delta x\tan\theta - n\Delta y$$

and

$$c=\begin{cases} P-m\Delta x & \text{for } \theta=-\frac{\pi}{2} \\ P+m\Delta x & \text{for } \theta=\frac{\pi}{2} \end{cases}$$

If the number I of pathlength measurements is equal to the number of elements K, a system of K linear algebraic equations of the form of equation (80) can be generated and solved for K unknown values f_k. This approach to the analysis of holographic interferograms was introduced by Alwang et. al.[25]

·Reconstruction from Localization Data

Earlier the equations describing fringe localization in holographic interferograms of diffusely-illuminated transparent media were derived in detail. We repeat the result of that discussion here in a notation convenient for the present discussion. We assume that the region of interest lies in the xy plane. Furthermore, we assume that the viewing telescope has a slit aperture oriented parallel to this plane; then a single equation will govern localization:

$$X_i' = \frac{\int_{-\infty}^{\infty} \frac{\partial f}{\partial y'} x' dx'}{\int_{-\infty}^{\infty} \frac{\partial f}{\partial y'} dx'} \tag{81}$$

The denominator of equation (81) can be evaluated from the interference pattern formed by rays traveling in the x' direction:

$$\int_{-\infty}^{\infty} \frac{\partial f}{\partial y'} dx' = \frac{d}{dy'} \int_{-\infty}^{\infty} f \, dx' = \lambda \frac{dN}{dy'} \tag{82}$$

Since N is fringe order, $dN/dy' = 1/\Delta y_f'$ where y_f' is the local fringe

spacing. If the subscript i denotes the i^{th} ray as in figure 9 it is convenient to introduce the quantity

$$\lambda q_i = \lambda \left(x_1' / \Delta y_t' \right) \tag{83}$$

The quantity q_i is the product of the wavelength and localization position divided by the fringe spacing. This will serve as the data from which the refractive index change f(x,y) is to be reconstructed.

We now must approximate the integral equation

$$\int_{-\infty}^{\infty} \frac{\partial f}{\partial y'} x' \, dx' = \lambda q_i = \lambda q(P, \theta) \tag{84}$$

Using the notation of the preceding subsection, this can be written as

$$\sum_{K=1}^{K} B_{Ki} \left(\frac{\partial f_K}{\partial y'} \right) = \lambda q_i \tag{85}$$

where

$$B_{Ki} = \left(\sum_{j=1}^{K-1} A_{ji} + \frac{1}{2} \right) A_{ji} \tag{86}$$

It is assumed that f = 0 outside the region of interest. Now we introduce a finite difference approximation for $\partial f_k / \partial y'$, after noting that

$$\frac{\partial f}{\partial y'} = \frac{\partial f}{\partial x} \cos\theta + \frac{\partial f}{\partial y} \sin\theta$$

For all interior nodes a central difference approximation can be used:

$$\frac{\partial f_K}{\partial y'} = \left(\frac{f_{m+1,n} - f_{m-1,n}}{2\Delta x} \right) \cos\theta + \left(\frac{f_{m,n+1} - f_{m,n-1}}{2\Delta x} \right) \sin\theta \tag{87}$$

If an element lies on the boundary, the central difference cannot be used; it must be replaced by an appropriate forward or backward difference.

Equations (83)-(85) together with the preceding definition of A_{ki}

constitute a set of linear equations which can in principle be solved for the K values of f_k.

In practice this procedure may be difficult to implement because it involves using data which are likely to have a rather high degree of uncertainty, and because it involves finite difference approximations to derivatives in the definition of B_{ki} and in the evaluation of the derivative of fringe order. It may be that these equations can best be used as ancillary equations to those discussed in the preceeding subsection, that is as a way of increasing the number of available linearly-independent equations. Solving both the optical pathlength and fringe localization equations together might be particularly helpful when the range of viewing angles is small, as it is likely to be in the subject experiments.

Fourier Transform Domain

·Reconstruction from Pathlength Measurements

Here we review the Central Section Theorem, which provides one of the most fruitful ways to consider the reconstruction problem. In the notation of figure 10, fringe order number is related to f(x,y) as

$$\int_{-\infty}^{\infty} f(x',y')\,dx' = \lambda N(y') \tag{88}$$

The one-dimensional Fourier transform of N(y') is

$$\mathcal{F}_1\left\{N(y')\cdot\lambda\right\} = \int_{-\infty}^{\infty}\lambda N(y')e^{-i2\pi\,\nu' y'}dy' \tag{89}$$

$$= \int_{-\infty}^{\infty}\int f(x',y')\,e^{-i2\pi\,\nu' y'}dx'\,dy'$$

Now note the definition of the two-dimensional transform of (f(x,y):

$$F(u,v) = \iint_{-\infty}^{\infty} f(x,y)\, e^{-i2\pi(ux+vy)}\, dx\, dy \tag{90}$$

Clearly,

$$\mathcal{F}_1\left\{\lambda N(y')\right\} = \lambda F(o,v') \tag{91}$$

i.e., the one-dimensional transform of fringe order data read from an interferogram yields the values of the two-dimensional transform of f (x,y) along a radial line, u' = 0 in the transform plane. This result, known as the Central Section Theorem is the basis of Fourier reconstruction methods. Clearly if we build up the transform along a large number of radial lines in the transform plane we can then take an inverse Fourier transform to reconstruct f (x,y).

·Reconstruction from Localization Data

Here we ask the question, what is the analog of the Central Section Theorem for localization data? Given

$$g(y') = \int_{-\infty}^{\infty} x' \frac{\partial f}{\partial y'}\, dx' \tag{92}$$

The two-dimensional Fourier transform of the integral is

$$\mathcal{F}_2\left\{x', \frac{\partial f}{\partial y'}\right\} = -v' \frac{\partial F(u',v')}{\partial u'} \tag{93}$$

The one-dimensional transform of g(y') is

$$\mathcal{F}_1\left\{g(y')\right\} = \int_{-\infty}^{\infty} g(y')\, e^{-i2\pi v'y'} dy' \tag{94}$$

$$= \iint_{-\infty}^{\infty} \frac{\partial f}{\partial y'}\, e^{-i2\pi v'y'} x'\, dx'\, dy' = \mathcal{F}_2\left\{x', \frac{\partial f}{\partial y'}\right\}_{o,v'}$$

Hence we have the result

$$\mathcal{F}_1\{g(y')\} = -v' \left.\frac{\partial F}{\partial u'}\right|_{u',0} \tag{95}$$

Even though this result is simple in form, we have not been able to deduce a reconstruction algorithm from it. One may not exist. Clearly it could play a useful role in conjunction with Fourier reconstruction from pathlength data in the following manner. The Central Section Theorem applied to interferometric data leads to known values of the Fourier transform along discrete radial lines. To use fast Fourier transform codes on the computer the values must be known on a rectangular grid of points. Hence it is necessary to interpolate from one format to the other. The derivatives of the transform given by equation (95), if accurate, would be useful for this interpolation.

Some Tentative Conclusions on Reconstruction of f(r) from Asymmetric Phase Objects

i. There are cases in which the refractive index field cannot be reconstructed from localization data alone. An obvious example is a radially symmetric field; in this case fringes localize in the center plane for all viewing directions. This does not provide sufficient data for reconstruction.

ii. For the general case it is possible to formulate a linear algebraic set of equations which relate refractive index to measured values of localization position. As far as we can discern at this point in time these can in principle be used to reconstruct the refractive index field, except in special cases. In any event, these equations increase the information available. For example if the localization methods are accurate, these equations could be combined with the reconstruction equations based on fringe order. This yields greater redundancy and should improve the accuracy of reconstruction, especially when only limited viewing angles are available.

iii. If Fourier reconstruction methods are used to invert fringe order data, fringe localization data in principle provides useful information for improving the accuracy on interpolation in the transform plane.

iv. Localization data could be used for iterative reconstruction from fringe order data. That is, at each step one could calculate the fringe localization position based on the reconstructed field and check for agreement with measured values of localization position.

v. The phenomenon of fringe localization is always useful in the sense that it discloses symmetries of the field, assists the viewer in locating the field in space, and helps one to form a qualitative impression of the structure of the field.

References

1. C. M. Vest, Holographic Interferometry, Wiley Interscience, New York, 1979, and unpublished reports via subcontract with TAI Corporation.

2. F. D. Bennett, W. C. Carter and V. E. Bergdolt, Interferometric Analysis of Air Flow About Projectiles in Free Flight. J. Appl. Phys. 23, 1952.

3. R. N. Bracewell, The Fourier Transforms and Its Applications, McGraw Hill, New York, 1965.

4. W. Hauf and V. Grigull, Optical Methods in Heat Transfer in Advances in Heat Transfer, Academic Press, New York, 1970.

5. R. Ladenburg, J. Winkler and C. C. Van Voarhis, Interferometric Study of Faster than Sound Phenomena, Part I, Phys. Rev. 73, 1948.

6. R. Barakat, Solution of an Abel Integral Equation for Band-Limited Functions by Means of Sampling Theorems, J. Math Phys., 43, 325-331, 1964.

7. D. W. Sweeney, A Comparison of Abel Integral Inversion Schemes for Interferometric Applications, J. Opt. Soc. Am., 64, 559, 1974.

8. P. B. Gooderum and G. P. Wood, NACA TN 2173, 1950.

9. E. T. Whittaker and G. N. Watson, A Course of Modern Analysis, 4th ed., Cambridge University Press, Cambridge, p. 229, 1962.

10. D. H. Nestor and H. N. Olsen, Numerical Methods for Reducing Line and Surface Probe Data, SIAM Rev., 2, 200-207, 1960.

11. W. L. Barr, Method for Computing the Radial Distribution of Emitters in a Cylindrical Source, J. Opt. Soc. Am., 52, 885-888, 1962.

12. K. Bockasten, Transformation of Observed Radiances into Radial Distribution of the Emission of a Plasma, J. Opt. Soc. Am., 51, 943-947, 1961.

13. J. W. Bradley, Density Determination from Axisymmetric Interferograms, AIAAJ., 6, 1190-1192, 1968.

14. R. South, An Extension to Existing Methods of Determining Refractive Indices from Axisymmetric Interferograms, AIAAJ., 8, 2051-2059, 1970.

15. S. I. Pollitz, A Method for Computing the Emission Distribution in Cylindrical Light Sources, Ark. Fys., 23, 571-574, 1963.

16. R. N. Bracewell, Strip Integration in Radio Astronomy, Aust. J. Phys., 9, 198-217, 1956.

17. I. D. Kulagin, L. M. Sorokin and E. A. Dubrovskaya, Evaluation of Some Numerical Methods for Solving Abel's Integral Equation Opt. Spectrosc. 32, 1972.

18. I. M. Gel'Fand, M. I. Graev, and N. Ya. Vilenkin, Generalized Functions, Vol. 5, Academic Press, New York, 1966.

19. M. V. Berry and D. F. Gibbs, The Interpretation of Optical Projections, Proc. Roy. Soc. (London), A314, 143-152, 1970.

20. D. Ludwig, The Radon Transform on Euclidean Space, Commun. Pure Appl. Math., 19, 49-81, 1966.

21. A. M. Cormack, Reconstruction of Densities from Their Projections, with Applications in Radiological Physics, Phys. Med. Biol., 18, 195-207, 1973.

22. C. M. Vest, Formation of Images from Projections: Radon and Abel Transforms, J. Opt. Soc. Am., 64, 1215-1218, 1974.

23. P. P. B. Eggermont, Three-Dimensional Image Reconstruction by Means of Two-Dimensional Radon Inversion, Report 75-WSK-04, Technological University, Eindhoren, The Netherlands, 1975.

24. D. W. Sweeney and C. M. Vest, Reconstruction of Three-Dimensional Refractive Index Fields from Multi-directional Interferometric Data, Appl. Opt., 12, 2649-2664, 1973.

25. W. Alwang, L. Cavanaugh, R. Burr, and A. Houer, Optical Techniques for Flow Visualization and Fluid Flow Measurement in Aircraft Turbo-Machinery, Item 1, Final Report PWA-3942, Pratt and Whitney Aircraft Co., Hartford, CT., 1970.

26. G. Golub, Numerical Methods for Solving Least Squares Problems, Numer. Math., 7, 206-216, 1965.

27. G. N. Ramachandran and A. V. Lakshminavayanan, Three-Dimensional Reconstruction from Radiographs and Electron Micrographs. Part III: Description of the Convolution Method, Indian J. Pure Appl. Phys., 9, 997-1003, 1971.

28. R. N. Bracewell and A. C. Riddle, Inversion of Fan Beam Scans in Radio Astronomy, Astrophys. J., 150, 427-434, 1967.

29. J. W. Cooley and J. W. Turkey, An Algorithm for the Machine Calculation of Complex Fourier Series, Math. Comp., 19, 297-301, 1965.

30. T.-F. Zien, W. C. Ragsdale, and W. C. Spring III, Quantitative Determination of Three-Dimensional Density Field by Holographic Interferometry, AIAAJ., 13, 841-842, 1975.

31. R. D. Matulka and D. J. Collins, Determination of Three-Dimensional Density Fields from Holographic Interferometry, J. Appl. Phys., 42, 1109-1119, 1971.

32. H.-G. Junginger and W. Van Haeringer, Calculation of Three-Dimensional Refractive Index Field Using Phase Integrals. Opt. Commun., 5, 1-4, 1972.

33. Yu. P. Presnyakov, Calculation of a Two-Dimensional Refractive Index Function, Opt. Spectrosc., 40, 69-70, 1976.

34. R. Gordon, A. Treatise on Reconstruction from Projections and Computerized Tomography (to be published).

C-2

SECTION V

QUANTITATIVE APPLICATION OF FRINGE LOCALIZATION AND INVERSION PROCESS THEORY TO A PRACTICAL EXAMPLE IN A TRANSPARENT MEDIUM

It is the objective of this section to discuss various applications of the theory presented in the last section. We provide a detailed discussion of the application of the theory of fringe localization (forward problem) to the special, practical case of a radially symmetric field with two refractive index variations. We then provide confirmation of this theoretical result using original experimentation from the simulated HOSS system. We further present several other original experiments, using the HOSS system, along with results and analysis of their data. Finally, we provide a collection, or recoup, of the conceptual theory to fix ideas, and provide a simplified computer code for analysis or inversion of data from the radially symmetric field using 9835A BASIC, with detailed instructions for implementation.

A Specific Application of the Theory of Fringe Localization

As shown earlier in Section IV, the optical pathlength difference for a radially symmetric field is:

$$\Delta \Phi (x) = 2 \int_{x}^{R} \frac{f(r)\, dr}{(r^2 - x^2)^{1/2}}$$

where x is normal to both the axis of symmetry and the viewing direction. We have indicated earlier that the fringes localize where the moment of the gradient of f (r) normal to the viewing direction vanishes, and for the radially symmetric phase object, the fringes will localize in the center plane of the object field. This is illustrated by original experimentation using the simulated HOSS system presented later in this section.

For the moment, let's pursue the details of an hypothetical experiment with regard to prediction of fringe localization. Then we will produce the results of a similar experiment which supports our theoretical conclusions.

Consider two radially symmetric phase objects, which are plumes of heated water above small, identical electrical heating elements. This experimental situation is displayed schematically in figure 1. Our viewing direction is along k_2, so that the optical axis passes diametrically through both heating elements. Because of symmetry, the moments of the gradient normal to the viewing direction vanish in the plane midway between the two objects. If our viewing direction is along, say k_2' of figure 1, then again because of symmetry, the fringes due to each phase object independently will separately localize in their respective center planes.

Let's assume that the radial distribution of refractive index change of our plumes of heated water is Gaussian. Then our plume (phase object) which is centered at $Z = Z_{01}$, has a refractive index distribution $f_1(r_1)$, given by

$$f_1(r_1) = f_{01} \exp\left[-\left(\frac{r_1}{r_{01}}\right)^2\right] \tag{1}$$

Similarly for our second plume, which is centered at $Z = Z_{02}$, has a refractive index distribution $f_2(r_2)$, given by

$$f_2(r_2) = f_{02} \exp\left[-\left(\frac{r_2}{r_{02}}\right)^2\right] \tag{2}$$

where f_{01}, and f_{02} represent the maximum value of refractive index and r_{01} and r_{02} are the characteristic radii of the respective plumes of heated water, i.e., phase objects.

Recall from Section IV that the equations of fringe localization for an interferogram viewed along the z axis, where $\vec{k}_2 = \vec{k}$, are given by

$$Z_l = \frac{\int_{-\infty}^{\infty} f^x z \, dz}{\int_{-\infty}^{\infty} f^x \, dz}$$

and

$$Z_l = \frac{\int_{-\infty}^{\infty} f^y z \, dz}{\int_{-\infty}^{\infty} f^y \, dz}$$

In our case where we view our interferogram along the z direction, localization is determined by the use of the first one of the two localization equations above. The second equation is not used since $f^y = 0$ for our case.

Further, recall that in our notation of Section IV $f^y = \partial f/\partial x$. We then must first evaluate the gradient of our refractive index distribution.

$$\frac{\partial f(x,y)}{\partial x} = \frac{\partial}{\partial x}\left\{ f_{01} \exp\left[-\frac{x^2+(z-z_{01})^2}{r_{01}^2}\right] + f_{02} \exp\left[-\frac{x^2+(z-z_{02})^2}{r_{02}^2}\right]\right\}$$

$$= -2x\left(\frac{f_{01}}{r_{01}^2}\right) \exp\left[-\frac{x^2+(z-z_{01})^2}{r_{01}^2}\right] -2x\left(\frac{f_{02}}{r_{02}^2}\right) \exp\left[-\frac{x^2+(z-z_{02})^2}{r_{02}^2}\right]$$

$$\therefore f^x = -2x\left\{\frac{f_{01}}{r_{01}^2} \exp\left[-\frac{x^2+(z-z_{01})^2}{r_{01}^2}\right] + \left(\frac{f_{02}}{r_{02}^2}\right) \exp\left[-\frac{x^2+(z-z_{02})^2}{r_{02}^2}\right]\right\} \quad (3)$$

Substitution of equation (3) into the first of the localization integrals and evaluation of this integral equation produces the equation of the surface of localization, i.e.

$$z_\perp = \frac{z_{01}\left(\frac{f_{01}}{r_{01}^2}\right) \exp\left[-\left(\frac{x}{r_{01}}\right)^2\right] + z_{02}\left(\frac{f_{02}}{r_{02}^2}\right) \exp\left[-\left(\frac{x}{r_{02}}\right)^2\right]}{\frac{f_{01}}{r_{01}^2} \exp\left[-\left(\frac{x}{r_{01}}\right)^2\right] + \left(\frac{f_{02}}{r_{02}^2}\right) \exp\left[-\left(\frac{x}{r_{02}}\right)^2\right]} \quad (4)$$

In our case $r_{01} = r_{02}$ and $f_{01} = f_{02}$, and

$$Z_1 = \frac{Z_{01}\left(\frac{f_{01}}{r_{01}^2}\right) \exp\left[-\frac{X}{r_{02}^2}\right] + Z_{02}\left(\frac{f_{01}}{r_{01}^2}\right) \exp\left[-\frac{X}{r_{01}^2}\right]}{\left(\frac{f_{01}}{r_{01}^2}\right) \exp\left[-\frac{X}{r_{01}^2}\right] + \left(\frac{f_{02}}{r_{01}^2}\right) \exp\left[-\frac{X}{r_{01}^2}\right]} \qquad (5)$$

and the surface of localization for our case becomes

$$Z_1 = \frac{Z_{01} + Z_{02}}{2} \qquad (6)$$

Using the simulated HOSS System, described earlier in Section III, we performed an experiment, designed as closely as possible to comply with the characteristics of the above described hypothetical experiment. (A similar, but separate, experiment has been presented and described qualitatively in Section III.) Presented below are some of the results of this experiment which are offered in support of the theoretical findings on fringe localization.

Double exposure holograms of two heating elements were taken as shown in Fig. 1. In the construction, the straight line bisecting the centers of the heating elements was normal to the plane of the diffuser yielding a hologram which showed the elements located "on-axis" in the object beam. The distances used were Z_{01} = 0.5 in (1.3cm) and Z_{02} = 3.5in (8.9cm) = distance to plane b. The distance to plane a may, therefore, be calculated from Equation 6 to be $Z_1 = 2_{in}$(5.1cm).

Upon reconstruction of the holograms, photographs of the real

images as projected using a ¼" x 2" vertical slit in the collimated reconstruction beam are shown in figure 2. The top row of pictures shows the results of exposing the first half of the double exposure during the quiescent state, then applying power to the heating elements for 30 seconds. Immediately after this 30 seconds of heat, the second half of the exposure was taken. The bottom row was taken with a 60 second delay between "heat off" and the second half exposure. The right-hand column of photos shows the image in plane b while the left-hand column displays plane a which is the plane of localization as predicted by Equation 6.

A Presentation of Several Experiments Using The Simulated HOSS System With Quantitative Data Analysis.

On obtaining an interferogram where the fringes are due only to a single radially symmetric disturbance, and with a temperature of the test cell, the index of refraction and thus the temperature (or vice versa) within the disturbance can be calculated in two ways. The first way is a quick way of determining the average temperature over a specific region of the disturbance. The second method (already presented in theory of Section IV), generates a reasonably detailed map of refractive index and temperature of a cross section taken through the disturbance.

In order to present the first of these methods, attention is directed to figure 3 which presents an interferogram of a doubly exposed hologram which has employed a diffuser in the object beam. The phase object is a plume of heated water rising from a heater element during the second exposure and has a temperature probe positioned in the plume as shown. We seek to determine the average temperature in the region of the temperature probe tip. The depth of the test cell (along the object beam) was 10cm.

This method of analysis uses the concept of zeroth order fringe (ZF) discussed in Section II.

As the heater element is turned on, between the exposures, the water in the entire test cell begins to slowly heat up from the top down to the bottom. This results in background fringes and provides us with the

zeroth order fringe. We wish to calculate the temperature on the left- and right-hand sides of the temperature probe.

From figure 3 there are only two bright fringes from the bottom up to the level of the temperature probe tip. This provides information for calculations of the temperature at the left-hand side of temperature probe due to its level in the water bath. We call this left-hand side the <u>outside</u> of the temperature probe and the right-hand side the <u>inside</u> respectively. In this way we reference to its position in the plume. Usings = 10 cm for test cell depth and λ = 514.5 nm in

$$\Delta n = \frac{N\lambda}{S}$$

we find for the <u>outside</u>

$$\Delta n \approx 1 \times 10^{-5}$$

From CRC tables for water at approximately 20°C a Δn of 1×10^{-5} corresponds to a ΔT of 0.1°C. Since the ambient temperature of the water bath after the first exposure and prior to heating was 20.2°C, then the temperature at the outside edge is

$$20.3^{\circ}C = \text{ambient temperature} + \Delta T$$

Because the sensor tip of the temperature probe was relatively large (4mm), it senses an average of the temperature across it. We must now determine the temperature of the inside edge of the probe.

On counting the fringes from left to right across the tip of the probe, figure 3, we find N = 4. Again, using probe diameter of 4mm

$$\Delta n = \frac{N\lambda}{S} = \frac{4\lambda}{4 \times 10^{-3}\,m} = 5.0 \times 10^{-4}$$

From CRC tables a Δn of 5×10^{-4} corresponds to a ΔT of $5.3^{o}C$ and the temperature at the inside of the temperature probe is

$$25.6^{o}C = \text{outside temperature} + 5.3^{o}C$$

The average temperature across the probe is then

$$\frac{20.3^{o}C + 25.6^{o}C}{2} \cong 23.0^{o}C$$

The temperature reading for this position sensed by the probe was $22.5^{o}C$.

We will now address the second, more detailed method and we will employ this method to the analysis of two distinctly different experimental techniques of recording basically the same phenomenon. In one of these experiments we employ a single exposure hologram and a single heater element with no diffuser. This constitutes use of a collimated light source and classical interferometer for fringe production. In the second experiment, everything remained the same except we employed a double exposure hologram with the diffuser in the object beam and utilized localized fringes. We describe and analyze the single exposure hologram experiment first.

A collimated beam of 514.5 nm radiation was incident (without diffuser) on the test cell of water after a single heater element had been turned on for thirty (30) seconds to create a radially symmetric disturbance as the phase object. A temperature probe was located in the center of the heat plume to provide a reference temperature determination. The ambient temperature was $22.0^{o}C$ and the temperature reading at the time of exposure was $33.4^{o}C$.

The hologram was processed and replaced in position to generate an interferogram using the simulated HOSS system shown in figure (12) Section III. The interferogram so generated is shown in figure 3, which labels the cross section under investigation. cross section number 1. This cross section was analyzed using the Abel inversion technique already described in Section IV under Inversion Techniques.

Using this technique, a computer code called "RINDEX", was produced which was a prototype of that code offered for analysis at the end of this section. This program provides for the mapping of refractive index and temperature from interferometric fringe data.

The basics of the analysis procedure is to first calculate the refractive index of H_2O at the ambient temperature of 22.0°C. This is done via an expression from reference 1:

$$n - 1.337253 = - (2.8767T + 0.14825T^2) \times 10^{-5}$$

This produced that $n_o = 1.33590$.

The Δn for each region or annulus of the disturbance is calculated using the equations from Section III for the Abel inversion techniques. This yields an annular map of the radially symmetric disturbance. The Δn calculated for each sequential annuli in the map, starting from the outside of the plume and reading in toward the center, are sequentially added to the calculated value of n_o. This yields the absolute index of refraction, n, for each region of the annular map. The indices of refraction for each region of the map are then converted to temperature values (°C) for the map by using the expression above.

Figure 5 shows an enlarged view of the selected fringe cross section number 1. Note that the fringe order is negative if the density decreases as we go from outside, n_0, toward the center of disturbance and the fringe order is positive if the density increases toward the center. (The reverse is appropriate for the temperature calculation and our computer program accounts for this.)

Figure 6 displays a table of the values found for index of refraction and temperature for the map of the first quadrant of the disturbance.

Figure 7 shows a plot of the temperature versus distance for the radius of the disturbance.

We now describe and analyze the double exposure hologram experiment, i.e., the second method. The double exposure experiment had the same collimated object beam except this time it was incident on a diffuser plate. The temperature probe was at a slightly different position in the radially symmetric disturbance. The first exposure was at ambient conditions with a temperature of 21.4°C. A single heater element was again turned on for thirty (30) seconds and a second exposure was recorded. The temperature probe reading at the time of the second exposure was 32.2°C.

The doubly exposed hologram was processed and the interferogram produced is shown in figure 8. The data from this interferogram was processed by the same computer code, RINDEX, in the same way as before. Figure 9 displays a table of values found for index of refraction and temperature for the map of the first quadrant of the disturbance.

Figure 10 shows a plot of the temperature versus distance for the radius of the disturbance.

A Summary of the General Theoretical Concepts Presented and Presentation of a Useable Computer Code for Analysis.

In order to summarize the general concepts presented thus far on the theoretical description of fringe localization and inversion of fringe data we once again direct attention to the radially symmetric phase object.

Consider the interpretation of a diffusely illuminated holographic interferogram of a radially symmetric phase object. To fix ideas, examine figure 11. Light is scattered by an input diffuser through a transparent fluid medium which has a homogeneous refractive index, n_o, at the time of the initial holographic exposure. A phase object, for example a thermal plume or a mass diffusion boundary layer, is then introduced and examined by either real-time or double exposure holographic interferometry. This object is assumed to be symmetrical about an axis, which for convenience, is assumed to be vertical. We now address the question of how the refractive index, $n(r)$, of this field can be determined from the fringe pattern. Here, r, is the radial coordinate measured from the centerline of symmetry.

Recall that two types of information are available from the interferogram.

(1) Fringe number, position and spacing.

(2) Fringe localization.

To determine the role of fringe localization in this case, assume that we view the object field (through the hologram) along the direction k_2, parallel to the z axis. Now consider the solution of the "forward problem" which has been derived in Section IV and above in its simplest form as

$$z_\ell = \frac{\int_{-\infty}^{\infty} f^x z \, dz}{\int_{-\infty}^{\infty} f^x dz}$$

&

$$z_\ell = \frac{\int_{-\infty}^{\infty} f^y z \, dz}{\int_{-\infty}^{\infty} f^y dz}$$

These equations were interpreted as indicating that fringes localize where the first moments of the refractive index distribution, f^x and f^y, normal to the z direction (direction of propagation) vanish. In the radially symmetric case if our viewing direction, k_2, lies in the xz plane, the numerators of the above fringe localization equations will vanish because of symmetry, if the origin is located along the axis of symmetry as shown in figure 12. Therefore the fringes for this case will localize in the center plane of the object field. The orientation of the xz coordinates is arbitrary, so this conclusion will be valid if we use any other viewing direction k_2 in the xz plane, as shown in figure 12. We therefore conclude that for radially symmetric phase objects the fringes will localize in the center plane of symmetry normal to any viewing direction k_2 which is normal to the axis of symmetry.

Now let us determine what this result implies for the "inverse problem". In Section IV this was approached in two ways: by finite differences in the spatial domain, and analytically in the Fourier transform domain. First consider the latter. The data, $g(y')$ as was given in Section IV is

$$g(y') = \int_{-\infty}^{\infty} x' \frac{\partial f}{\partial y'} dx'$$

where x' is along the viewing direction and y' is normal to it. We have shown above that this is a <u>constant</u> for any given viewing direction i.e., fringes localize in a plane orthogonal to the viewing direction. When we use this fact in

$$\mathcal{F}_1\{g(y')\} = -v' \frac{\partial F}{\partial u'}\Big|_{u',0}$$

of Section IV, the result simply indicates that the transform is radially symmetric. This result is correct, but it does not contribute a reconstruction.

Similarly the spatial domain formulation leads to a set of algebraic equations which, from Section IV, we can represent as

$$\sum_{K=i}^{K} C_{ki} f_K = \lambda g_i$$

where the coefficients C_{ki} are determined by geometry and the finite difference representation of derivatives of $f = n - no$, f_k are the unknown values of f, and g_i are the data of fringe localization defined by

$$\lambda g_i = \lambda\left(x_i' / \Delta y_f'\right)$$

from Section IV. For simplicity, assume that we locate our coordinate origin at the axis of symmetry of the phase object. In this case $g_i = 0$, and the above equation will be homogeneous. Since there are no unknown parameters to serve as eigenvalues, this set will have no solutions. Again, the localization data cannot be inverted to determine n(r). We conclude that:

·The role of fringe localization in the case of radially symmetric phase objects is to disclose whether or not the phase object does indeed have radial symmetry. Radial symmetry is assured if, as the observer changes viewing direction about an axis, he observes that the fringes always localize in a plane which contains that axis and is normal to the viewing direction.

·By symmetry, the fringe pattern will be the same in any localization plane.

·Once radial symmetry is recognized by the localization effect, f(r) can be reconstructed by use of the Abel inversion technique to interpret fringe order data.

Inversion of Fringe Order Data

This section includes a listing of computer code, written in Hewlett Packard 9835, BASIC, which enables the user to interpret fringes formed by holographic interferometry of a radially symmetric transparent object field. Given the fringe pattern, the refractive index as a function of radius is computed. If diffuse illumination is used to form the interferogram, the analysis applies to the fringe pattern in the plane of localization. If collimated illumination is used, the analysis applies to the fringe pattern recorded by a camera focussed on the center plane of the radially symmetric object.

The computer code presented here is based on the discussion in the subsection on Inversion Techniques discussed in Section IV of this report (and applied via a prototype program above). Figure 13 depicts a fringe pattern and indicates the manner in which fringe order would be assigned to dark and bright fringes if the object has a refractive index which increases from n_o at the periphery to some maximum value at the center. The numbering scheme, for the fringe order data, would be the same, but all orders would be negative if the refractive index decreased toward the center. (In either case only the sign would be different.) The objective is to determine $f(r) \equiv n(r) - n_o$ in the horizontal plane which contains the line $\overline{aa}$ in figure 13. The data are to be plotted as shown at the bottom of this figure. Either graphically or by curve fitting, the operator should fit a smooth curve to the data as indicated. We assume that we deal with objects for which $f(r)$ goes smoothly to zero at some maximum radius R.

To prepare data for the computer program, the x axis is divided into a number of equal increments or widths Δx, and the values of fringe orders, N_i, are recorded at each point, $x(i)$. The number of intervals to be used cannot be specified by any rule. It depends largely on the smoothness and amount or density of data. The best approach is to use some exactly invertable function which is roughly similar to the object under study and to ascertain accuracy of reconstruction and sensitivity to data errors as a function of increment size prior to analyzing the experimental data.

The approximate reconstruction of $f(r)$ is effected by dividing the region of interest into discrete annular rings or zones of width Δr (which is identical to the width Δx of the data intervals along $\overline{aa}$). Following the detailed development in Section IV, Inversion Techniques, one can construct a linear system of equations relating the unknown values of $f(r)$ in each annulus to the discrete values of fringe order N_i. The approximation made in this approach is that $f(r)$ has a uniform value throughout the annular ring $r_i \leq r \leq r_{i+1}$. The set of equations can be denoted symbolically as

$$\sum_{K=i}^{I_{max}-1} A_{Ki} f_K = \left(\frac{\lambda}{2\Delta r}\right) N_i$$

The coefficients are given by

$$A_{Ki} = \left\{\left[(K+1)^2 - i^2\right]^{1/2} - \left(K^2 - i^2\right)^{1/2}\right\}$$

f_k is the vector of values of $f(r)$ to be computed, λ is the wavelength of the light employed, Δr is the increment in radius and N_i is the vector of data values.

The program fully prompts the user at each step. The procedure for using the program is:

1. Read the instructions which appear on the output device, carefully noting that the outermost radius must be one for which fringe order N = 0.

2. Enter "1" to continue execution.

3. The computer will prompt "How many data points will be entered?" Enter the <u>total</u> number of data points including both the center of the field and the outermost radius.

4. The computer will prompt "What is the radius of the outer fringe (N = 0) in mm?" Enter this value.

5. The computer will prompt "What is the wavelength of light in nm?" Enter this value in <u>nanometers</u> (e.g. 632.8 for He-Ne light).

6. The computer will prompt "Enter data as requested". It will then ask for the fringe order at each required radius. The operator enters each value, as read from the graph in figure 3, when requested.

7. The entered pairs of radius and fringe order are then displayed on the screen. The operator is asked to review the data, and is given explicit instructions for correcting any errors in the data and then continuing.

8. To alleviate operator boredom, the values of the coefficients A_{ki} are flashed on the screen as they are computed.

9. The computer will then pause as the system of equations is solved. The coefficient matrix of this system is triangular, so the solution is by a very simple and fast back substitution.

10. The results are displayed in the format:

"at R = 0, F = - - - - - at R = .2, F = - - - - -

at R = .3, F = - - - - - etc."

11. If another data set is to be analyzed, the program is simply rerun.

The BASIC program accompanying this report is of the simplest form possible. It can be upgraded easily to carry out more sophisticated Abel inversion algorithms if desired. Many other algorithms simply require that more complicated coefficients A_{ki} be used. Some other algorithms may have better suppression of experimental error; however, if a sufficient amount of smooth, accurate data are available, the accompanying code should be adequate.

SECTION VI

CONCLUSIONS

The phenomenon of fringe localization plays an important, fundamental and practical role in the analysis of holographic interferograms of opaque objects. An understanding of localization is important in all but the most trivial quantitative analysis of holographic interferometry in solid mechanics. This phenomenon of fringe localization also plays an increasingly important role in holographic interferometry of transparent mediums using diffuse backlighting arrangement. To date, however, its role in this casehas been insufficiently pursued. The analysis carried out by this effort suggests that there is a potentially important role for localization in the interpretation of diffuse illumination holographic interferograms of transparent media.

Information about the structure (that is, the spatial distribution) of changes of refractive index is displayed in two ways in a holographic interferogram:

(1) Fringe number, position and spacing,

(2) Fringe localization.

Traditionally, only data of the first kind has been used, however, the analyses presented in this report indicate that data of the second kind contain quantitative information about the object field which can be used in conjunction with fringe order data, or possibly alone, for the numerical reconstruction of refractive index fields.

It was pointed out in this report that there are two distinct localization problems:

(1) The Forward Problem: Given a refractive index distribution, determine the surface in which the fringes appear to localize when viewed from a specified direction.

(2) The Inverse Problem: Using measurements of fringe localization, determine the refractive index distribution (or use the measurements to augment the reconstruction based on fringe number, position, and spacing).

The forward problem was discussed in Section IV of this report. This work was basically an expansion, adaptation and clarification of work conducted by C.M. Vest, of the University of Michigan, under contract/consultant to the TAI Corporation for this purpose. Section IV also contains analysis of the inverse problem. To the best of our knowledge, this was the first treatment of this problem. It is useful at this point to review the conclusions of this report:

(1) The solution of the forward problem is given by equations (51) and (52) of Section IV. They describe the curve of fringe localization for a given distribution $f(x,y,z) = n(x,y,z) - n_0$. These two equations can also be written in the more compact, but not necessarily more convenient form of equations (67) and (68) of Section IV.

(2) There are cases in which the refractive index field cannot be reconstructed from localization data alone. An obvious example is a radially symmetric field, for which fringes localize in the center plane for all viewing directions. This does not provide sufficient data for reconstruction. However, it does provide sufficient data for specific structure resolution and thereby indicates the inversion technique to

be employed for reconstruction.

(3) For the general case of asymmetric fields, it is possible to formulate a linear algebraic set of equations, (see Section IV), which relate refractive index change to measured values of localization position. It appears that these can, in principle, be used to reconstruct refractive index fields, except in special cases. In any event, they increase the available information and might be combined with the usual fringe order equations to improve accuracy and error suppression when only a limited range of viewing angles is available.

(4) If Fourier reconstruction methods are used to invert fringe order data, fringe localization data, in principle, provide information for increasing accuracy of interpolation in the transform plane.

(5) Localization data might be used in an iterative reconstruction scheme. That is, at each step one could calculate the fringe localization position based on the field reconstructed from fringe order data and check for agreement with measured values of localization position.

(6) The phenomenon of fringe localization is always helpful in the sense that it discloses symmetries of the field, assists the viewer in locating the field in space, and helps one to form a quantitative impression of the structure of the field.

(7) An exhaustive literature search was performed and the analysis of this literature is provided in Section II.

(8) The simulated HOSS system, which was constructed during this effort, was successfully employed to provide the determination of feasibility and application of localized fringes. Multiple holograms

of various phase objects were constructed and their data and analysis are included in this report.

SECTION VII

RECOMMENDATIONS FOR FURTHER STUDY

This report has treated the problem of localized fringes in the holographic interferometry of transparent media. In so doing it has provided solutions to the two specific areas of what is called the Forward Problem and the Inverse Problem. Treatment of the forward problem was handled rather generally, but the general equations were rather complicated. Treatment of the inverse problem, of necessity, was not as successful for the general case. However, use of the special but important case of a radially symmetric disturbance did prove to be successful, and quantitative analysis was performed for this case.

We feel that the general state of knowledge on this subject is adequately represented in this report. However, we further feel that this state of knowledge is itself inadequate for the appropriate realization of the apparent potential that this subject holds for the investigation of fluid flow visualization. We further feel that the effort spent on this investigation by the TAI Corporation personnel has allowed us to specify areas in which further investigation should prove most beneficial to the appropriate understanding and realization of the potential of this area of knowledge and its application to the investigation of fluid flow visualization.

Specifically the areas needing further investigation are:

(1) Write the equation for depth of localization and relate it to fringe spacing.

(2) Computer program for localized formulation.

(3) Relation of localization to reconstruction theory.

(4) Effects on localization of refraction.

(5) What are the limitations due to fringe resolution.

(6) Difference between real and virtual images.

(7) Investigate absolute localization.

(8) The effect of aperture geometry and orientation on the extraction of information from localized fringes.

(9) Further effort to attempt the simplification of the general localization equations.

(10) Pursue other approaches to the solution and simplification of the general inverse problem.

We wish to thank the NASA for allowing us the opportunity to work with them on this important problem and wish to request their sincere consideration of the necessity for performing the further study indicated above.

APPENDIX I

Sample Problem

An artificially contrived test problem which can be used to check the program user procedure is: Maximum radius = 1, No. of data = 11, Wavelength = 1E6

DATA: x	N(x)	RESULTS: r	f(r)
0	3000	0	2082.35
.1	2960.1	.1	2052.08
.2	2841.6	.2	1982.01
.3	2648.1	.3	1874.42
.4	2385.6	.4	1730.76
.5	2062.5	.5	1552.4
.6	1689.6	.6	1340.49
.7	1280.1	.7	1095.17
.8	849.6	.8	813.018
.9	416.1	.9	477.299
1.0	0	1.0	0

FIGURES

FOR

SECTION III

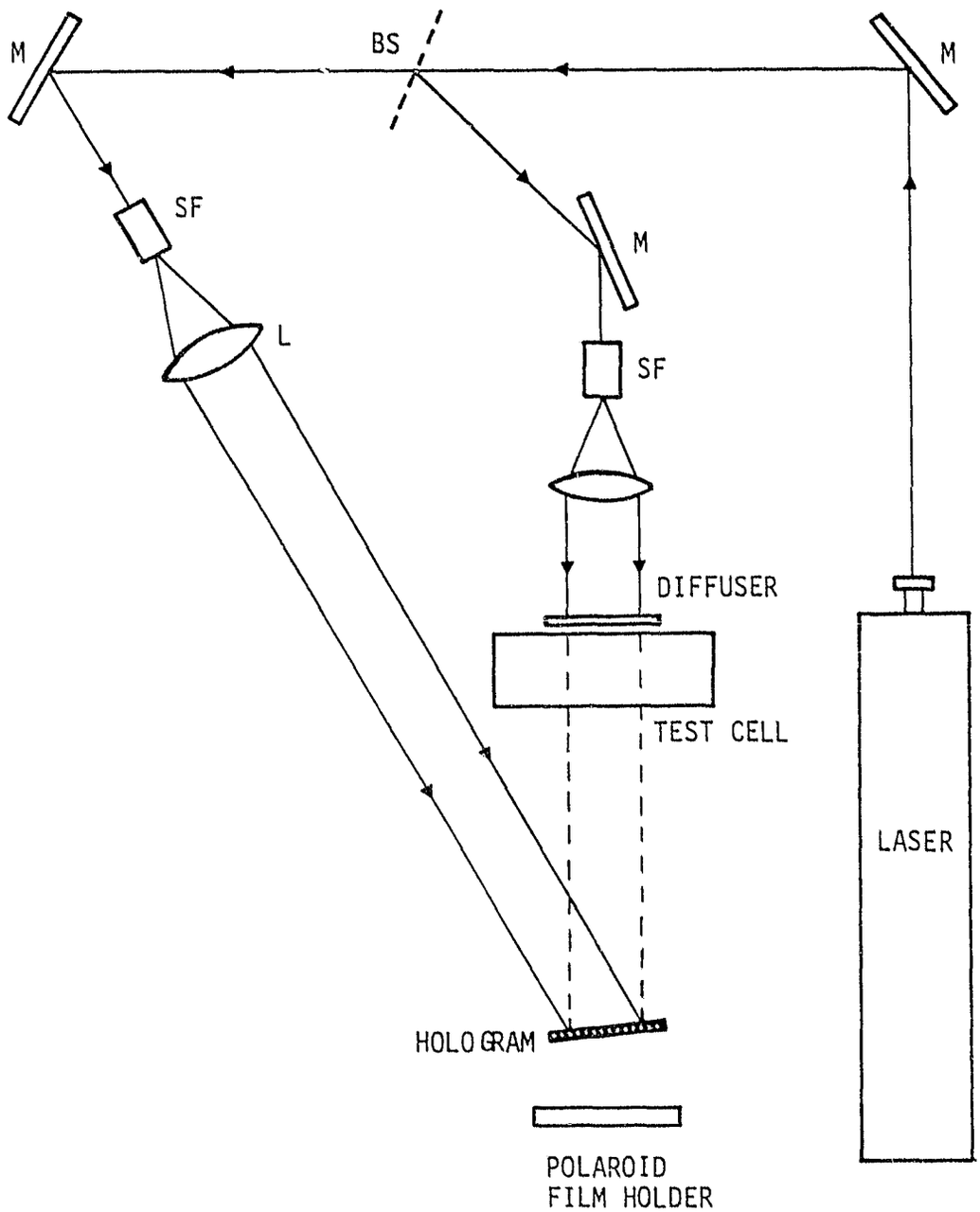

Fig. 1 Typical side band holographic arrangement used to show the feasibility of fringe localization.

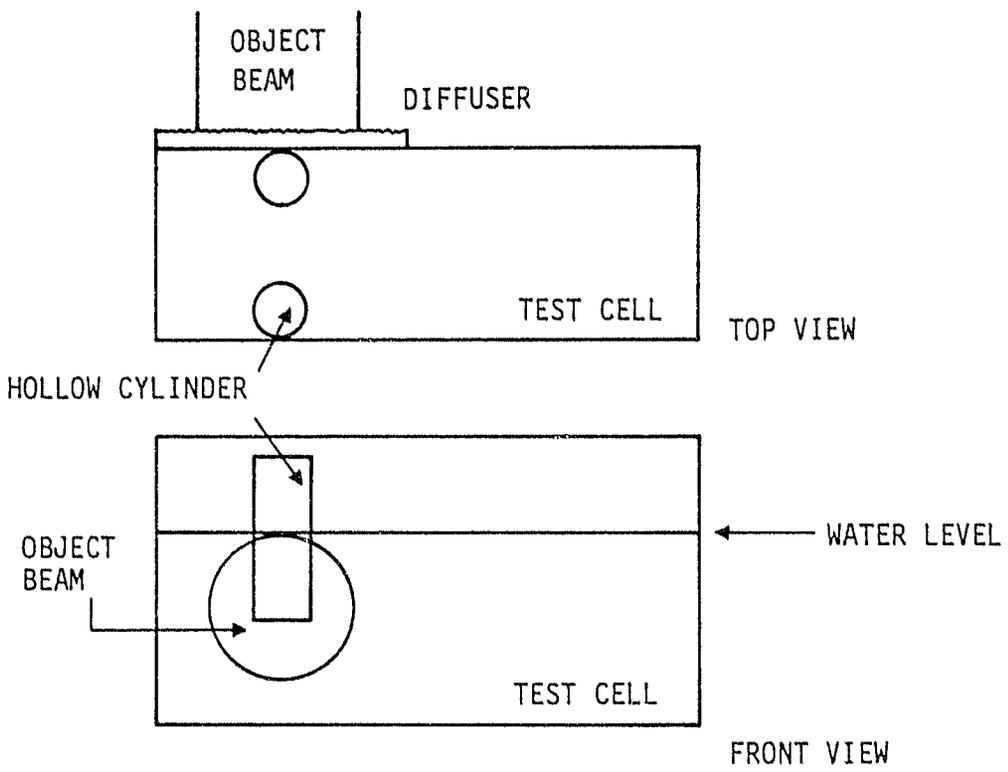

Fig. 2 Test cell with two hollow cylinders in place.

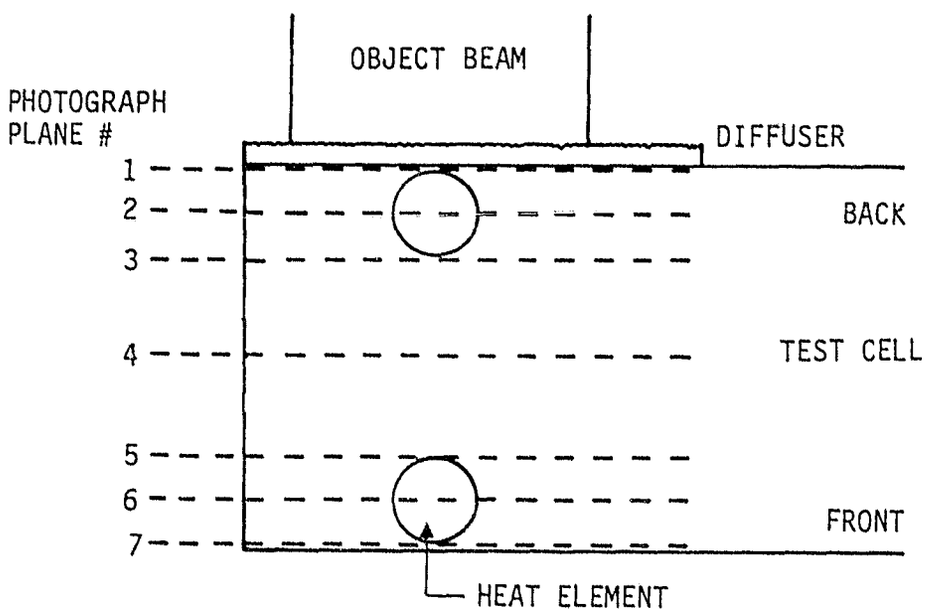

Fig. 3 Real image sample planes

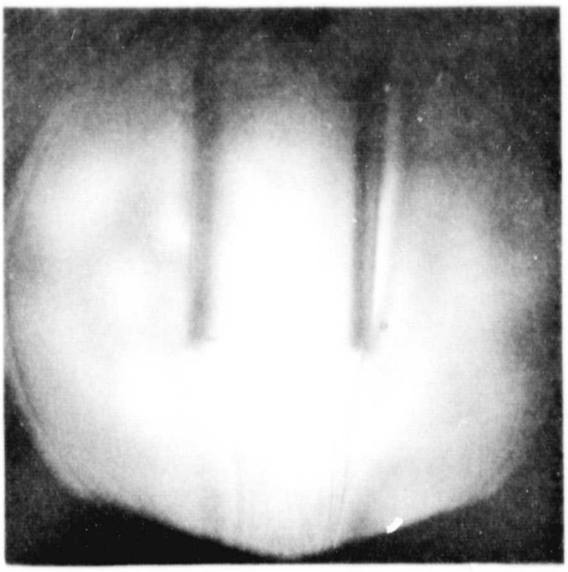

PLANE 1

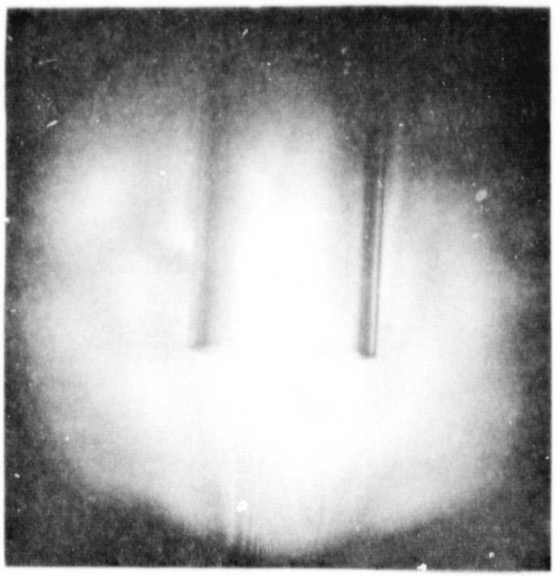

PLANE 2

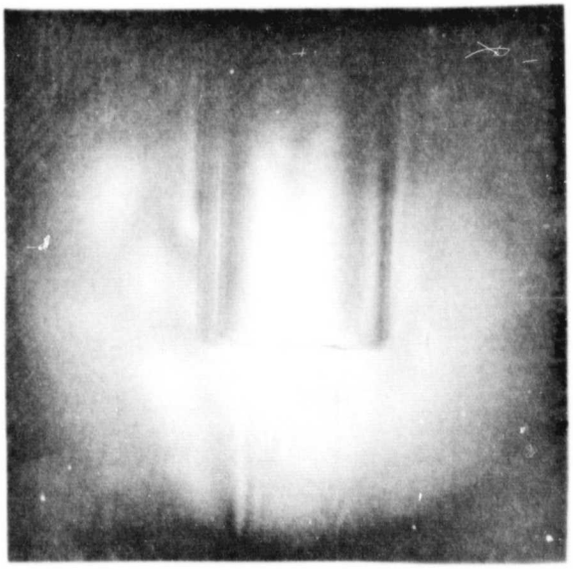

PLANE 3

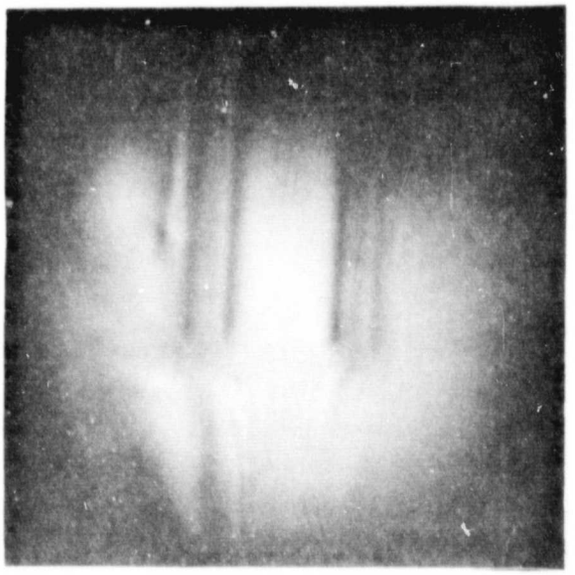

PLANE 4

Fig. 4 Photographs of real image planes shown in Fig. 3

PLANE 5

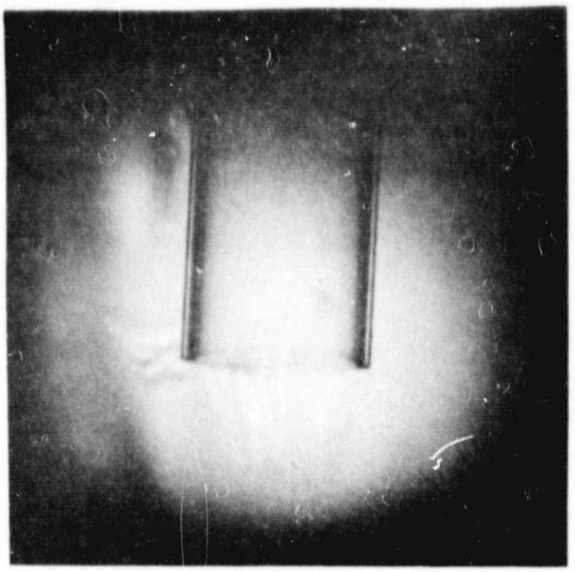

PLANE 6

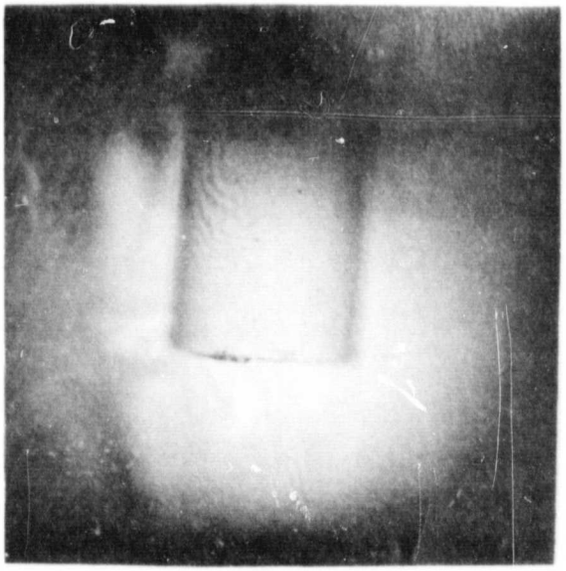

PLANE 7

Fig. 4 cont.

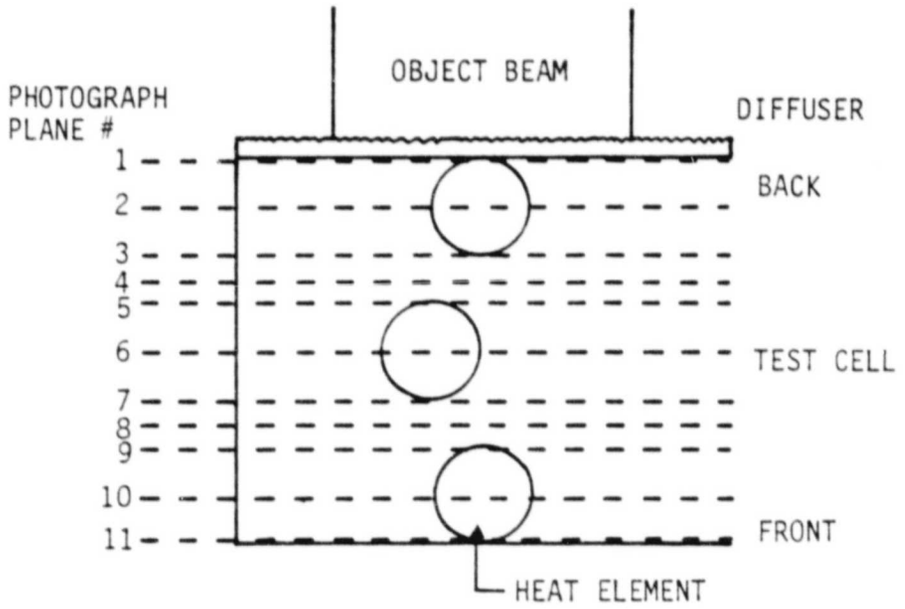

Fig. 5 Real image sample planes

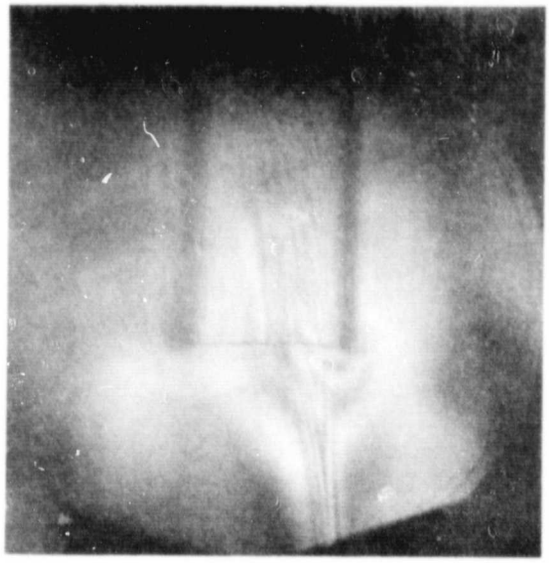

PLANE 1

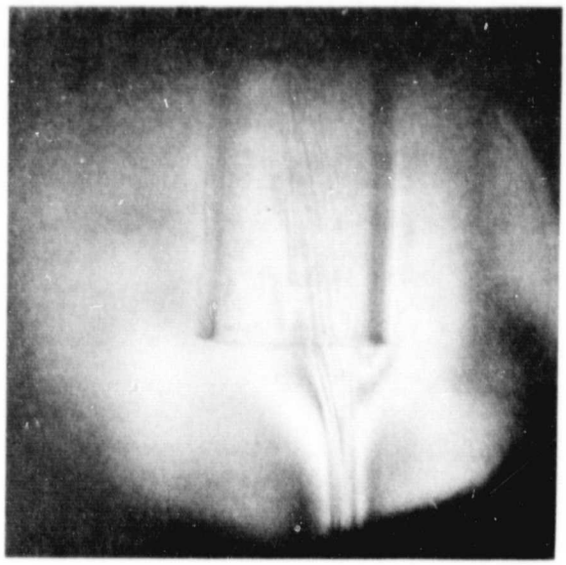

PLANE 2

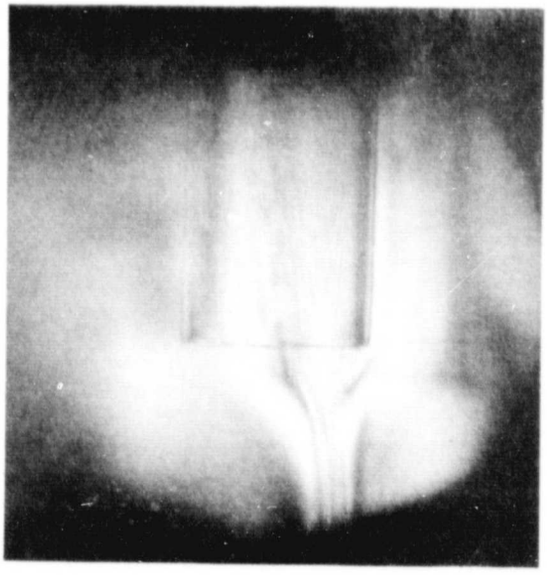

PLANE 3

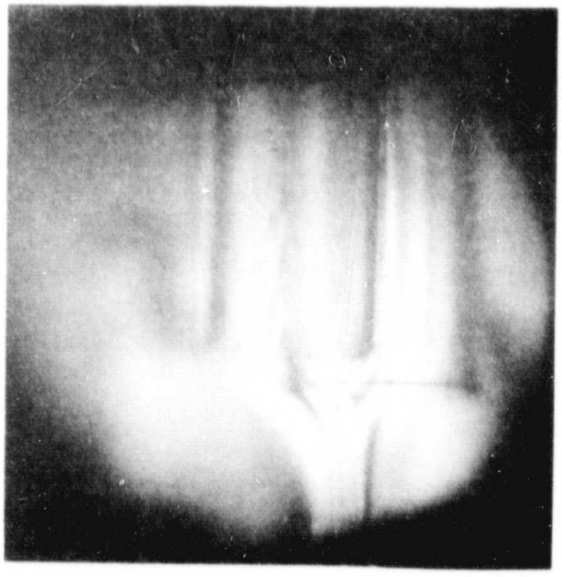

PLANE 4

Fig. 6 Photographs obtained from Fig. 5

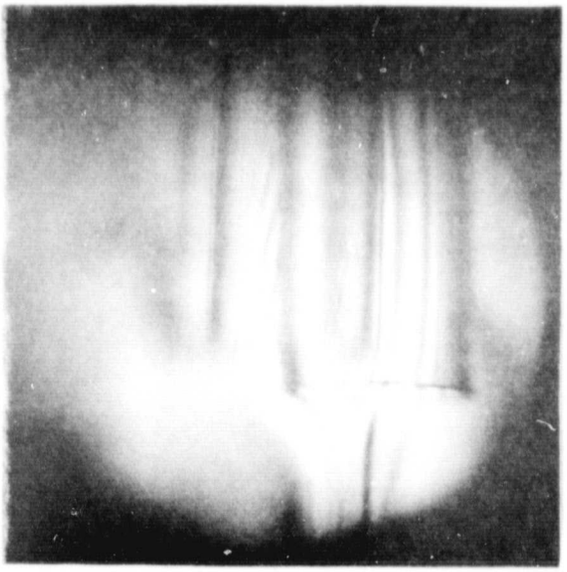

PLANE 5

PLANE 6

PLANE 7

PLANE 8

Fig. 6 cont.

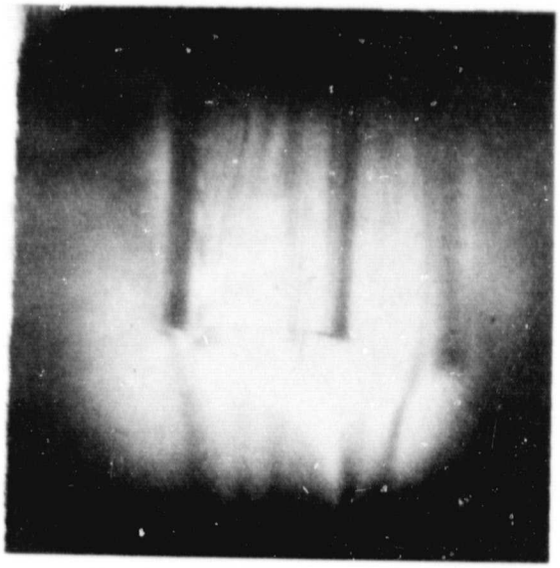

PLANE 9

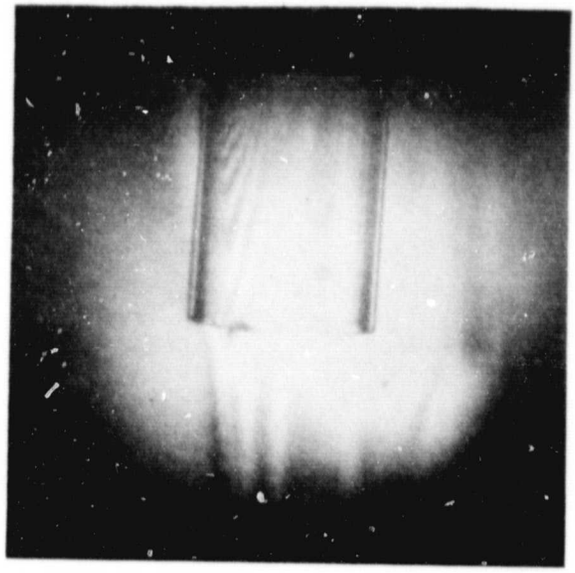

PLANE 10

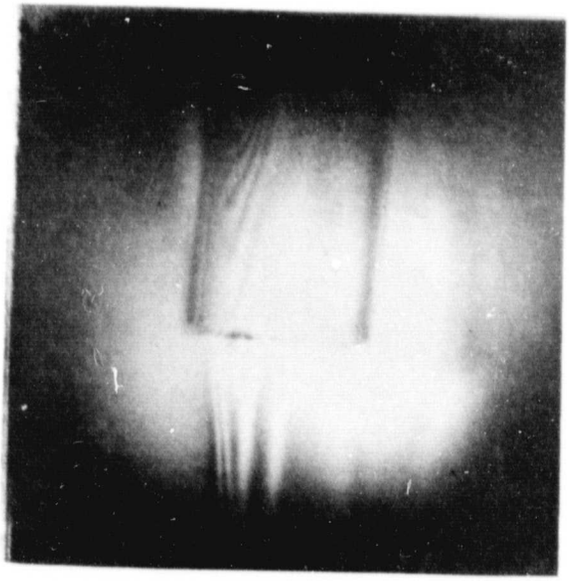

PLANE 11

Fig. 6 cont.

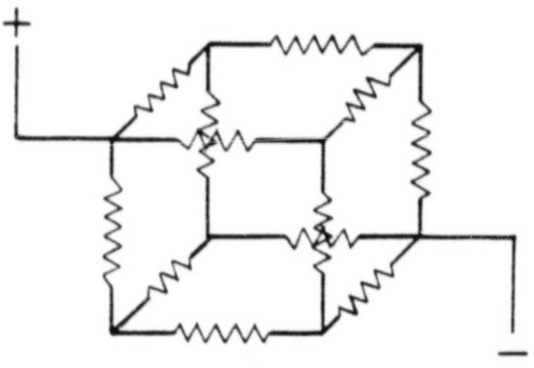

Fig. 7 Resistor-simulated crystal

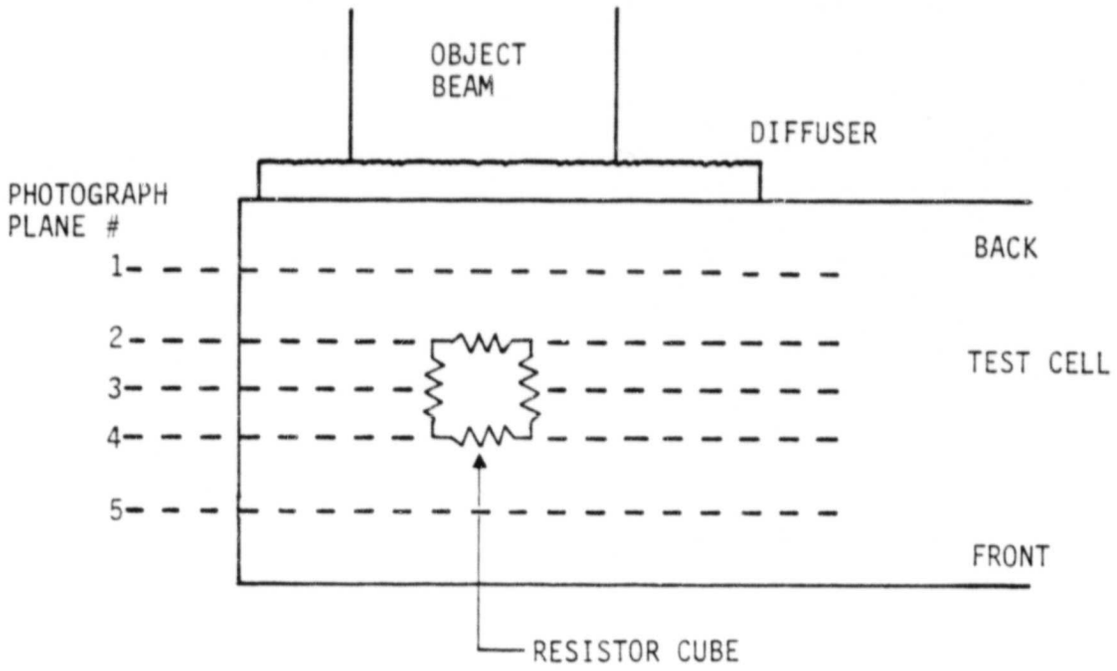

Fig. 8 Photographic planes of real image

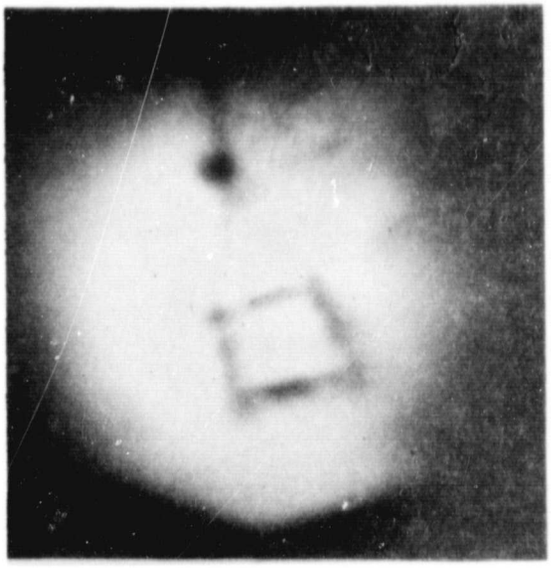

PLANE 1

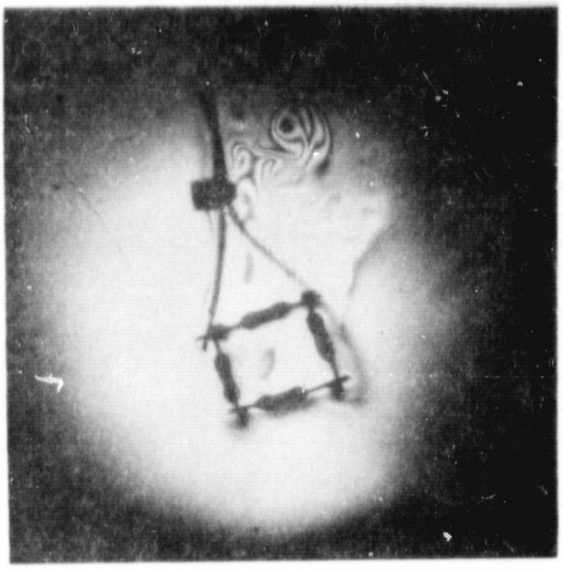

PLANE 2

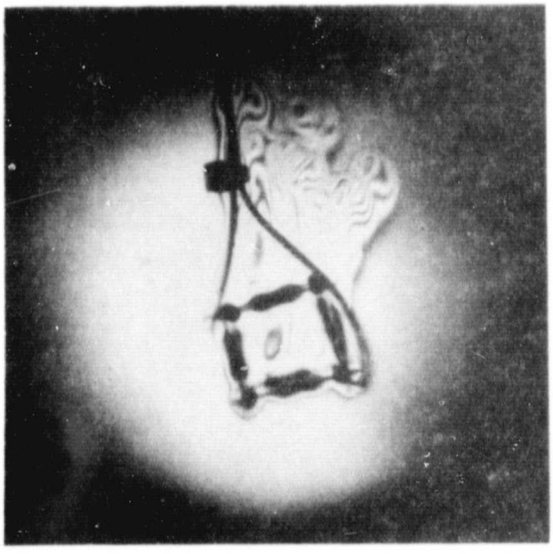

PLANE 3

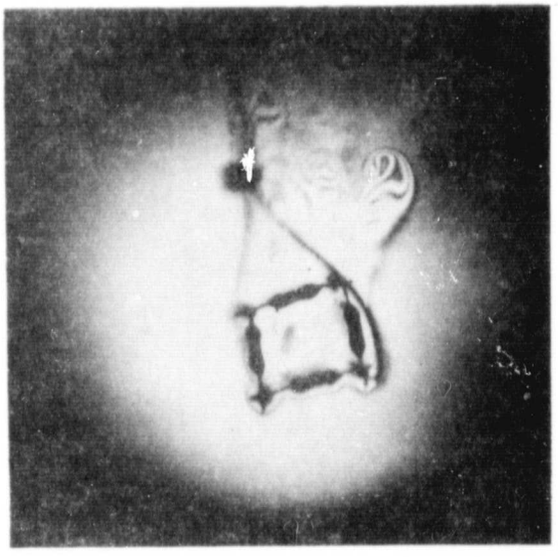

PLANE 4

Fig. 9 Photographs showing the planes of Fig. 8

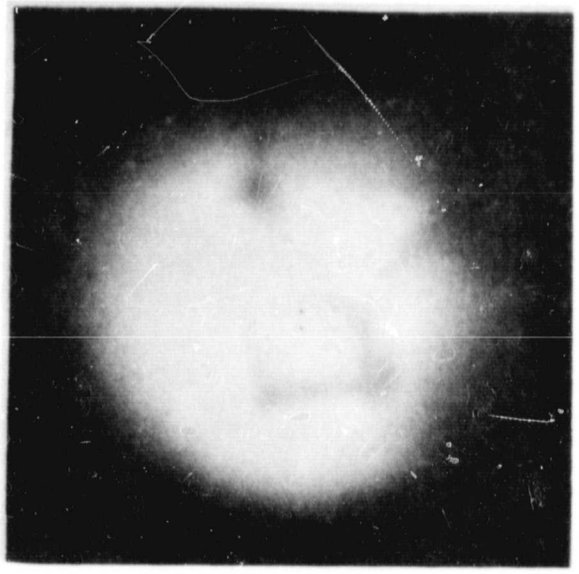

PLANE 5

Fig. 9 cont.

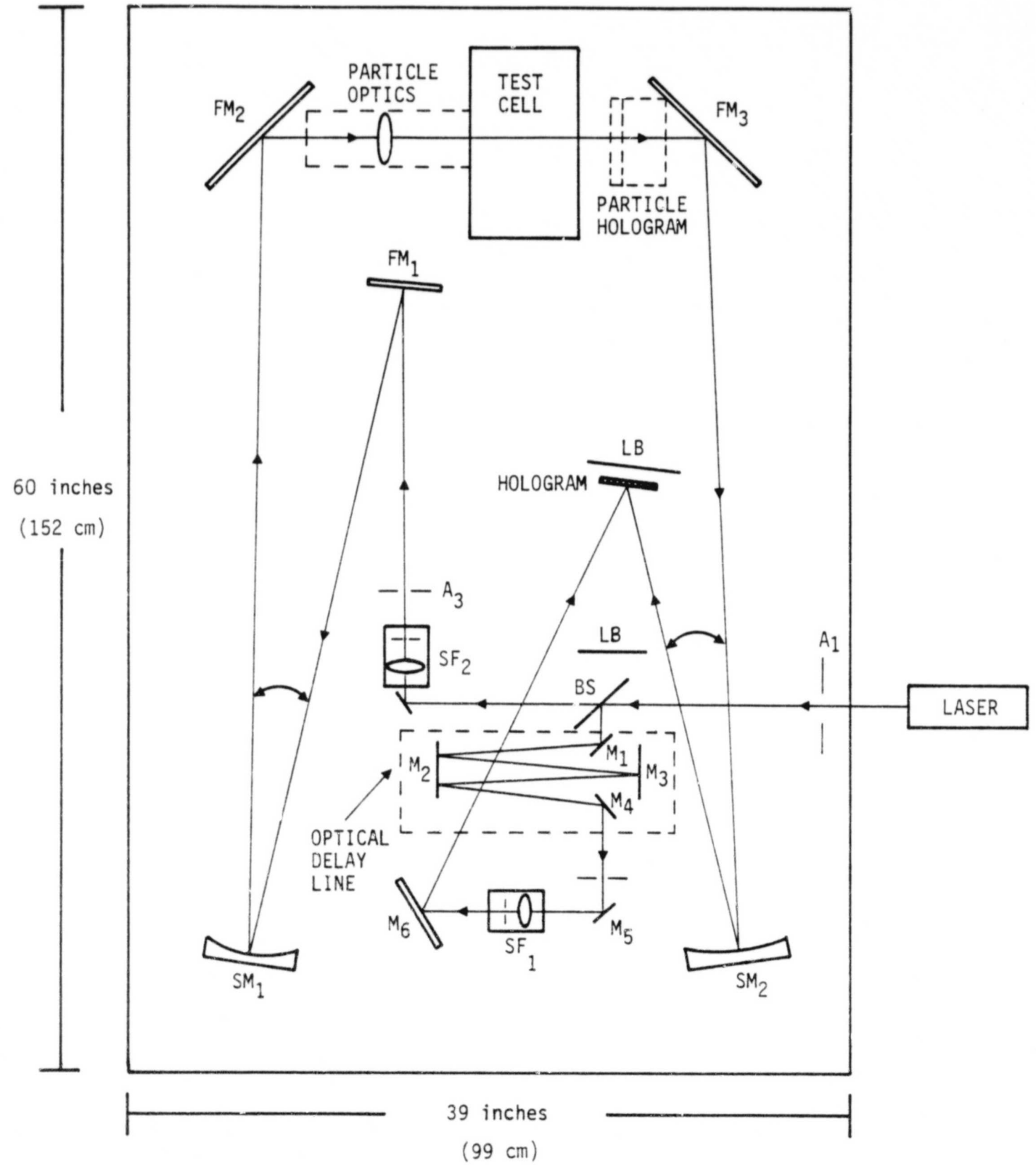

Fig. 10 Present HOSS configuration

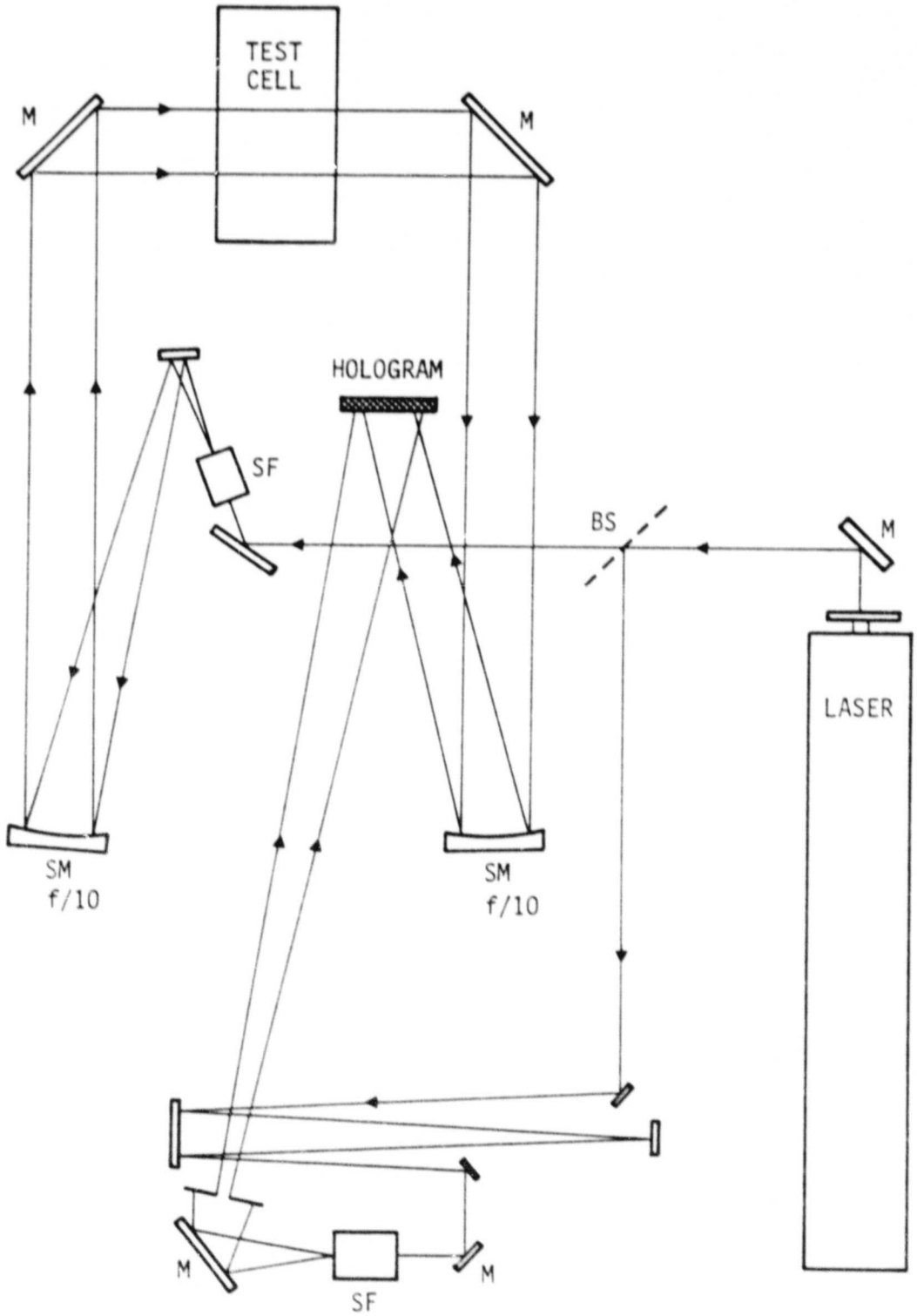

Fig. 11 Scaled-down version of the HOSS employing half-size optics.

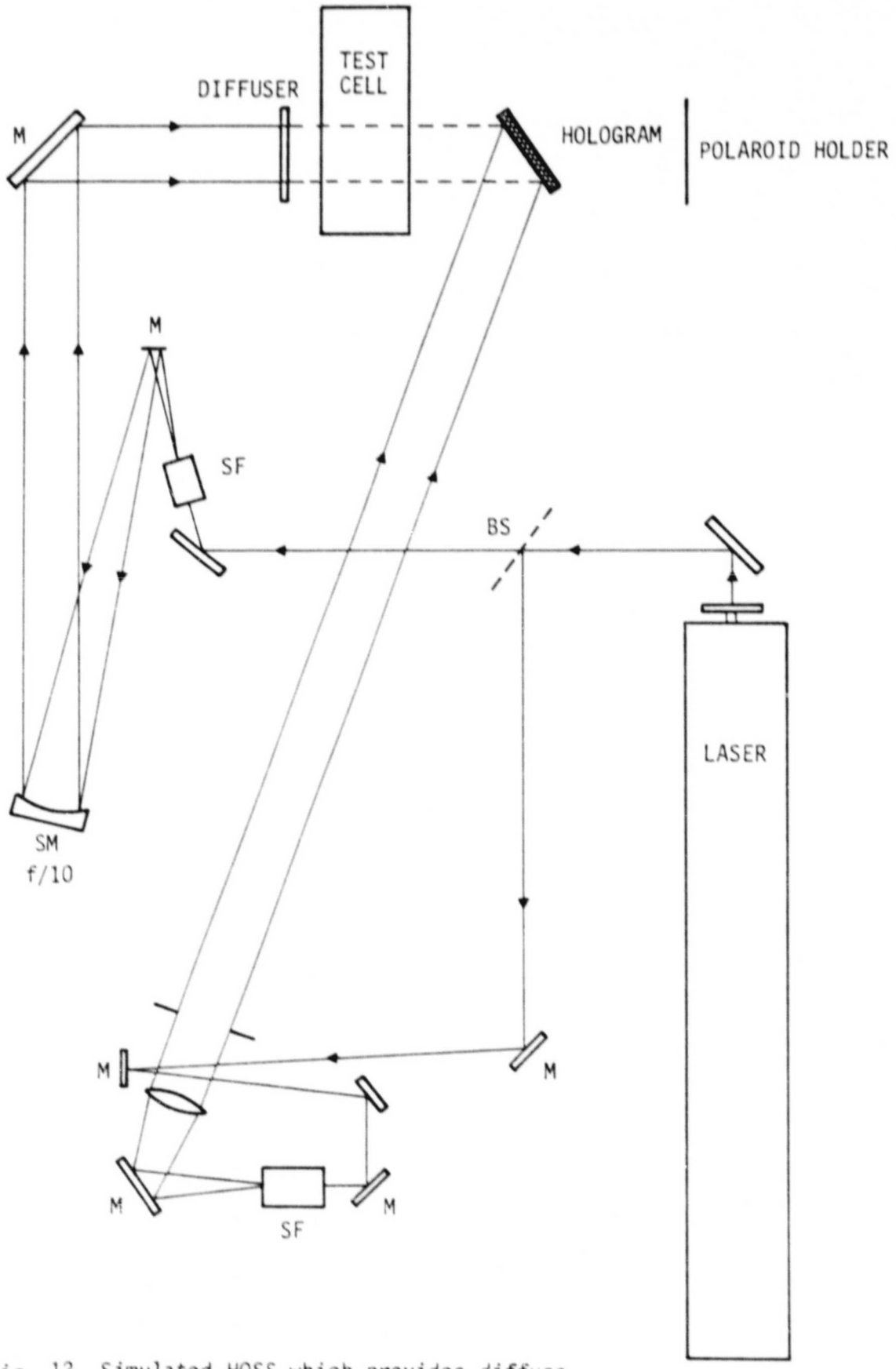

Fig. 12 Simulated HOSS which provides diffuse illumination of object.

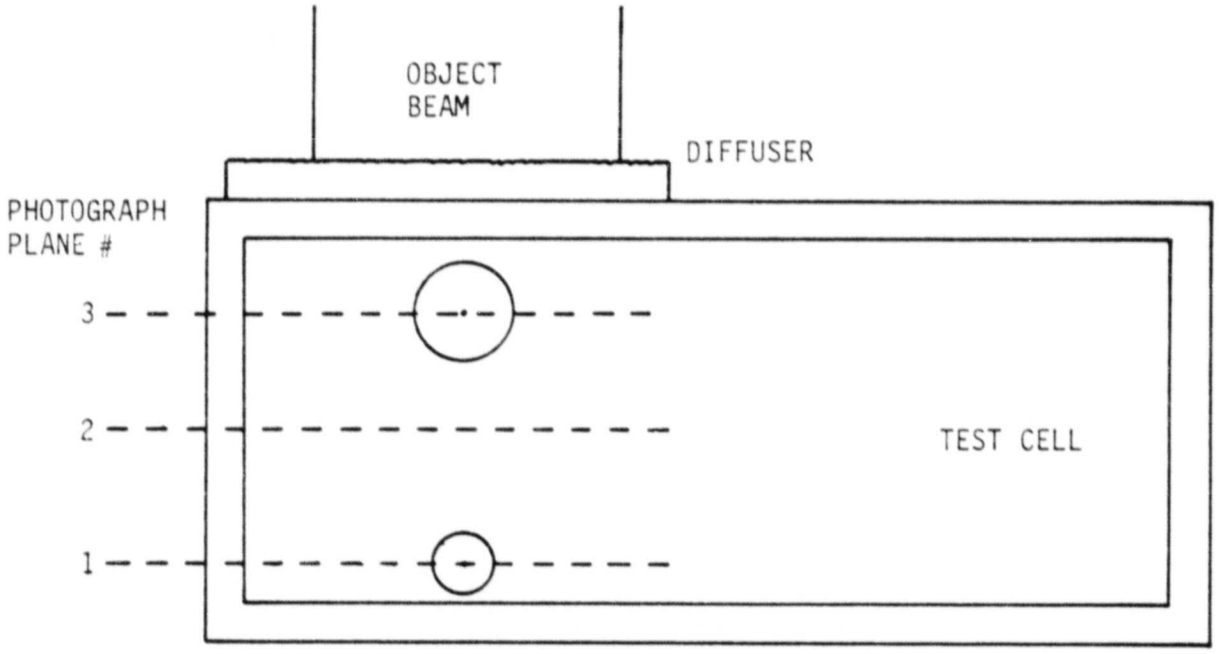

Fig. 13 Location of large and small heating elements in test cell.

PLANE 3

PLANE 2

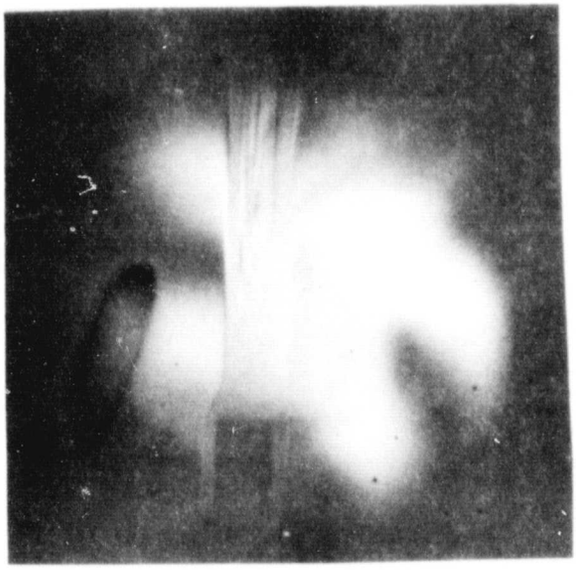

PLANE 1

Fig. 14 Fringes obtained when heat was applied to elements for 30 seconds.

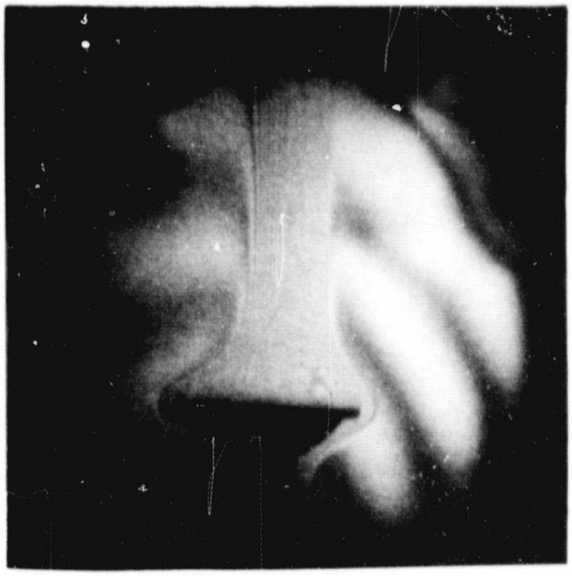

PLANE 3

PLANE 2

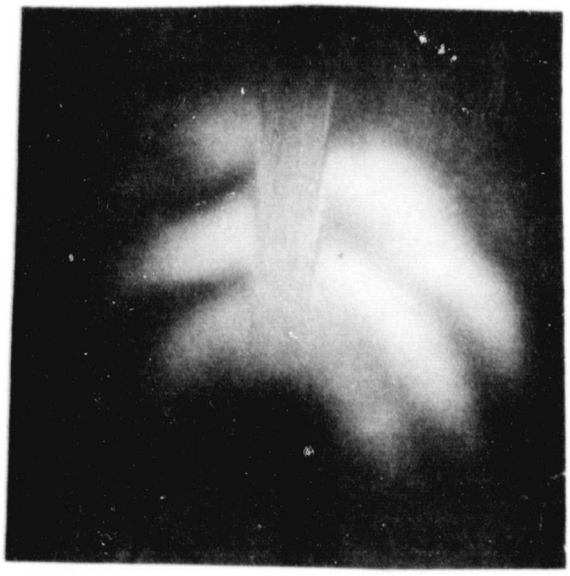

PLANE 1

Fig. 15 Fringes obtained when elements were heated for 60 seconds.

PLANE 3

PLANE 2

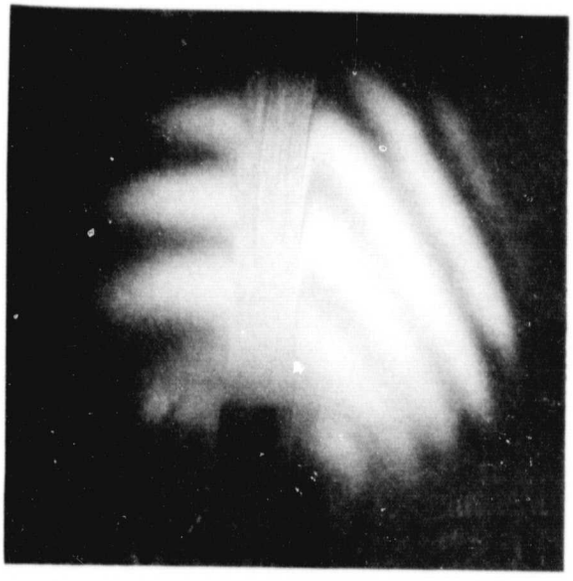

PLANE 1

Fig. 16 Fringes obtained when elements were heated for 90 seconds.

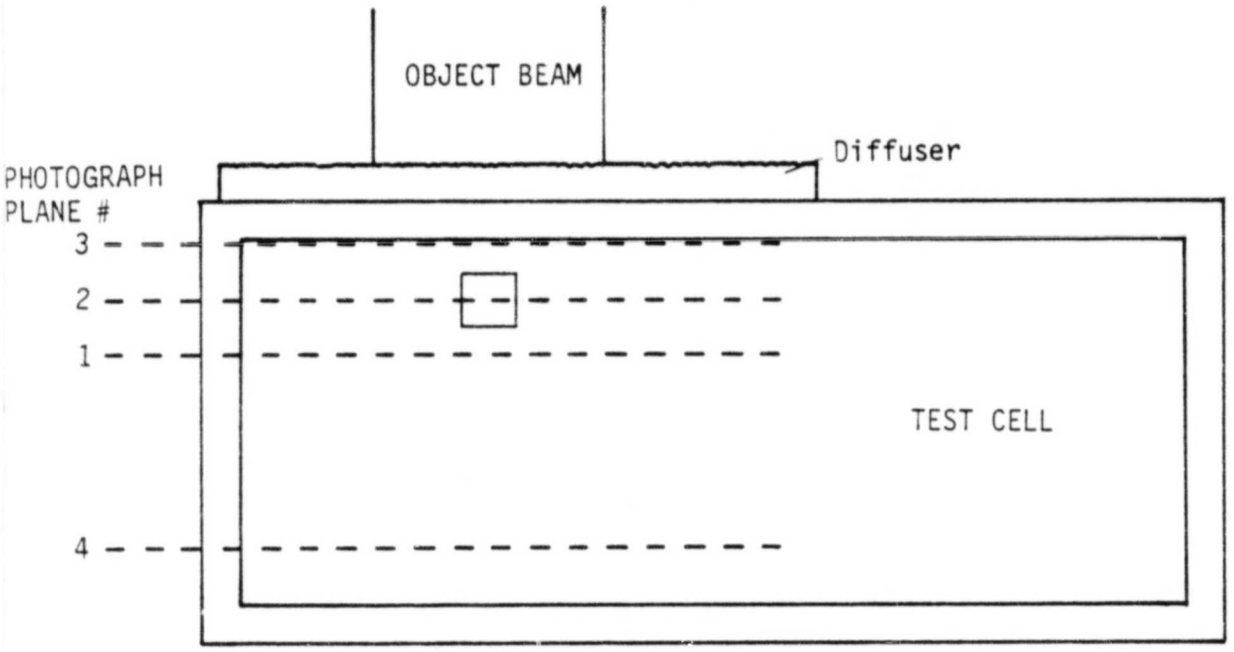

Fig. 17 Location of photograph planes

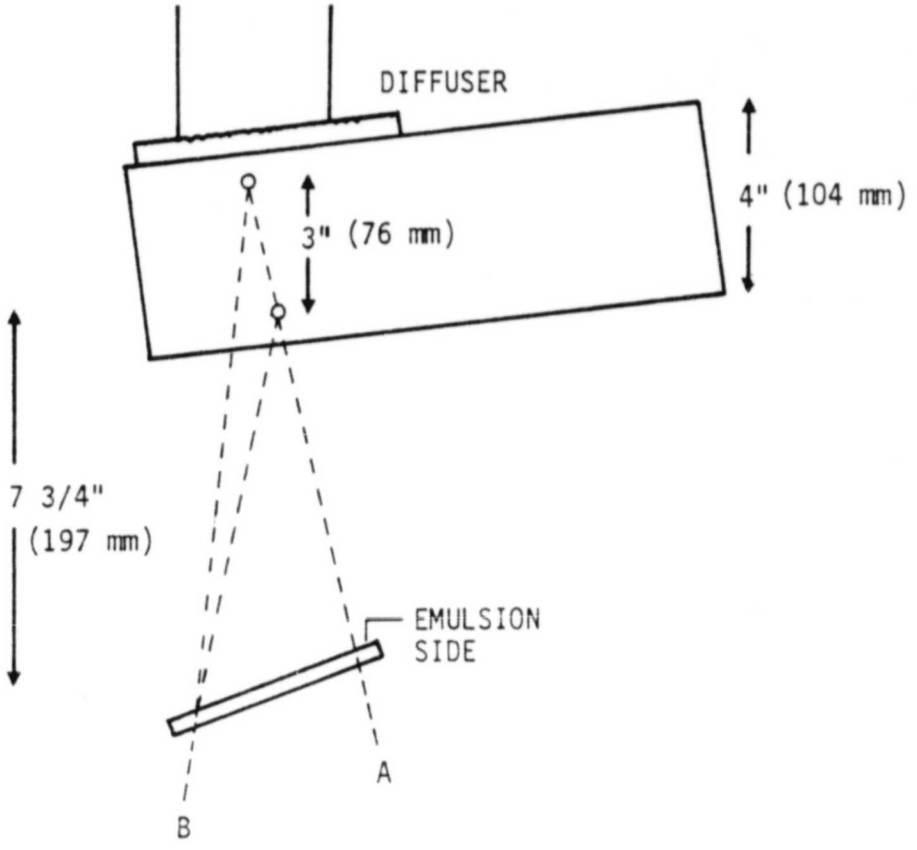

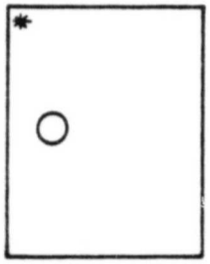

PHOTOS 1 & 2

A

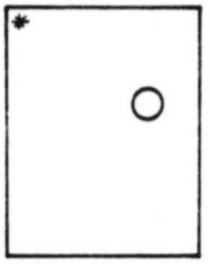

PHOTOS 3 & 4

B

Fig. 19 Fringe localization and parallax planes

PLANE 1

PLANE 2

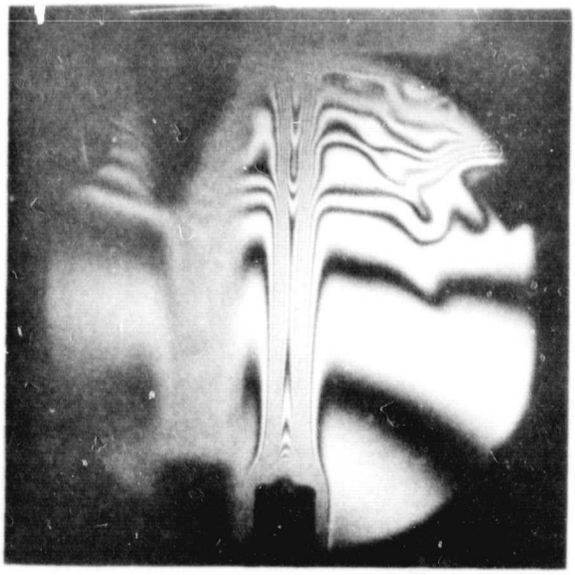

PLANE 3

PLANE 4

Fig. 20 Photographs of planes shown in Fig. 19

FIGURES

FOR

SECTION IV

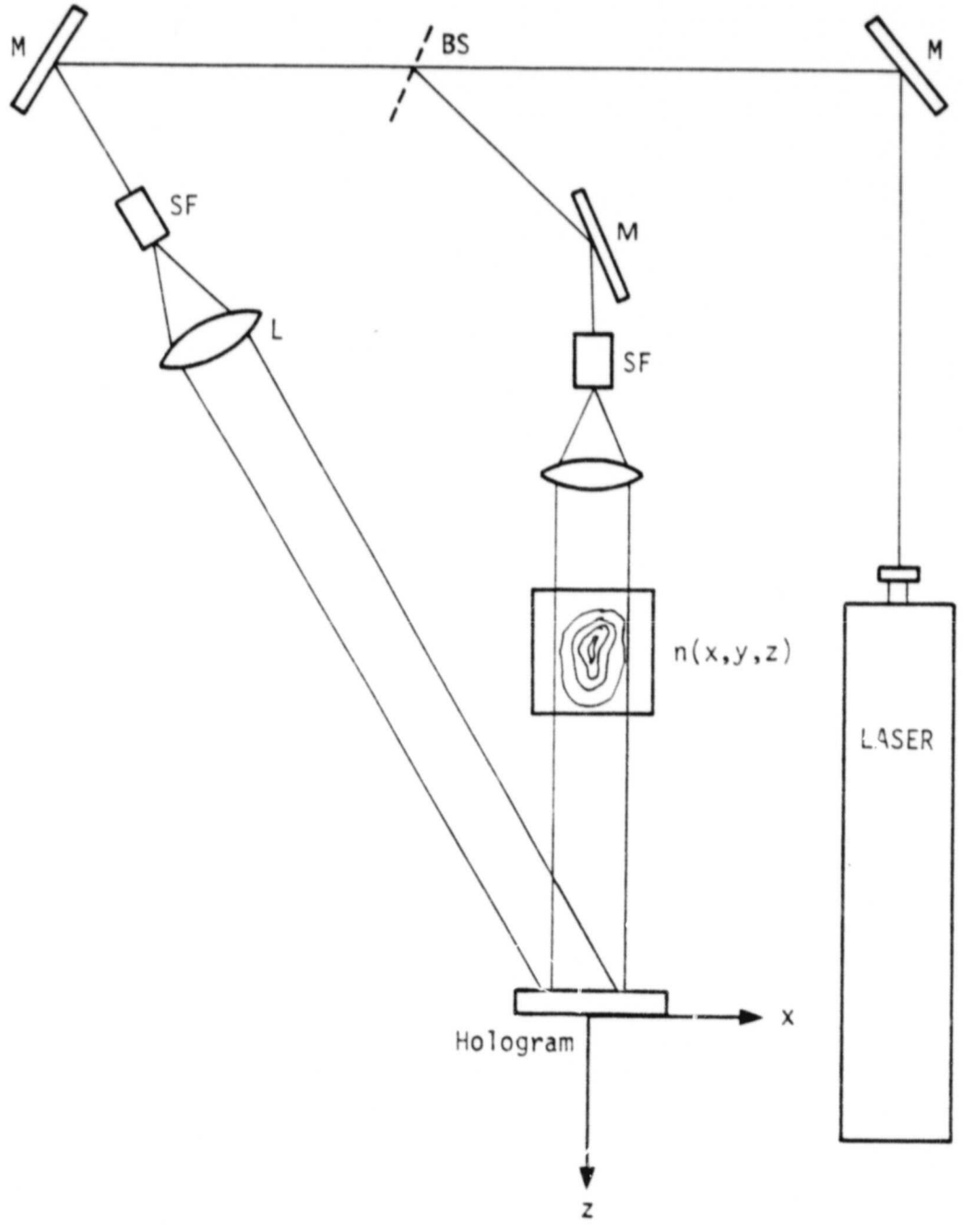

Figure 1. Typical side band holographic arrangement

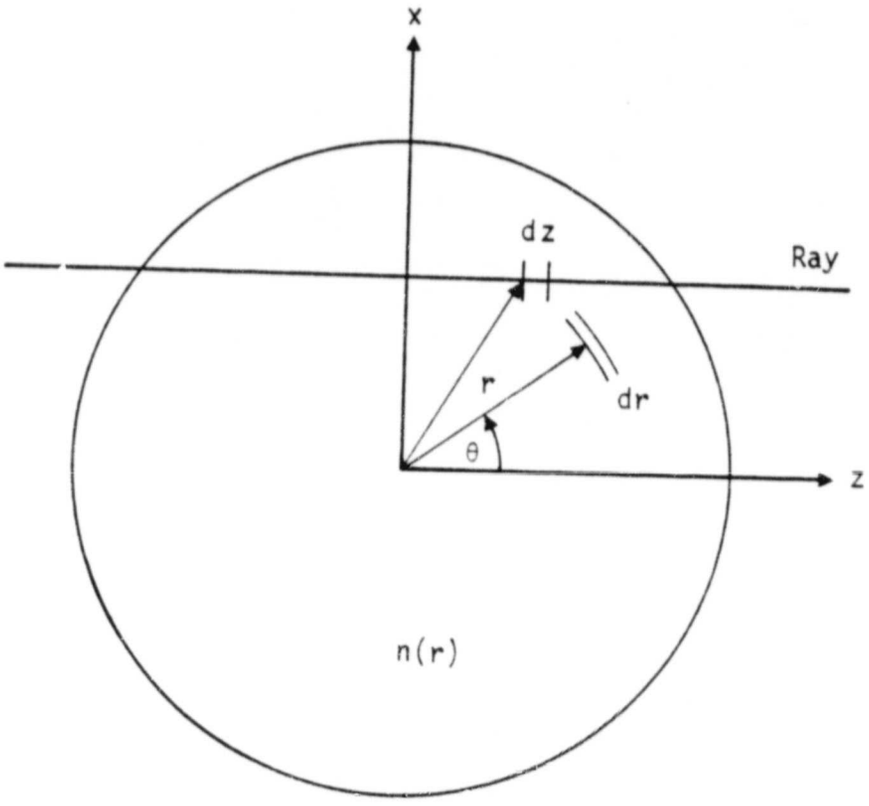

Figure 2. Schematic for radially symmetric phase object notation.

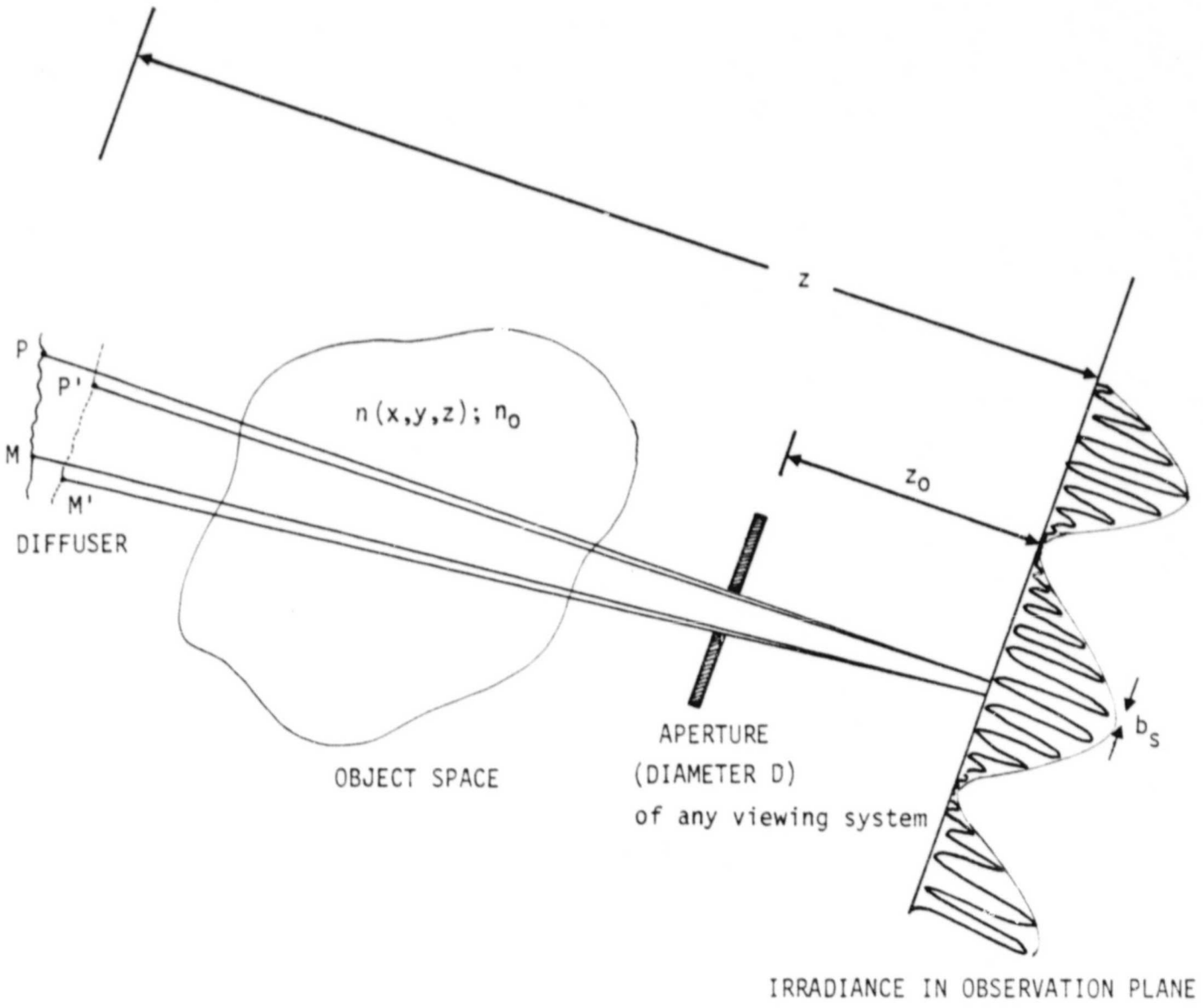

Fig. 3. Schematic diagram of fringe formation from phase object space.

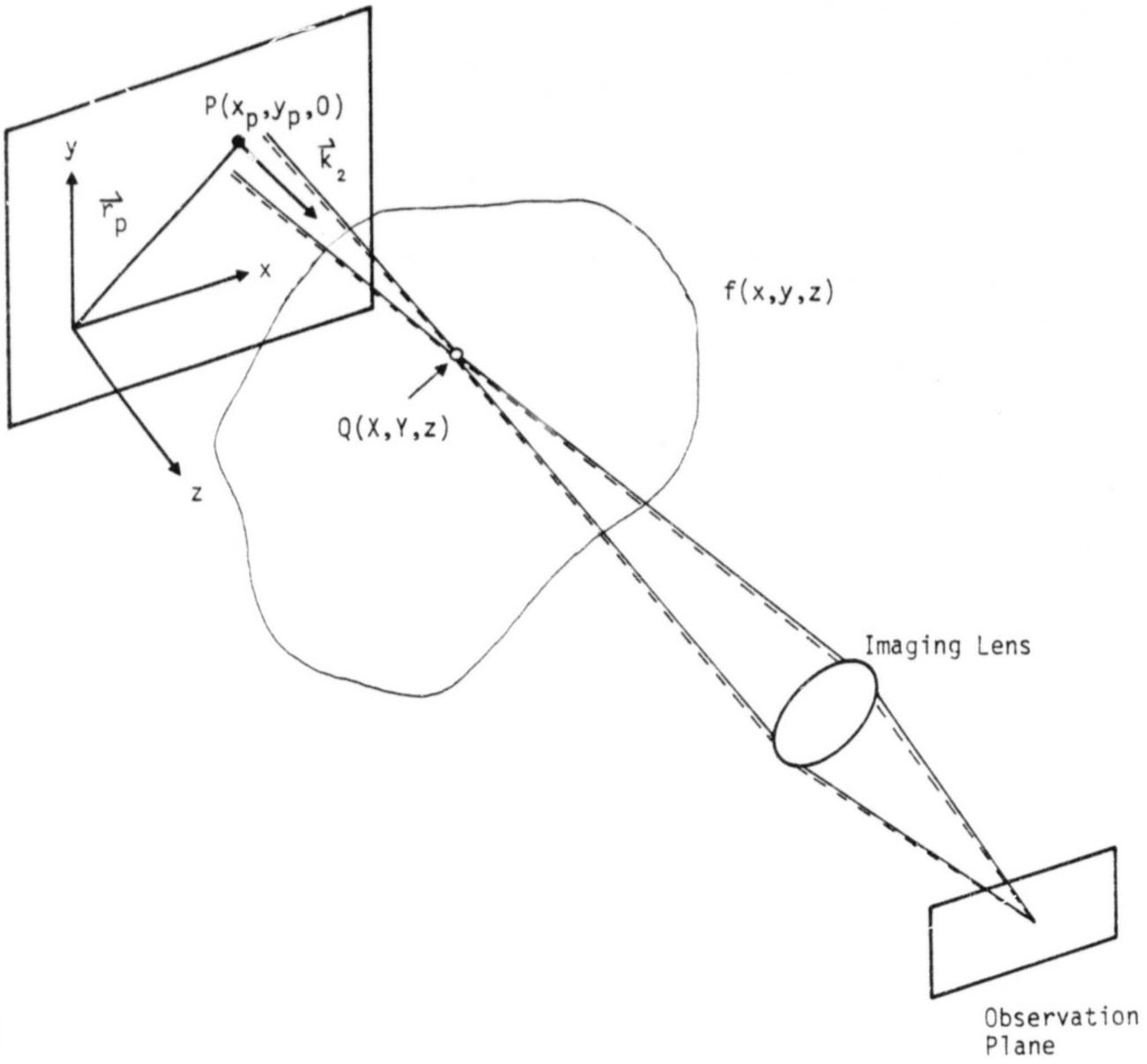

Fig. 4. Notation diagram for derivation of fringe localization equations.

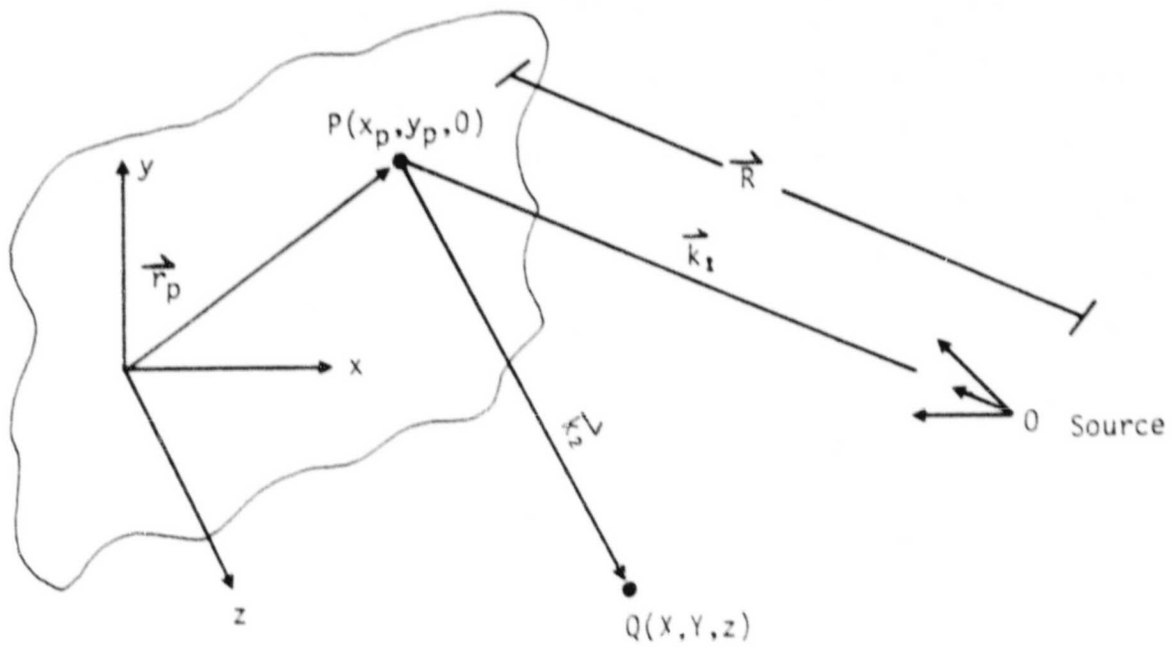

Figure 5. Nomenclature for analysis of fringe localization. Points P and Q correspond to P and Q in figure 2. 0 is the illumination source.

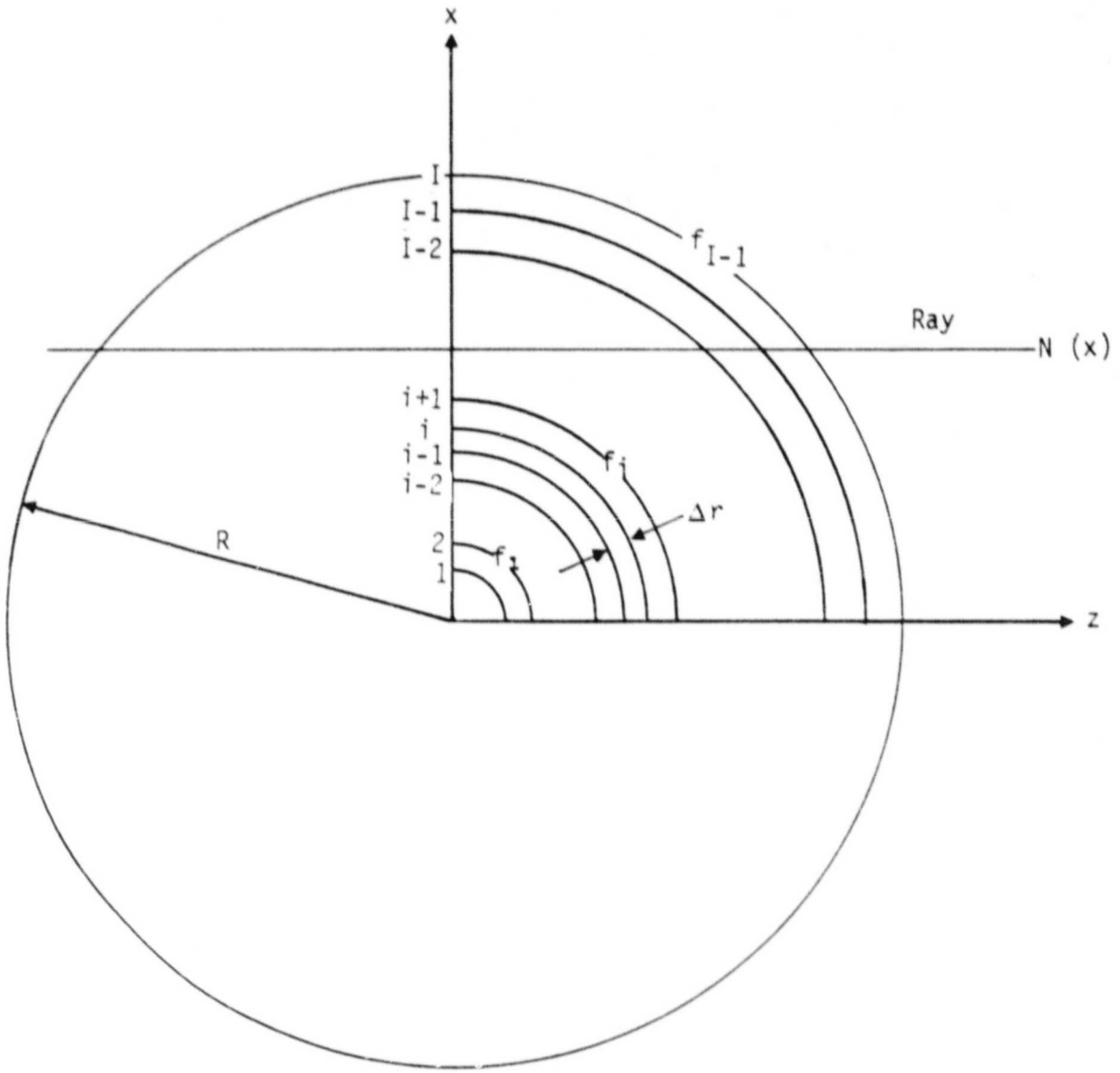

Figure 6. Cross section of a radially symmetric phase object divided into discrete annular elements of width Δr.

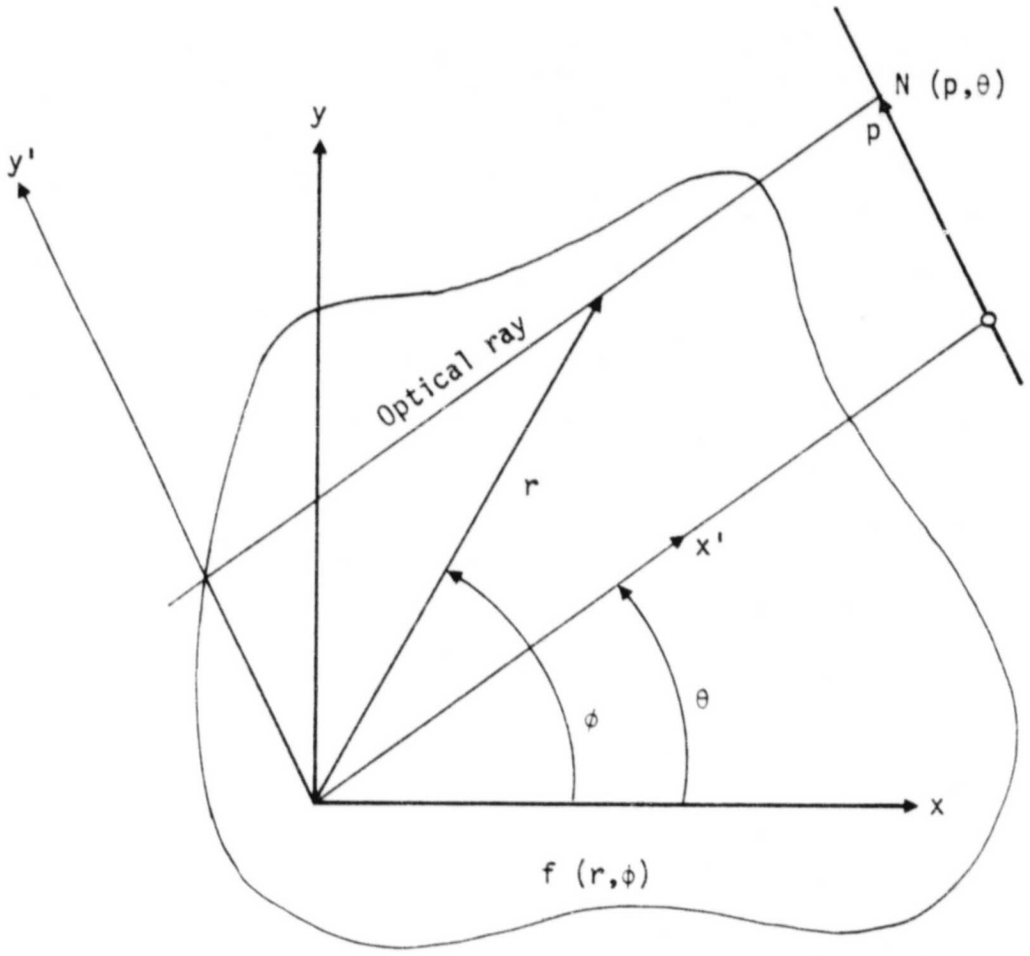

Figure 7. Notation for equations (77) and (78). A typical optical ray is shown passing through an asymmetric phase object $f(r,\phi)$ and impinging on a particular observation plane where an interferogram is recorded. Here θ defines the observation direction, and p locates a probing ray oriented in this direction.

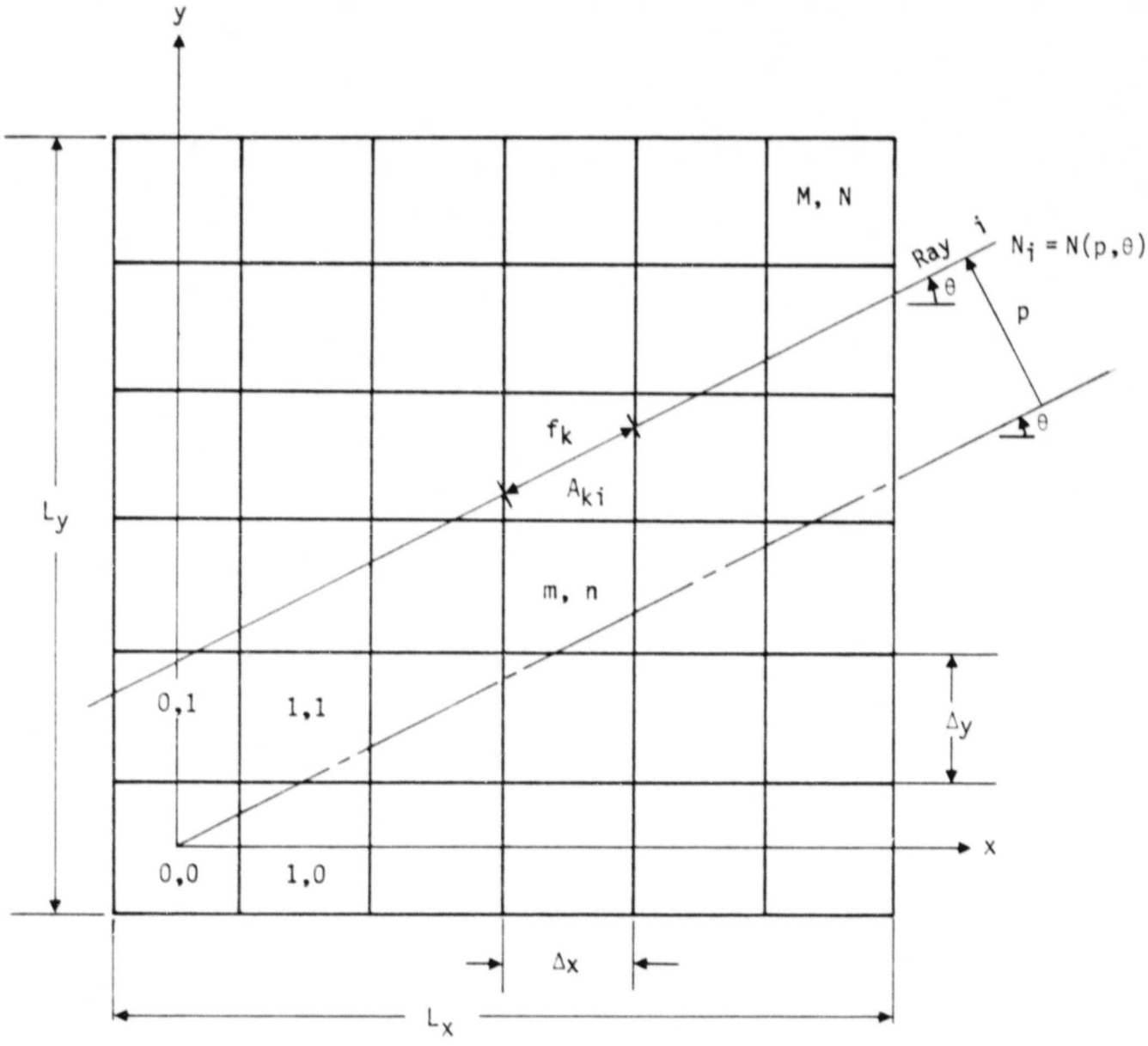

Figure 8. Cross section of an asymmetric phase object divided into discrete rectangular elements of dimension $\Delta_x X \Delta_y$. A typical probing ray, denoted by the index i, is shown traversing the object.

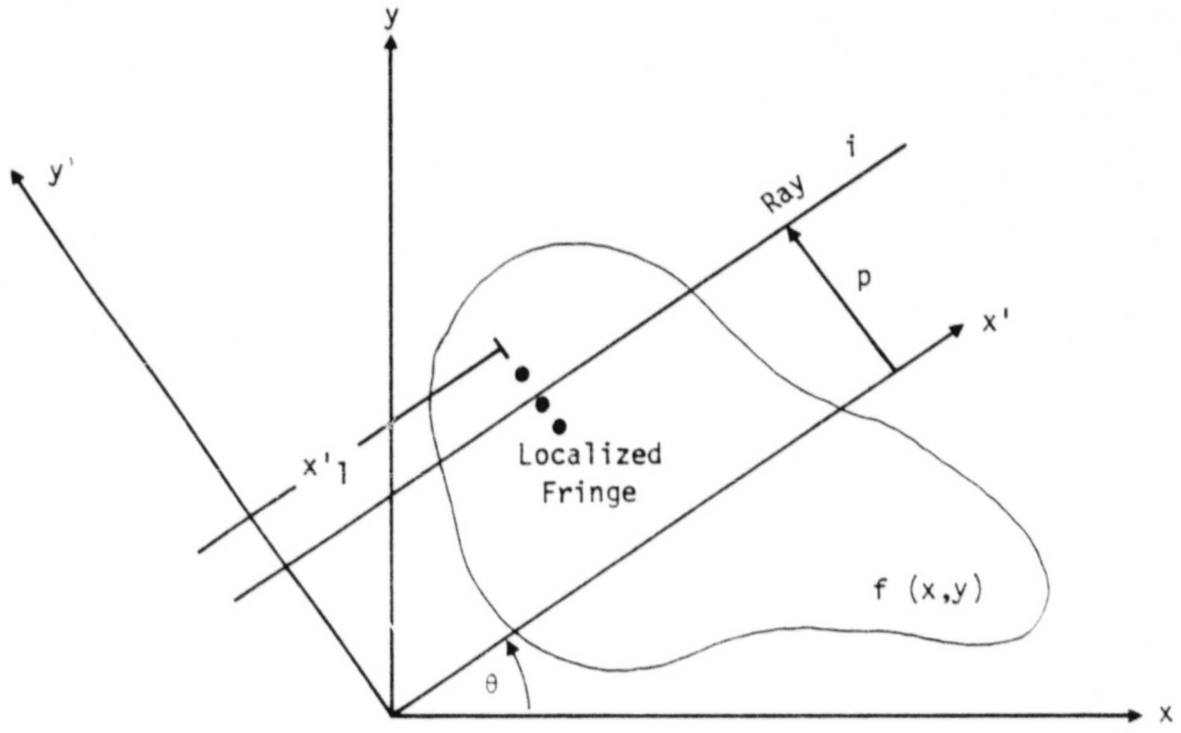

Figure 9. Notation for Localization Reconstruction

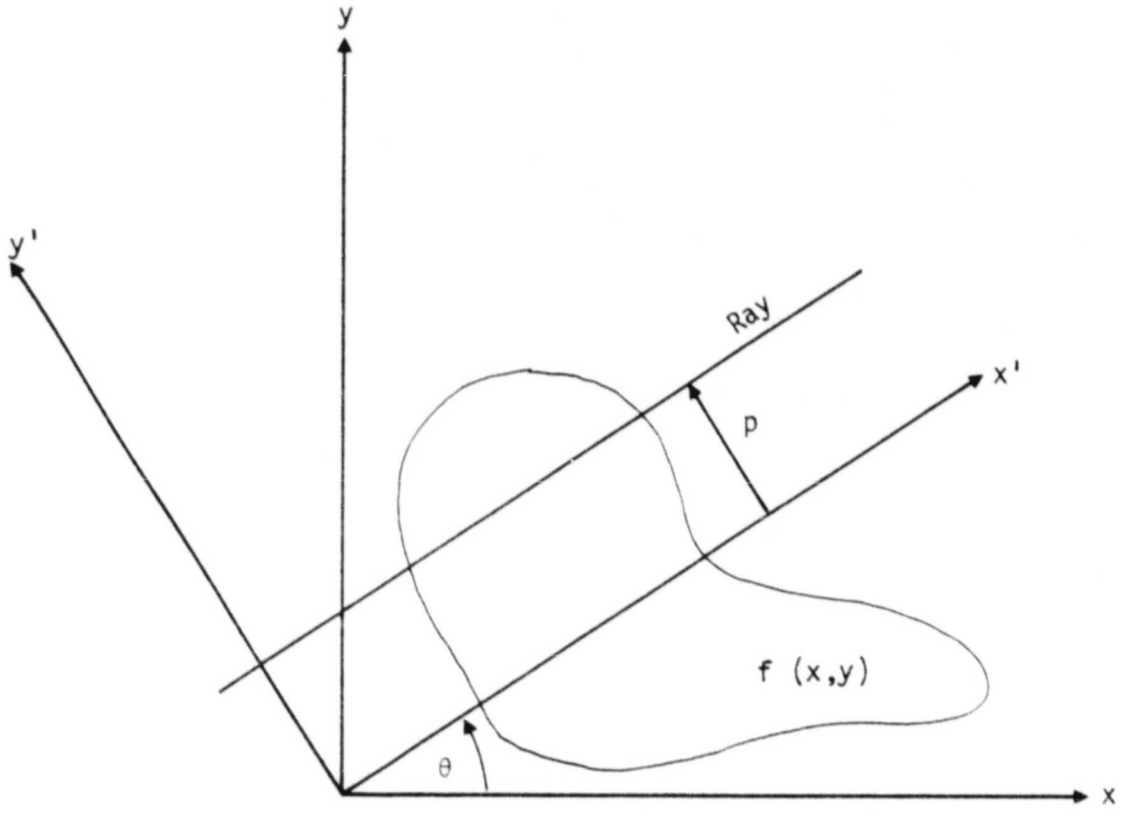

Figure 10. Notation for Fourier transform Domain-Pathlength

FIGURES

FOR

SECTION V

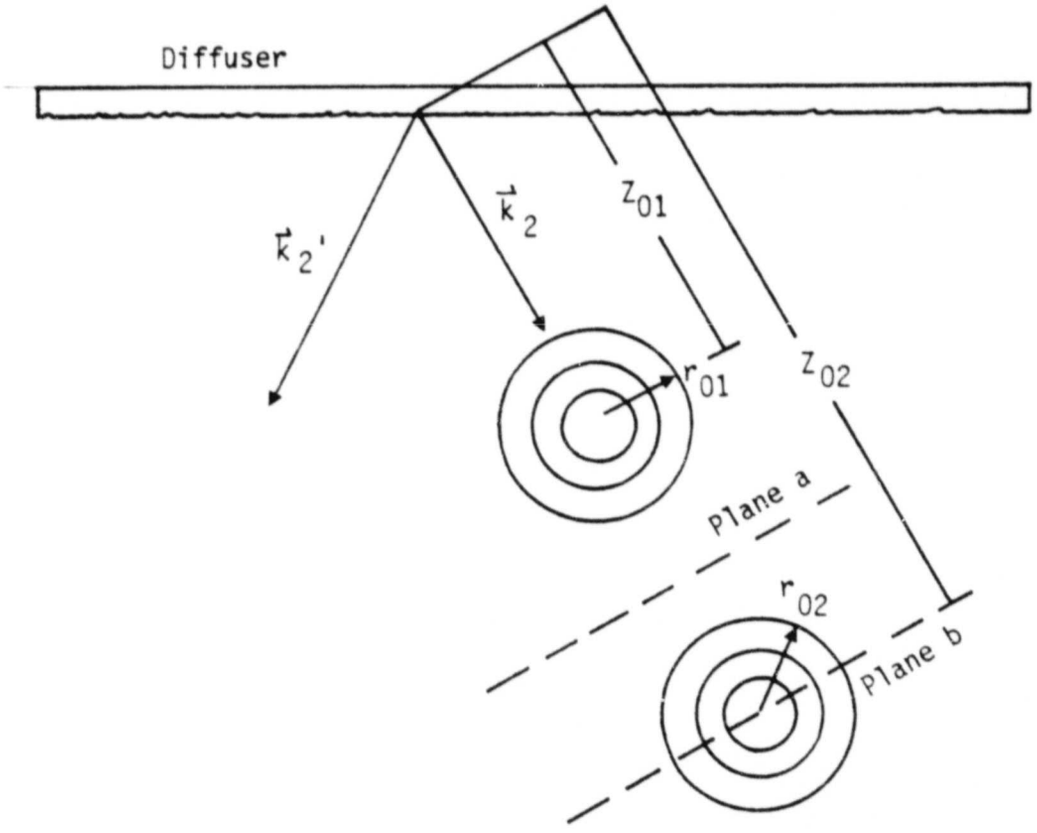

Figure 1. An example of fringe localization.

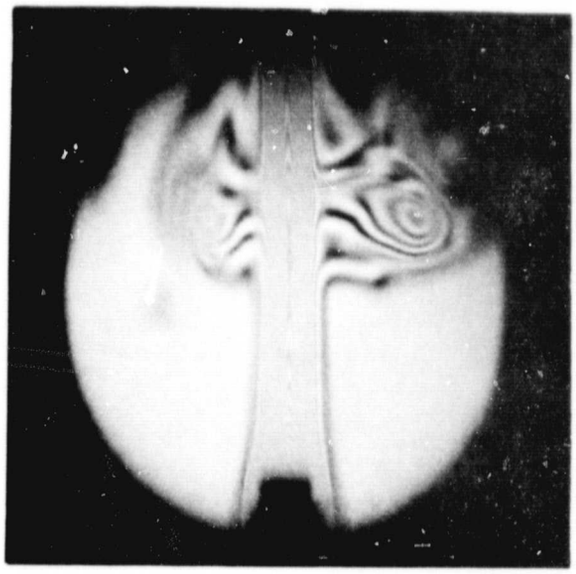

Plane a - no delay

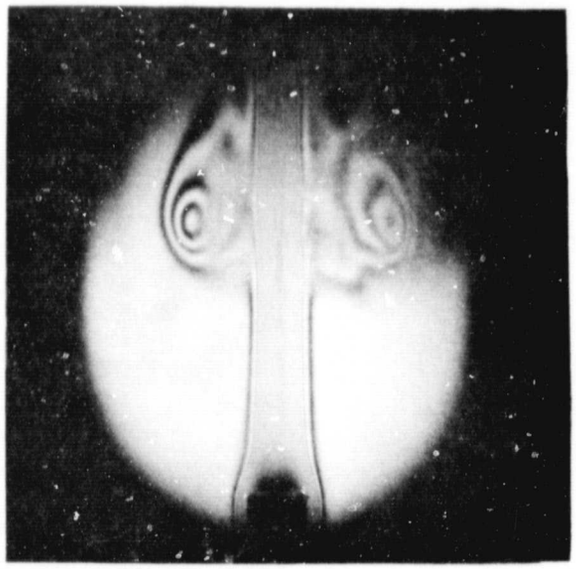

Plane b - no delay

Plane a - 60 sec. delay

Plane b - 60 sec. delay

Figure 2. Experimental data on 2-element radially symmetric phase objects showing fringe localization.

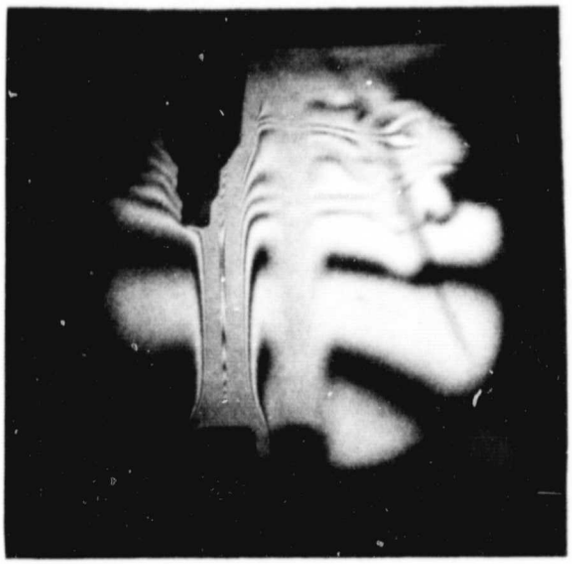

Figure 3. Interferogram of double exposed hologram - Number 26.

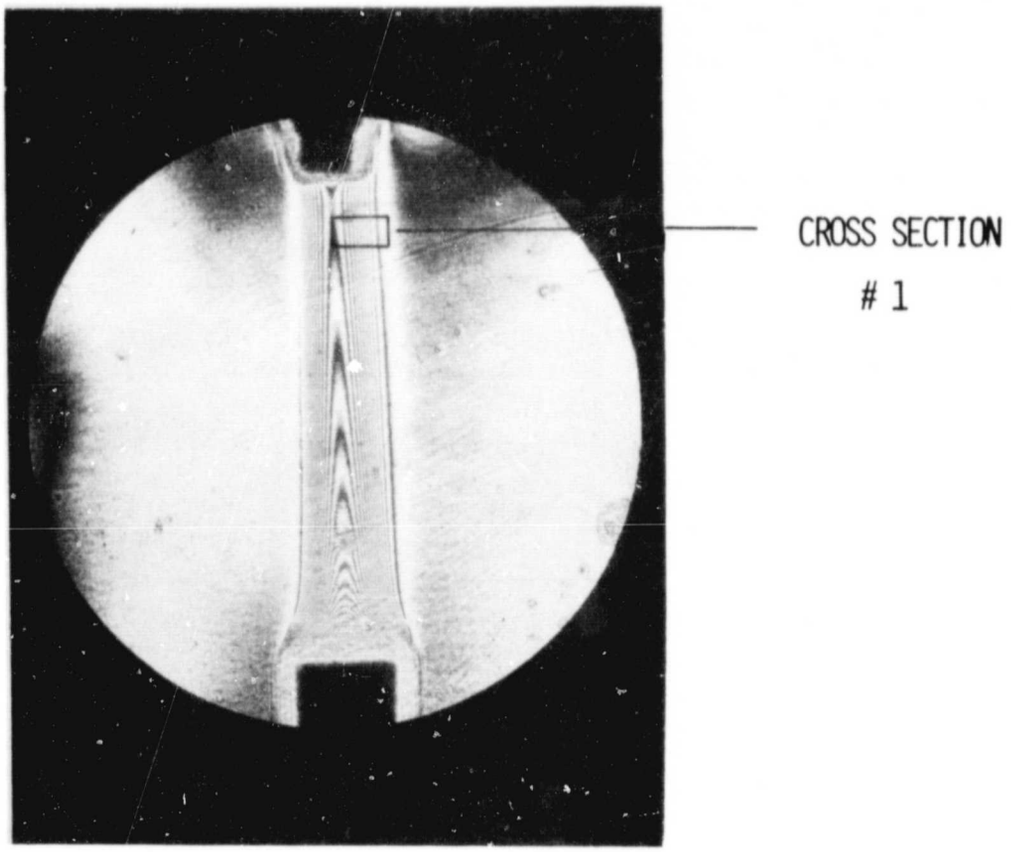

Figure 4. Fringe production by classical interferometer for collimated beam, single exposure and radially symmetric phase object. Hologram #29, cross section #1.

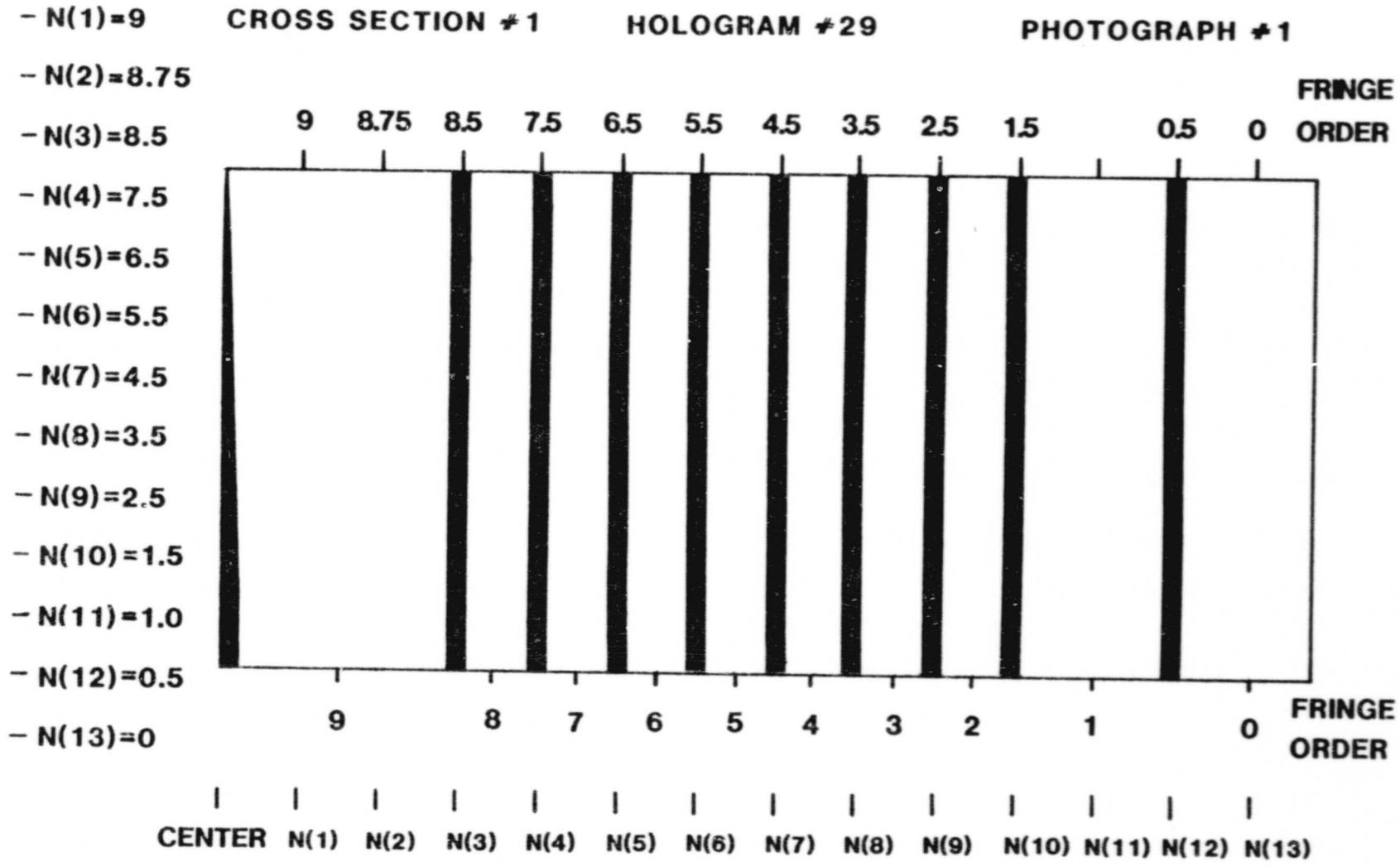

Figure 5. Enlarged view of cross section #1 from Figure 4.

HOLOGRAM # 29 PHOTOGRAPH # 1 CROSS SECTION # 1

ANNULUS #	INDEX OF REFRACTION	TEMPERATURE
1	1.33499	31.1
2	1.33501	30.9
3	1.33492	31.9
4	1.33506	30.4
5	1.33518	29.2
6	1.33529	28.1
7	1.33539	27.2
8	1.33548	26.2
9	1.33559	25.2
10	1.33572	23.8
11	1.33577	23.4
12	1.33582	22.8
13	1.33590	22.0 AMBIENT

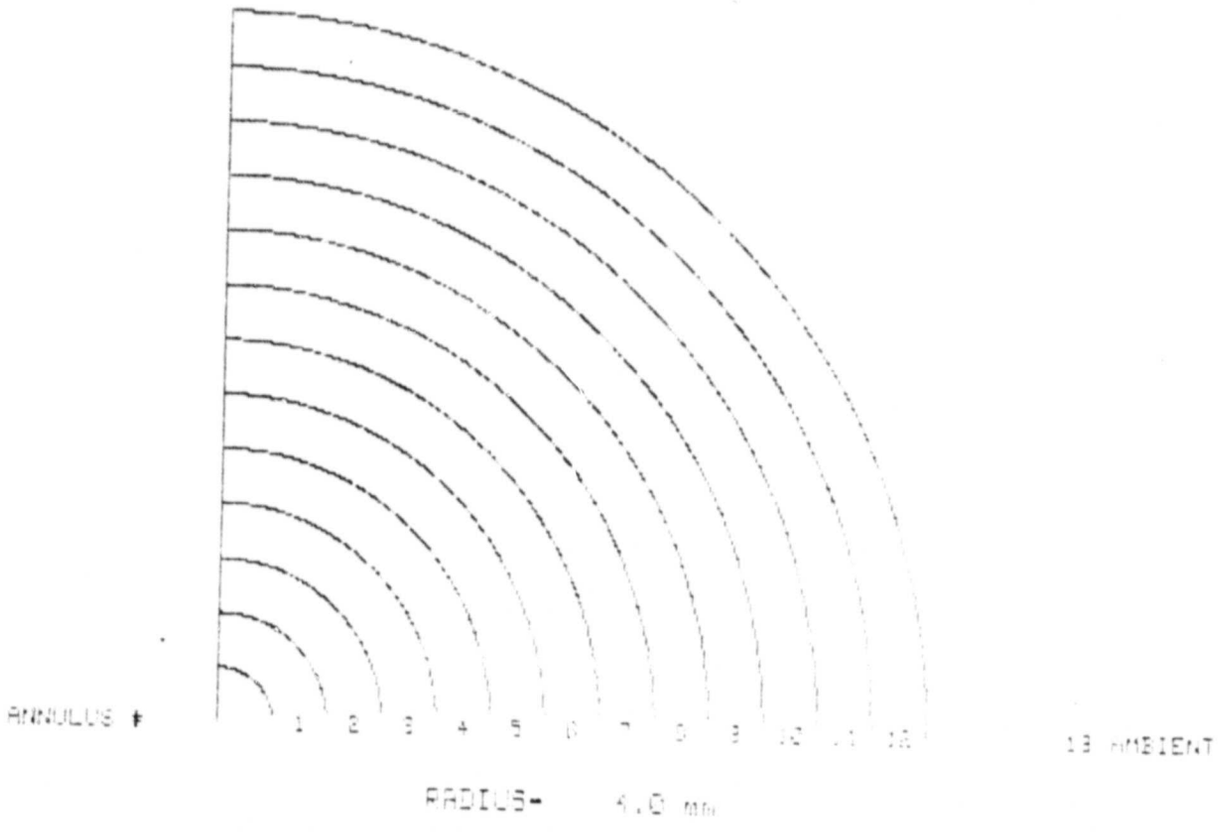

QUADRANT MAP OF REFRACTIVE INDEX FIELD

Figure 6. Table of values for index and temperature from hologram #29.

HOLOGRAM # 29 PHOTOGRAPH # 1 CROSS SECTION # 1

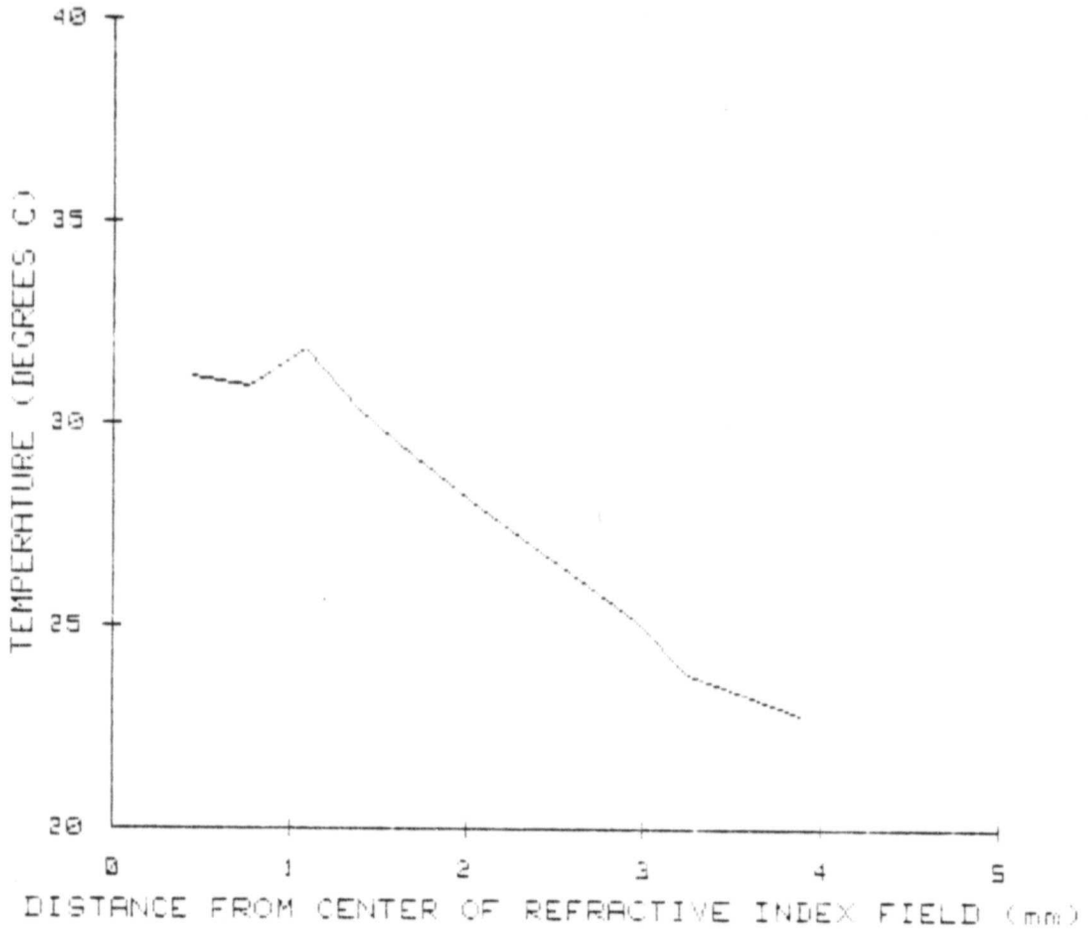

Figure 7. Plot of temperature versus radial distance for hologram #29.

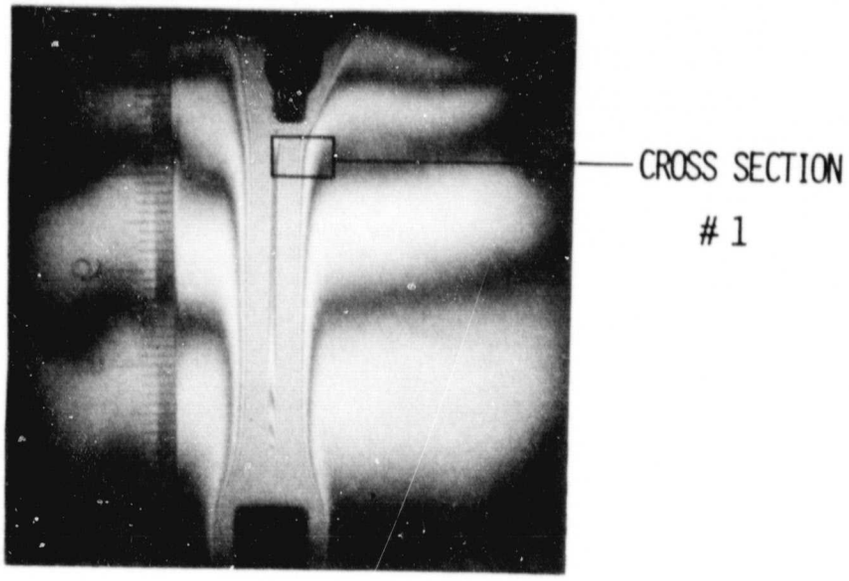

Figure 8. Fringe production by double exposure. Localized fringes of radially symmetric phase object. Hologram #31, cross section #1.

HOLOGRAM # 31 PHOTOGRAPH # 1 CROSS SECTION # 1

ANNULUS #	INDEX OF REFRACTION	TEMPERATURE
1	1.33477	33.2
2	1.33499	31.1
3	1.33508	30.2
4	1.33528	28.1
5	1.33548	26.2
6	1.33571	23.9
7	1.33578	23.2
8	1.33589	22.0
9	1.33592	21.8
10	1.33596	21.4 AMBIENT

Figure 9. Table of values for index and temperature from hologram #31.

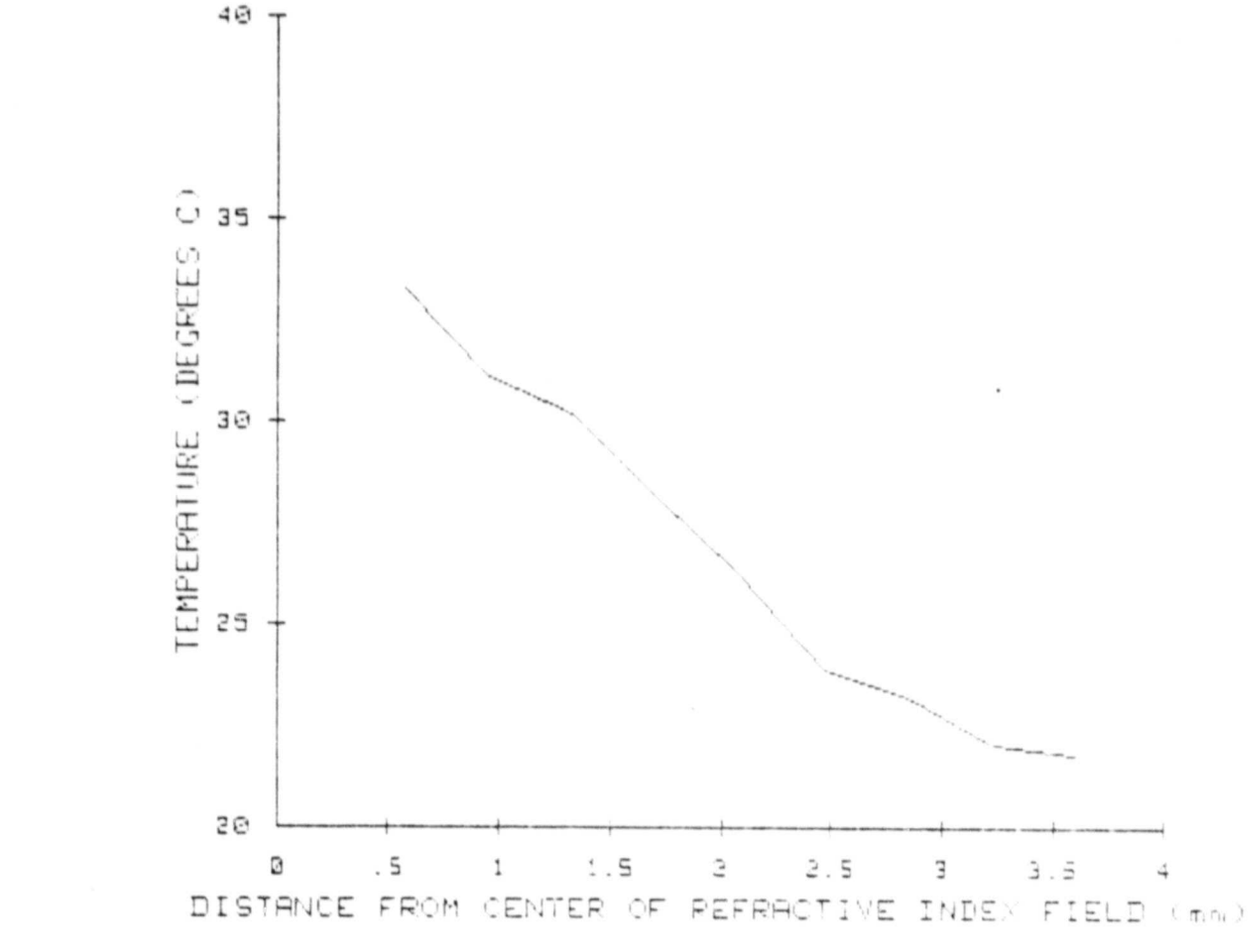

Figure 10. Plot of temperature versus radial distance for hologram #31.